UNIVERSITY OF CALIFORNIA, MERCED

Variability, Stability, and Vulnerability of Buried Soil Organic Carbon: Differences Along Depositional and Erosional Transects

DISSERTATION

submitted in partial satisfaction of the requirements

for the degree of

DOCTOR OF PHILOSOPHY

in Environmental Systems

by

Manisha Dolui

Dissertation Committee

Prof. Teamrat A. Ghezzehei (Chair)

Prof. Sora L. Kim

Prof. Erika Marin-Spiotta (University of Wisconsin, Madison)

Prof. Rebecca Ryals

2022

_____

Sora Kim

_____

Erika Marin-Spiotta

_____

Rebecca Ryals

_____

Teamrat A. Ghezzehei (Chair)

Dedication

To

My parents, husband, and friends

in recognition of their help and support through this journey

TABLE OF CONTENTS

LIST OF FIGURES

LIST OF TABLES

ACKNOWLEDGEMENTS

I would like to express my deepest gratitude to my advisors' Professor Asmeret Asefaw Berhe (previous advisor) and Professor Teamrat A. Ghezzehei (current advisor), for their excellent guidance, caring patience and for providing me with an excellent atmosphere for doing research. I am heartily thankful for their excellent guidance and encouragement that enabled me to undertake this research and complete it successfully.

I would like to express my gratitude to my committee members Dr. Rebecca Ryals, Dr. Sora Kim, and Professor Erika Marin-Spiotta, for their valuable suggestions and contributions throughout the project and refining of this thesis. I would also like to thank the NSF EAR-1623814 grant for funding this research.

Also, I am thankful to Dr. Karis McFarlane for giving me the opportunity to work as a graduate summer intern in 2021 at LLNL under her guidance and for allowing me to use her laboratory instrument to finish all the required gas analyses in 2022. Also, a big Thank you to Dr. Robin Trayler for helping me with all the isotope analysis.

This work would not have been possible without the help of all these above-mentioned people and including my lab mates, our postdoctoral scholars, and laboratory assistants, who have immensely helped me to reach the finish line.

Asmeret Asefaw Berhe was a co-PI of the research project that resulted in this dissertation, until May 2022 when she was confirmed by the US Senate to serve as the Director of the DOE Office of Science.

VITA

Manisha Dolui

EDUCATION

Ph.D., Environmental Systems (Soil Biogeochemistry), University of California, Merced 2022

M.S., Agricultural Science (Plant Science major), Tennessee State University 2017

M.Sc., Environmental Science, University of Calcutta 2011

B.S., Zoology (major) and Botany and Chemistry (minor), University of Calcutta, 2009

ADDITIONAL TRAINING:

Summer Soil Institute, Colorado State University June 17th -25th, 2018

- Advanced concepts and methods in soil organic matter biogeochemistry and pedology

Radiocarbon in Ecology and Earth System Science, UC Irvine August 11th-16th, 2019

- Introduction to Accelerator Mass Spectrometry and application of radiocarbon (14C) in soil science and ecology, including determining the mean residence time of soil organic matter (SOM).

RESEARCH EXPERIENCE

Ph.D. Dissertation (in progress) August 2017- Fall 2022

Variability, stability, and vulnerability of buried soil organic carbon: difference along eroding and depositional transects

M.S. Thesis January 2015- May 2017

An Attenuated Total Reflectance Fourier Transform Infrared (ATR-FTIR) Spectroscopic Study on The Oxytetracycline (OTC) Sorption Mechanism on Variable Charge Minerals"

- ATR-FTIR experiments to see the sorption capacity of OTC or P (V) alone at different pH by adsorption isotherm experiment

- pH envelope experiment to understand the effect of P and OTC sorption
- macroscopic competitive sorption experiment on kaolinite between P and OTC by manually controlling the pH

M.Sc. Dissertation January 2011-April 2011

Documentation of Biodiversity and Related Traditional Knowledge in a Village

- *Project 1*: "Sustainable Development in India Updates on Possible Role of States" (Kolkata, India, August 2013-August 2014)
- *Project 2*: "A Study on Solid Waste Disposal Mechanism, Practiced in Marketplaces of Kolkata and Immediate Surroundings" (Kolkata, India, February 2013-May 2013)

- *Project 3*: "A Study on the Risk Pattern, Preparedness and Possible Impacts cum Vulnerability of Kolkata and Howrah to Phenomenon of Climate Change" (Kolkata, India, December 2011-March 2012)

PUBLICATIONS

1. Roy, J., Bhowmik, R., **Dolui, M.** 2014. Actions for sustainable development evidence-based assessment for the state of West Bengal. *Arthaniti* 13 (1-2)/2014/1
2. Dolui, M., Rakshit, S., Lefevre, G., Sarkar, D., and Elzinga, E.J. 2018. "Probing Oxytetracycline Adsorption Mechanism on Kaolinite in a Single Ion and Binary Mixtures with Phosphate Using in situ ATR-FTIR Spectroscopy." *Soil Science Society of America Journal* Vol. 82:826–838, doi:10.2136/sssaj2018.01.0020
3. Dolui, M., Ghezzehei. T. 2022. Differences in soil organic matter composition and partitioning along eroding and depositional transects in buried vs. modern soil layers: A case of the Brady paleosol at Wauneta, Nebraska (in preparation)
4. Longbottom, T., Wahab, L., Min, K., Jurusik, A., Moreland, K., **Dolui, M.,** Thao, T., Gonzales, M., Rojas, Y. P., Alverez, J., Malone, Z., Yan, J., Ghezzehei, T. A., and A. A. Berhe. May 2022. What's soil got to do with climate change? The Geological Society of America, Vol.32, No.5
5. Szymanski, L. M., McMurtry, A. R., **Dolui, M.,** de Graaff, A. M, Berhe, A. A., Mason, J. A., and Marín-Spiotta, E. 2021. Vulnerability of ancient carbon in buried soils to microbial decomposition with landscape disturbance, Soil Biology, and Biochemistry (Submitted)

CONFERENCE PRESENTATIONS

1. Poster presentation on "An *in-situ* ATR-FTIR investigation of the influence of phosphate on oxytetracycline sorption on kaolinite" at Southeast Regional Meeting of American Chemical Society, Columbia, South Carolina, October 23rd-26th, 2016.
2. Oral presentation on "Evaluating surface interaction mechanisms of antibiotic oxytetracycline on a mixed clay and iron oxide mineral system: A molecular level investigation using in situ spectroscopic probes" at 18th Biennial research symposium of Association of 1890 Research Directors, Atlanta, GA, April 1st-4th, 2017.
3. Poster presentation on "Distribution and composition of soil organic matter in a buried soil: differences along eroding and depositional transect" at American Geophysical Union Fall 2019 meeting in San Francisco, December 9th -13th, 2019.
4. Poster presentation on "Variability in soil organic matter composition in a buried soil: differences along eroding and depositional transects" at American Geophysical Union Fall 2020 meeting online, December 1st - 17th, 2020.
5. Oral presentation on "Vulnerability of buried soil organic carbon: insights from radiocarbon" at American Geophysical Union Fall 2021 meeting online, December 13th – 17th, 2021.

AWARDS, SCHOLARSHIPS, FELLOWSHIPS

1. 2nd prize for the poster presentation on "*In situ* ATR-FTIR spectroscopic study of antibiotic oxytetracycline adsorption on variable charge minerals" at 38th Annual University-Wide Research Symposium Research and Sponsored Programs, Tennessee State University, 2016.
2. University of California, Department of Environmental Systems Summer fellowship (2018 and 2019)
3. University of California, Department of Environmental Systems Professional Development Fellowship (2018 Summer, 2019 Summer, 2019 Fall, Summer 2021)
4. Received a fellowship of $1000 to attend the Sumer Soil Institute at Colorado State University, June 17th -25th, 2018.
5. Graduate Summer internship at Lawrence Livermore National Laboratory (LLNL), 24th May- 14th August 2021

INDUSTRIAL EXPERIENCE (APRIL 2012- DECEMBER 2012):

1. Worked in an Environmental Laboratory (Mitra S K Pvt. Ltd, ISO 9001:2008 by DNV certified) in the Water Department at Kolkata, India.
2. The main area of work was analyzing –

    a. Dissolved oxygen of surface water
    b. Biochemical oxygen demand of effluent, ground & surface water

c. Chemical oxygen demand of effluent, surface & groundwater
d. Bioassay of effluent water
e. pH, EC, Total dissolve solid (TDS), phosphate, nitrate

TECHNICAL AND OTHER SKILLS:

1. Instrument operation, data analysis, and interpretation
    a. Attenuated Total Reflectance- Fourier-transform infrared (ATR-FTIR) spectroscopy
    b. Diffuse reflectance infrared fourier transform- Fourier-transform infrared (DRIFT-FTIR) spectroscopy
    c. Inductively coupled plasma atomic emission spectroscopy (ICP-OES)
    d. Ultra-violate visible spectroscopy (UV-Vis)
    e. Gas chromatography (GC)
2. Data analysis using R
3. Organizing weekly Enviro-Lunch seminar at UC Merced (Fall 2020 to Spring 2022)
4. Office/Project management skills (Leading, planning, and owning end-to-end independent research studies)
5. Team player and resilient nature
6. Passionate about working with the community and stakeholders

ABSTRACT OF THE DISSERTATION

Variability, Stability, and Vulnerability of Buried Soil Organic Carbon: Differences Along Depositional and Erosional Transects

by

Manisha Dolui

Doctor of Philosophy in Environmental Systems

University of California, Merced, 2022

Dr. Teamrat A. Ghezzehei, Chair

Paleosols are formed when the topsoil gets buried by the lateral distribution of soil and can store large quantities of soil organic matter (SOM) that may persist over millennial timescales due to its detachment from the disturbances at the surface. We studied buried SOM dynamics in the Brady paleosol, a deep loess (aeolian) deposit in Nebraska, USA, where climate has historically driven varying rates of loess deposition during the late Pleistocene and Holocene, burying soils up to 50m below the surface. Soils were sampled along the depositional and erosional transects at depths from 0.2 to 5.5m to understand the variability in the physical and chemical composition of the soils. We used elemental and isotopic compositions of C, N, ^{13}C, and ^{15}N, along with radiocarbon, base cation concentrations, and Fourier Transformed Infrared Spectroscopy (FTIR) to determine the distribution, stabilization, and composition of SOM and organic carbon in the soil profiles. Our results show a general decreasing trend of $\delta^{13}C$ and $\delta^{15}N$ values with depth, suggesting root input to soil carbon pools and the presence of less decomposed SOM in the deeply buried soil layers. Radiocarbon analysis of bulk soil indicated a loss of ancient carbon and incorporation of new photosynthate carbon in the eroding transect. Our stabilization study indicated, modern and buried Brady soil both are flocculated in physical structure and Brady soils has more monovalent cations compared to the modern soils. To determine the vulnerability of the SOM to the addition of moisture, we added water to soil from the different transects and depths at 60% pore space capacity in two different experimental setups – repeated wet and dry cycles and continuously wet. We found that repeated wetting and drying led to higher CO_2 efflux for buried Brady soils from erosional transects compared to the modern soils collected from the depositional transects. Our findings indicate that change in soil moisture status can play a critical role in destabilizing previously protected ancient carbon. Finally, our study highlights the need for furthering our understanding of how a predicted increase in precipitation quantity and intensity coupled with accelerated erosion can release large quantities of greenhouse gases by mineralization of previously protected old carbon stocks.

Chapter 1.
Introduction

Globally, the soil system has stored more carbon (C) than the atmosphere and vegetation combined, making it possibly an important part of the solution to climate change (Le Quéré et al., 2018). However, the projected warming of the Earth's atmosphere is expected to increase the decomposition of soil C with the potential to release high levels of greenhouse gases (GHGs) into the atmosphere (Berhe et al., 2007). But large uncertainty remains on the response of subsoil C, especially below 30 cm depth (stores 30-70% C) to climate change. Soil down to 1 m has been predicted to release an equivalent to a third of current fossil fuel emissions with a 4 C increase (Berhe et al., 2007). Paleosols, formerly topsoils buried by deposition of newer material, have been highlighted for their potential to play important roles in soil C storage (Marin-Spiotta et al., 2011; Hoffmann et al., 2013). For example, an aeolian buried soil in northeast Siberia, Russia, is estimated to store about 8465 Mg C/ha at a depth of 1-16 m (Chaipricha and Marin-Spiotta, 2014; Zimov et al., 2006). Subsoil soil organic matter (SOM) has a long residence time (i.e., persistence) compared to topsoil SOM owing to its mineral association, aggregate protection, burial, chemical composition (less plant litter and more microbial byproducts), reduced contact with microbes, low moisture status (Chabbi et al., 2009; Marin-Spiotta et al., 2014). However, deep-buried C may become an active source for microbial growth if the factors responsible for stabilization are altered. Paleosol can play a growing role in the global C cycle under predicted future climate. Predicted higher rates of erosion and exposure of formerly buried layers to oxidizing and wetter near-surface environments can accelerate the rate of decomposition of SOM in buried layers (Fontaine et al., 2007). To understand and predict buried C vulnerability to changes in climate and landscape disturbance, we need to identify the mechanisms that are contributing to storage and turnover in these pools and evaluate their response to changing environmental conditions *in situ*.

Paleosols are soils that developed in different environmental conditions (Johnson 1998) when the topsoil was transported downhill and was buried by alluvial, colluvial, aeolian deposition, volcanic eruption, or human activities (Chaipricha and Marin-Spiotta, 2014). These processes can take place over centuries to millennia, promoting efficient chemical interactions with soil particles (Rumpel and Kogel-Knabner, 2011; Rasse et al., 2006) storing large quantities of soil organic C due to reduced moisture, reduced microbial diversity, and a high rate of evapotranspiration that limits the downward movement of SOM (Chaipricha and Marin-Spiotta, 2014; Schmidt et al., 2018). *In situ* primary production such as root and bioturbation (Chaipricha and Marin-Spiotta, 2014) at the sites of burial can lead to additional C storage (Berhe et al., 2012) as accumulating sediments also transport varying amounts of C that are buried at the downhill (Nadeu et al., 2012) due to soil erosion (Berhe et al., 2007). If we understand the geochemistry of this buried soil, then it will help us to predict the release of the C sink present in this area and will give us an estimation of the increasing release of ancient C in the environment (Marin-Spiotta et al., 2014). In general, the radiocarbon age of SOC increases with the soil depth due to precipitation and clay content (Billings and de Suza 2020), and analysis of this helps us to understand C stabilization processes. Radiocarbon analysis can also be

used as a tool to understand C turnover and CO_2 production and how precipitation can affect C protection (Billings and de Suza 2020).

Erosion caused by precipitation affects the structure of the ecosystem (Pimentel et al., 1995), and the IPCC 2013 report has indicated that there will be an increase in interannual rainfall variability, possibly inducing further soil erosion. Topsoil C is annually redistributed across the landscape by erosion and deposition (Berhe et al., 2007), which can have a significant influence on the global C budget if they cause a release of CO_2 into the atmosphere (Guo and Gifford 2002). Due to the topsoil removal by erosion, more stable C from the deep layers is incorporated into the top layer and gets mixed with the new labile material, which affects the turnover of these previously stable C compounds (Doetterl et al., 2012). The total amount of C in soil buried during ancient and modern times is not known, but the occurrence of landscape change and disturbance by various climatic, geologic, and anthropogenic events suggests that it is likely significant. The vulnerability of buried SOC to the changing climate depends on the types of soil minerals present and the soil's response to the change in annual to decadal timescale (Harrison et al., 2011). The presence of polyvalent cations, metals, or reactive minerals has an influence on increased SOC stock, and it can resist microbial degradation by forming aggregates in the presence of polyvalent cations that can get cemented in the presence of carbonates, Fe oxides, and poorly crystalline minerals (Zhao et al., 2017; Whittinghill and Hobbie, 2012). Along with the erosion-surface exposure of the buried soil due to human-induced changes or changes in soil hydrology and plant rooting depths can also reconnect the ancient SOC to conditions favorable for decomposition. This research will help us to understand the heterogeneity of buried C at the landscape scale and estimate the amount and rate of the release of this ancient C from this massive C sink with changes in climate.

Paleosols give powerful insight into understanding modern and future projections of soil processes, landscape disturbance, C persistence, vegetation, and previous climate when the soil was formed. We can use the information of the buried soil C persistence as a model system -to understand the C accumulation, long time stabilization, and its vulnerabilities to climate change in deep soil horizons. Finally, we can identify how the buried soil can be a part of the climate change solution. One important aspect of this research is to understand the vulnerability of soil C that depends on the landform position, as the SOM protection mechanism can differ in a tableland compared to an erosional landform and thus providing a unique opportunity to predict the response of soil C to two different landscapes impacted by climate change.

In the past, most of the soil research on soil C persistence has focused on topsoil C dynamics, and hence our understanding of the mechanisms of deep soil C storage and its vulnerability to future climate change is currently incomplete. So, in this dissertation research, I investigated C persistence due to the difference in the chemical composition of SOM in buried vs modern soils owed to a shift in vegetation and burial, the presence of different polyvalent cations and its association with SOM; and finally, the effect of anticipated changes in precipitation on buried SOM in different landform (burial and erosional) scenarios in the central Great Plains.

To address these major knowledge gaps, I performed a detailed comparison of SOM composition at two different landforms, burial (depositional or table landform) and erosional, to understand the spatial variability in buried vs modern soils (Chapter 2). The

objective of this chapter is to elucidate the difference in SOM chemical composition and C amount in eroded and depositional landforms in buried compared to modern soil layers.

In Chapter 3, I address the extent to which SOM stabilization can be explained by the presence of polyvalent cations. Specifically, the goal of this chapter was (a) to identify differences in concentration and types of polyvalent cations in buried and modern soils, (b) to identify the relationships between SOC concentration and various polyvalent cation concentrations in depositional and erosional landform buried vs modern soils, and (c) the importance of soil particle size and exchangeable base cation content in the SOC stabilization in buried and modern soils.

Finally, given the differences in SOM composition and differences in the stabilization mechanism of the buried vs modern soils in depositional and erosional landforms, I assessed the vulnerability of SOC to the addition of moisture (Chapter 4). The specific objectives of this chapter were to quantify the response of Brady soil SOM to the input of water under ambient environmental conditions (near-surface aeration and room temperature). I also tested the patterns of soil CO_2 efflux in response to dissimilar water addition (continuous wet vs wet-dry-rewet) events.

1.1 References

Berhe, A. A., Harte, J., Harden, J. W., and Torn, M. S. (2007). The significance of the erosion-induced terrestrial carbon sink. Bioscience, 57, 337-346, https://doi.org/10.1641/B570408

Berhe, A. A., Harden, J. W., Torn, M. S., Kleber, M., Burton, S. D., and Harte, J. (2012). Persistence of soil organic matter in eroding versus depositional landform positions. J. Geophys. Res., 117, G02019, doi:10.1029/2011JG001790.

Billings, S.A., and de Souza, L.F.T. (2020). Earth's soil harbours ancient carbon. Nat. Geosci. 13, 527–528. https://doi.org/10.1038/s41561-020-0614-1

Chaopricha, N. T., and Marin-Spiotta, E. (2014). Soil Burial Contributes to Deep Soil Organic Carbon Storage. Soil Biology and Biogeochemistry, 56, 251-264, https://doi.org/10.1016/j.soilbio.2013.11.011

Climate Change 2013: The Physical Science Basis. Contribution of Working Group I to the Fifth Assessment Report of the Intergovernmental Panel on Climate Change (2013), p. 33

Doetterl, S., Six, J., Van Wesemael, B., and Van Oost, K. (2012). Carbon cycling in eroding landscapes: geomorphic controls on soil organic C pool composition and C stabilization. Global Change Biology, 18(7), 2218-2232.

Fontaine, S., Barot, S., Barré, P., Bdioui, N., Mary, B., and Rumpel, C. (2007). Stability of organic carbon in deep soil layers controlled by fresh carbon supply. Nature, 450(7167), 277-280.

L. B., and Gifford, R. M. (2002). Soil carbon stock and land use change: a meta-analysis, Global Change Biology,8(4), 345-360, https://doi.org/10.1046/j.1354-1013.2002.00486.x

Harrison, R. B., Footen, P. W., & Strahm, B. D. (2011). Deep soil horizons: contribution and importance to soil carbon pools and in assessing whole-ecosystem response to management and global change. Forest Science, 57(1), 67-76.

Hoffmann, T., Schlummer, M., Notebaert, B., Verstraeten, G., and Korup, O. (2013). Carbon burial in soil sediments from Holocene agricultural erosion, Central Europe. Global Biogeochemical Cycles, 27(3), 828-835.

Johnson, D. (1998). Paleosols are buried soils. Quaternary International, 51, 7.

Le Quéré, C., R. M. Andrew, P. Friedlingstein, S. Sitch, J. Hauck, J. Pongratz, P. A. Pickers, J. I. Korsbakken, G. P. Peters, J. G. Canadell, A. Arneth, V. K. Arora, L. Barbero, A. Bastos, L. Bopp, F. Chevallier, L. P. Chini, P. Ciais, S. C. Doney, T. Gkritzalis, D. S. Goll, I. Harris, V. Haverd, F. M. Hoffman, M. Hoppema, R. A. Houghton, G. Hurtt, T. Ilyina, A. K. Jain, T. Johannessen, C. D. Jones, E. Kato, R. F. Keeling, K. K. Goldewijk, P. Landschützer, N. Lefèvre, S. Lienert, Z. Liu, D. Lombardozzi, N. Metzl, D. R. Munro, J. E. M. S. Nabel, S. Nakaoka, C. Neill, A. Olsen, T. Ono, P. Patra, A. Peregon, W. Peters, P. Peylin, B. Pfeil, D. Pierrot, B. Poulter, G. Rehder, L. Resplandy, E. Robertson, M. Rocher, C. Rödenbeck, U. Schuster, J. Schwinger, R. Séférian, I. Skjelvan, T. Steinhoff, A. Sutton, P. P. Tans, H. Tian, B. Tilbrook, F. N. Tubiello, I. T. van der Laan-Luijkx, G. R. van der Werf, N. Viovy, A. P. Walker, A. J. Wiltshire, R. Wright, S. Zaehle, and B. Zheng (2018). Global Carbon Budget 2018, Earth Syst. Sci. Data, 10, 2141–2194, https://doi.org/10.5194/essd-10-2141-2018.

Marin-Spiotta, E., Chadwick, O. A., Kramer, M., and Carbone, M. S. (2011). Carbon delivery to deep mineral horizons in Hawaiian rain forest soils. Journal of Geophysical Research: Biogeosciences, 116(G3).

Marin-Spiotta, E., Chaopricha, N. T., Plante, A. F., Diefendorf, A. F., Muller, C. W., Grandy, A. S., Mason, J. A. (2014). Long-term Stabilization of Deep Soil Carbon by Fire and Burial During Early Holocene Climate Change. Nature Geoscience, May 25, 2014. DOI: 10.1038/NGEO2169

Nadeu, E., Berhe, A. A., de Vente, J., & Boix-Fayos, C. (2012). Erosion, deposition and replacement of soil organic carbon in Mediterranean catchments: a geomorphological, isotopic and land use change approach. Biogeosciences, 9(3), 1099-1111.

Pimentel, D., Harvey, C., Resosudarmo, P., Sinclair, K., Kurz, D., McNair, M., Crist, S., Shpritz, L., Saffouri, L., and Blair, R. (1995). Environmental and economic costs of soil erosion and conservation benefits. Science, 267(5201), 1117-1123.

Rumpel, C., and Kögel-Knabner, I. (2011). Deep soil organic matter—a key but poorly understood component of terrestrial C cycle. Plant Soil, 338**,** 143–158

Rasse, D. P., Mulder, J., Moni, C., and Chenu, C. (2006). Carbon turnover kinetics with depth in a French loamy soil. Soil Science Society of America Journal, 70(6), 2097-2105.

Schmidt, M. W. I., Torn, M .S., Abiven, S., Dittmar, T., Guggenberger, G., Janssens, I. A., Kleber, M., Kogel-Knabner, I., Lehmann, D J., Manning, A. C., Nannipieri, P., Rasse, D. P., Weiner, S., and Trumbore, S. E. (2011). Persistence of soil organic matter as an ecosystem property, Nature, 478, 49-56, doi:10.1038/nature10386

Whittinghill, K.A., and Hobbie, S.E. (2012). Effects of pH and calcium on soil organic matter dynamics in Alaskan tundra. Biogeochemistry, 111, 569–581. https://doi.org/10.1007/s10533-011-9688-6

Zimov, S. A., Davydov, S. P., Zimova, G. M., Davydova, A. I., Schuur, E. A. G., Dutta, K., & Chapin III, F. S. (2006). Permafrost carbon: Stock and decomposability of a globally significant carbon pool. Geophysical Research Letters, 33(20).

Zhao, J., Chen, S., Hu, R., & Li, Y. (2017). Aggregate stability and size distribution of red soils under different land uses integrally regulated by soil organic matter, and iron and aluminum oxides. Soil and Tillage Research, 167, 73-79.

Chapter 2.
Differences in soil organic matter composition and partitioning along eroding and depositional transects in buried vs. modern soil layers: A case of the Brady paleosol at Wauneta, Nebraska

Abstract

Paleosols are formed when the topsoil gets buried by a lateral distribution of soil and can store large quantities of soil organic matter (SOM) that may be persistent over millennial timescales due to its detachment from the disturbances at the surface. We studied buried SOM dynamics in the Brady paleosol, a deep loess (aeolian) deposit in Nebraska, USA where climate has historically driven varying rates of loess deposition during the late Pleistocene and Holocene, burying soils up to 50m below the surface. Soils were sampled along the burial and erosional transects at depths from 0.2 to 4.2m to understand the variability in the physical and chemical composition of the soils in buried vs modern surfaces. We determined SOM composition using Fourier Transformed Infrared Spectroscopy (FTIR) analysis to provide a better understanding of the relationships between carbon and nitrogen amounts, sources, and other soil physio-chemical properties with SOM composition and turnover time along depth gradients from modern to buried soil layers in the Brady paleosol. Our results show a general decreasing trend of $\delta^{13}C$ and $\delta^{15}N$ values with depth, suggesting root input to soil carbon pools and the presence of less decomposed SOM in the deeply buried soil layers. FTIR data shows that the buried soil organic matter tends to be enriched in aliphatic compounds similar to the modern soils and that the turnover rate of SOM decreases significantly due to exposure of buried soil layers by erosion. Our study showed that soil physical and chemical properties play important roles in controlling SOC composition across the site, suggesting that buried SOM may be vulnerable to any environmental changes that may directly or indirectly affect a range of soil physio-chemical properties.

2.1 Introduction

Soils are one of the largest carbon (C) reservoirs in the terrestrial ecosystem, storing about 3000Gt C (Le Quéré et al., 2018). Subsoil carbon (below 30 cm depth) can comprise 30-70% of total soil carbon (Moreland et al., 2021). Typically, carbon can accumulate into the subsoil through- dissolved organic matter, root biomass, particulate organic matter that is physically or biologically transported from topsoil layers to subsoil due to movement of water and/or bioturbation, and deposition or burial of soil C that is laterally redistributed by aeolian erosion—all of which depend on climate, soil type, and land use (Rumpel and Kogel-Knabner, 2011; Marin-Spiotta et al., 2014). Subsoil can stabilize a large amount of C compared to topsoil due to the availability of mineral surfaces for sorptive interactions with organic compounds, unfavorable environmental conditions (low oxygen concentration) for microbes leading to a slower rate of organic matter (OM) decomposition, and less physical disturbance (disconnected from water, microbes, and the enzymes that facilitate OM breakdown) (Alcantara et al., 2017;

Schmidt et al., 2011). Moreover, subsoils are likely to receive a large proportion of the C input from roots which is more persistent in soil than the above-ground carbon (ex., leaves, and needles) and promotes efficient chemical interactions with soil particles (Rumpel and Kogel-Knabner, 2011; Rasse et al., 2006).

In addition, subsoil organic carbon (OC) can be derived when ancient topsoil gets buried due to human activities, floods, landslides, volcanic eruptions, or loess deposition. Paleosols are ancient, buried soils, developed under different environmental conditions than present-day and retain properties of past soil-forming processes (Johnson, 1998). Paleosol can store a large amount of carbon in subsoils as they are former topsoil layers, generally rich in SOC that is buried beneath the surface (D'Elia et al., 2017). The carbon preserved in paleosols can be derived from residues of previous plant materials and may over time incorporate carbon derived from new root inputs and dissolved C leached from the upper soil horizons (Hoffman et al., 2013; Marin-Spiotta et al., 2011, Berhe et al., 2012). The disconnection of the buried soil from the atmospheric conditions (Chaopricha and Marín-Spiotta, 2014; Johnson, 1998) and reduced moistures in buried soils can restrict the diffusion of extracellular enzymes and inhibit microbial activity, especially in arid and semi-arid regions where a high rate of evapotranspiration limits the downward movement of water from precipitation (Schmidt et al., 2011) leading to the long-term preservation of C in deep soil layers for centuries to millennia (Chaopricha and Marín-Spiotta, 2014). Over time, additional new organic matter can be incorporated into the deep soil layers due to human activities and sudden environmental events such as a fire, landslides, etc (Leopold et al., 2011). In dryland or seasonality dry ecosystems, significant soil C burial can occur due to loess deposition (Chaipricha and Marín-Spiotta, 2014) as the wind can result in detachment and transportation of the sediment (Sankey et al., 2009); in particular, events when the vegetation that covers the soil surface is removed due to fires (Vermeire et al., 2005; Sankey et al., 2009).

Soil stores most of the terrestrial carbon pool in the earth (Jobbágy and Jackson, 2000; Lal, 2008), however, this SOC is projected to be mineralized with the warming of the earth's climate (Xu et al., 2019; Gao et al., 2020; Jiang et al., 2022). Projected warming of the earth's atmosphere is expected to increase the decomposition rate of soil carbon with the potential to release large amounts of greenhouse gases (GHGs) into the atmosphere. Large uncertainty remains on the response of subsoil C to climate change, with studies predicting the potential release of subsoil carbon due to warming that is equivalent to 1/3rd of current fossil fuel emissions (Berhe et al., 2007). The amount of soil carbon that is stabilized by climate change depends on the mechanisms of its stabilization, as the persistence of organic carbon in the soil is an ecosystem property (Schmidt et al., 2011) and depends on environmental conditions that affect the rate of chemical and biological reactions in the immediate environment where soil organic carbon (SOC) is located. Hence, the direction and magnitude of all soil carbon, including buried soil, deep soil, or subsoil C, released due to changes in climate will depend on the sensitivity of soil C to environmental change (Bellamy et al., 2005) as dictated by the SOC's location and nature.

Our understanding of SOC stability, turnover time, long-time storage, and the age of organic carbon present at different depths and landforms/ transect of a paleosol is little known (Chaopricha and Marin Spiotta, 2014). There is a shortage of research focusing on soil carbon pools at different landforms, depths, and the resident time of these soils compared to the modern topsoil. This kind of local and regional information can help us

to understand biogeochemical changes and paleoclimate reconstruction (Tabor and Myers, 2015).

Therefore, the objective of this study is to determine 1) differences in SOC composition between buried and modern soil and 2) how exposure of the formerly buried soil layers due to erosional transport affects the biochemical composition and persistence of soil organic carbon (SOC) in buried vs. modern (top) soil layers. The study was conducted on a well-studied paleosol, the Brady soil, in the southern great plain of Nebraska, where we characterized the soil's physical and chemical composition, SOM concentration, composition, and mean residence times along depth profiles of a burial transect (representing landscape positions where the buried soil is located at different depths below the soil surface) and an erosional transect (that represents portions of the landscape where the buried soil is located at different depths because it is being exposed by modern erosion). We hypothesized that: 1) the biochemical composition of SOM in the paleosol layer is enriched in more processed, microbially derived compounds, and that the SOM associated with the Brady soil will have less labile compounds compared to the modern soil layers, and 2) SOM will remain more persistent in depositional sites compared to the erosional site due to less disturbance leading to the Brady soils located at shallow depths to reflect shorter mean residence time due to input of newer carbon to the soil from recent photosynthate, compared to the deeper Brady soil. Our study will advance our understanding of how exposure to previously buried SOM by modern erosion may destabilize C buried across the landscape.

2.2 Materials and Method

2.2.1 Site description and soil sampling

The study site is located in Wauneta, Nebraska, Great Plains, where climate-driven varying rates of loess deposition during the Late Pleistocene and Holocene resulted in sequences of buried soils in thick loess deposits (Johnson et al., 2007). The mean annual temperature of this area is 9.7°C, mean annual precipitation is 495 mm (seasonal). The vegetation is mixed C3, C4, and short grass prairie and the land is cultivated where the topography permit and grazed where the topography doesn't. The Brady soil was formed between cs. 13 to 10 kya and was buried by loess (Mason et al., 2008). In our study site, the modern soils are loess derived and classified as Mollisols.

Brady soil is a morphologically distinct stratigraphic and paleoenvironmental marker in the central great plains (Johnson and Willy, 2000) which is prominent in central Nebraska, northern Kansas, and northeastern parts of Colorado. Its soil was formed due to aeolian deposition, which has an important beneficial effect such as nutrient transportation to the terrestrial and aquatic system (Sankey et al., 2009; Neff et al., 2008; Lal et al., 2003; Jickells et al., 2005; Reynolds et al., 2001). Jacobs and Mason (2004) study found that the Brady soil has A, B, and C horizon morphology. The A horizon is very dark greyish brown, and the texture is invariably silt loam. The dark color of the Brady soil A horizon is suggested to come from the recalcitrant clay-organic matter complexes (Jacobs and Mason, 2004) depending on a Mollisols study in that region, but the organic carbon chemistry in the Brady soil is not studied well. Secondary calcium carbonates are present in the A and other horizons of the Brady soil. Previous works have suggested that Brady soil was formed in a stable landscape (Mason and Kuzila, 2000), and it had time to form because of the reduction in the deposition rate (Jacobs and Mason, 2007).

Soil samples from the buried Brady soil and overlying modern soils were collected from two different topographical sequences- erosional and burial (depositional) transects in the summer of 2016 and 2017 to account for the differences in depth of burial and increasing exposure of buried soils due to erosional processes and modern soil formation processes (Figure 1). The burial transect Brady soil samples were collected from depths of ~5.5m(A), ~3m(B), and ~1m(C), whereas the erosional transect Brady soil samples were collected from the depth of 1-1.5m(B), ~0.5m(C) and ~0.2m(D), where the letters-A, B, C, and D represent different depths within the transects (Detail sampling technique in Figure 1: B and C) where Brady soil has been located. Soils were sampled using Giddings's probe (Giddings Machine Company; Windsor, CO) in 10.2 or 8.9m sampling tubes for the burial transect and by digging pits for the erosional transect (see details in Szymanski et al., 2022, in preparation). For all the locations, the sampled depths include Modern upper (0-30cm), Modern Lower (30-60cm), and as soon as we hit the buried Brady layer, Brady upper (0-30cm) and Brady lower(30-60cm) soils were collected. All the reported values presented in figures 2 (A, B), 3, 4, 5, and 8 are the mean of the three replicates of the 6 sequential depth categories of the continuum of buried to ~5.5 m, ~3m, ~1m and eroded to ~1.5m, ~0.5m, and ~0.2m for a total of 18 sample locations identified as either burial or erosional. Soil transects, sampling locations, and different depth categories of Brady soil were selected using information from prior research (Jacobs and Mason, 2004; Marin-Spiotta et al., 2014; Mason et al., 2008). We measured bulk soil pH and electrical conductivity (EC) to understand the solubility of nutrients and measure the dissolved salts in the aqueous solution of the soil. To determine the changes in total elemental and stable isotope concentration of the bulk soil, we analyzed total organic carbon (TOC%), total nitrogen (TN%), $\delta^{13}C$, $\delta^{15}N$, and C: N, which influence the decomposition procedure. $\delta^{13}C$ can tell us the source of the carbon, and $\delta^{15}N$ will help us to understand the decomposition state of the organic matter. We used the diffuse reflectance infrared fourier transform (DRIFT-FTIR) spectroscopic technique to understand organic matter functional group-level components that might be involved in the molecular interaction with minerals or help in mineralization by the microbes in the soil. This helped us to understand the aliphatic and aromatic ratio of SOM present in these buried and modern soils. Finally, we also analyzed ^{14}C of the bulk soil to understand how old the carbon that is present in these soils, and through a time-dependent steady-state model, we analyzed the turnover time of this buried carbon.

2.2.2 Basic Physical and Chemical Soil properties

Soils were air-dried and passed through a 2 mm sieve. All the roots and other organic debris were handpicked and removed from the soil sample before analysis before airdried soils were ground using a SpexMill-8000D (SPEX SamplePrep; Metuchen, NJ) ball grinder. Bulk soil pH was measured in a 1:2 (suspension: solution) slurry in deionized water and 0.01M $CaCl_2$ (Mason and Kuzila 2000), and soil electrical conductivity (EC) was measured in a 1:1 (soil: water) (soil survey laboratory manual (1996). The modern surface moist soil color was 10YR 5/3 whereas Brady soil's moist color was reported as 10YR 3/2; the soil structure was weak subangular blocky for both modern surface and Brady soil (Szymanski, et al. 2022 in preparation); we also find a similar description in Jacobs and Mason (2004) and Mason et al. (2008). Borrows created due to bioturbation was common in Brady soils (Mason and Kuzila 2000; Mason et al., 2003), along with the presence of calcium carbonate filaments and small masses, which were confirmed by placing a small amount of diluted HCl when effervescence was detected. The average soil bulk density was 1.44 g cm-3 with a notable soil geochemistry difference among transects, and there was no evidence of weathering of the Brady soil (Szymanski,2021;

Jacobs and Mason 2007), which might relate to drier climatic condition. Rainfall mostly doesn't infiltrate Brady soil more than 2m (McDowell, 2020), which indicates a possibility that Brady soil has not changed physically or chemically and might have homogeneity in the carbon content. Smectite, vermiculite, and illite proportions were similar between Brady and modern soils, along with kaolinite.

2.2.3 Concentration and stable isotope composition of C and N

We determined total elemental and stable isotope composition to determine stoichiometric differences and the source (C3 or C4 plant) of organic matter in the buried vs. modern soil layers (Bender, 1971). Before measuring organic $\delta^{13}C$ and percent organic C of the bulk soil, we removed carbonates using acid fumigation with 12.1(M) hydrochloric acid (HCl) (Harrison et al., 2001). Stable isotope analyses were conducted at the Stable Isotope Ecosystems lab of University of California, Merced (SIELO) using a 4010-elemental analyzer (Costech) that is interfaced with a ThermoFisher Delta V Plus isotope ratio mass spectrometer (IRMS) with a Conflo IV. Reference materials used include USGS 40 L-Glutamic Acid, USGS41a L-Glutamic Acid, EA sediment, and Costech Acetanilide to normalize and correct for drift and mass linearity. Stable isotope values are expressed in delta (δ) notation

$$\delta X = \left(\frac{R_{sample}}{R_{s\,tan\,dard}} - 1\right) * 1000 \quad (2.1)$$

where, X = ^{13}C or ^{15}N, R = ratio of $^{13}C/^{12}C$ or $^{15}N/^{14}N$ and the standards used were Vienna Pee dee belemnite-limestone (V-PDB) for carbon and air for nitrogen. All samples were analyzed in duplicate. Afterward, percentage of C4 and C3 plant derived SOC was determined using a simple linear mixing (Nordt et al., 2002), as:

$$\delta^{13}C_{Soil} = (\delta^{13}C_{C4})(x) + (\delta^{13}C_{C3})(1-x) \quad (2.2)$$

where, $\delta^{13}C_{Soil}$ is the $\delta\ ^{13}C$ of the soil's organic carbon, $\delta\ ^{13}C_{C4}$ is the average $\delta^{13}C$ value of C4 plants (-13 ‰), $\delta\ ^{13}C_{C3}$ is the average value of C3 plant's $\delta\ ^{13}C$ (-27 ‰), x is the proportion of carbon from C4 plant source, (1-x) is the proportion of carbon from C3 plant source.

2.2.4 Diffuse Reflectance Infrared Fourier Transform (DRIFT) spectroscopy

We determined the bulk composition of SOM using DRIFT. Before IR spectroscopy, soil samples were oven-dried overnight at 60°C to reduce moisture that might have accumulated during sample storage. The spectra were recorded using a BrukerIFS 66v/S IR system (Ettlingen, Germany) equipped with a Praying Mantis DRIFT apparatus (Harrick Scientific Corporation, Ossining, NY) and background correction was carried out using OPUS-6.5 software. We recorded IR absorbances in the mid-IR range (400 to 4000 cm^{-1}) at a resolution of 4 cm^{-1}. In all cases, 500 scans of the sample were recorded with KBr background. We reported baseline corrected peak areas for specific regions (Table 1). The areas under each peak (between the specific endpoints) were calculated using the "approxfun" and "integrate" functions in R s in Hall et al. (2018). Primary peak assignment for this study included C-H asymmetric stretch (2898-2976), C-H symmetric stretch (2839-2870), C=O and C=C stretch of amide (1570-1710), aromatic C=C (1500-

1550) and C-O(COO) stretch (1360-1450) according to Hall et al. (2018) and Tatzber et al. (2007). Five DRIFT peak height ratios were calculated to understand the relative decomposition, transformation and reduced biological activity according to Hall et al. (2018). C-H/COO- [(2898-2976 + 2839-2870)/ 1360-1450]; C-H/C=O [(2898-2976 + 2839-2870)/ 1570-1710]; and C-H/ C=C [(2898-2976 + 2839-2870)/ 1500-1550].

2.2.5 Radiocarbon (^{14}C) analysis

Radiocarbon values of the bulk soils were measured using a Van de Graaff FN accelerator mass spectrometer (AMS) or NEC 1.0 MV Tandem Accelerator Mass Spectrometer (AMS) at the center for accelerator mass spectrometry (CAMS) at Lawrence Livermore National Laboratory (LLNL). Prior to measurement, bulk soils were acid treated with 1(M) HCl to remove the carbonates. Samples were prepared for ^{14}C measurement into a sealed-tube and combusted to CO_2 in the presence of Ag and CuO and then reduced into iron powder in the presence of H_2 (Vogel et al., 1984). Radiocarbon data are reported as per mil (‰) from a standard to fixed isotopic composition.

$$\Delta X = \left(\frac{R_{sample}}{R_{standard}} - 1\right) * 1000 \quad (2.3)$$

where, X = ^{14}C, R = ratio of $^{14}C/^{12}C$ and the standards and the standard are selected so that $D^{14}C$ is zero (F= 1.000) for atmospheric CO_2 (Trumbore, 2000). Previously measured $d^{13}C$ values has been used to mass-dependent fractionation and ^{14}C values has been reported into $D^{14}C$ notation. The radiocarbon values were finally corrected to the year of measurement for ^{14}C decay since 1950 (Stuiver and Polach, 1977). We report ^{14}C values as fraction modern values ($F^{14}C$), where:

$$F^{14}C = \left(\frac{As}{0.95AOX1}\right) \times \left(\frac{0.975}{0.981}\right) \times \left(\frac{1 + \frac{\delta^{13}C_{OX1}}{1000}}{1 + \frac{\delta^{13}C_s}{1000}}\right) \quad (2.4)$$

where A= $^{14}C/^{12}C$, S=sample, OX1= oxalic acid 1 which is the ^{14}C international standard.

We used a time dependent steady state model to determine mean residence time (Torn et al. 2002; Gaudinski et al. 2000; McFarlane et al., 2013). For our bulk soil samples, a four-pool model was used to determine the turnover times of all the four different sequential depth categories (modern upper, modern lower, Brady upper and Brady lower) using the mass balance of carbon following Torn et al. (2009).

$$F'_{SOM(t)} = \left[I * F'_{atm(t-1)} + C_{(t-1)}F'_{SOM(t-1)}(1 - k - \lambda)\right] / \left[C_{(t)}\right] \quad \text{Equation 1}$$

where $F' = (D^{14}C * 1000^{-1})-1$; I = inputs of carbon to a pool of SOM (g C m^{-2} y^{-1}); C = stock of carbon for the given SOM pool; k = decomposition rate constant for the given SOM pool per year, equal to reciprocal of turnover time; F'_{atm}= atmospheric $^{14}C_{CO2}$; F'_{SOM} = ^{14}C value of the given SOM pool; λ = radioactive decay rate of ^{14}C per year; t = year of calculation. The model assumes steady-state conditions; lag time of 1 year between atmospheric ^{14}C and new input of SOM (Gaudinski et al. 2010; McFarlane et al., 2013); and that the pool of SOM is homogenous, where every carbon has equal probability of exiting the pool, and thus the SOM in the pool is equal in ^{14}C signature (McFarlane et al., 2013).

2.2.6 Statistical Analysis

Data are presented as mean ± standard error. All statistical tests were conducted using CRAN-R (version 3.5.1; R Development Core Team, 2017). To test for significant differences in the soil physical and chemical properties, we used the Kruskal-Wallis's test with an alpha = 0.05, followed by Dunn's post-hoc test to determine pair-wise differences. To determine the variability of soil physical and chemical data due to soil-landform-transect (burial- modern, burial- Brady, erosional-modern, erosional-Brady) we combined the data of transect (burial vs erosional) with landform (modern vs Brady) where modern upper, modern lower soils were combined as modern burial or modern erosional depending on from which transect they were collected and Brady upper, Brady lower were combined into burial Brady and erosional Brady depending on the transect they were collected irrespective of depth category [A (~5.5m), B (~3m), and C (~1m) for burial sites and B (~1-1.5m), C (~0.5m) and D (~0.2m) for erosional sites]. To understand the soil layer (upper vs lower) variability - all upper modern, all lower modern, all upper Brady, and all lower Brady were combined irrespective of transect and depth categories of Brady soils and made groups of upper modern, lower modern, upper Brady, and lower Brady. Finally, to understand how different depths might be affecting the Brady soil's physical and chemical composition compared to modern soil, we combined their transect, landform, and soil layer identification along with the depth category groups.

2.3 Results

2.3.1 Soil pH and EC

The details of these data have been given in Szymanski, 2021. Soil pH increased along with depth from modern soil to Brady soil at all depths. The pH for modern upper soil in the burial transect averaged ~6.9±0.41 compared to an average of ~7.41±0.11 in the modern upper soil layer at the erosional transect (Fig. 2 A). In the burial transect, soil pH was significantly higher in the Brady soil, but in the erosional transect, modern and Brady soil pH has no significant difference (Fig. 2 C). We found significant differences in soil pH among the groups modern upper with Brady upper and lower ($p < 0.001$) and modern lower with upper Brady ($p = 0.003$) lower Brady ($p = 0.002$) (Table.2). Across both eroding and depositional transects, we found statistically significant differences in pH with depth and for corresponding modern and buried soil layers ($p < 0.05$) which is reported in Table 2. Similarly, the EC value increased along with the depth for the burial transect (Fig. 2 B) and ranged from 176 to 590 mS/cm in both burial and erosional transect; we found statistically significant differences when comparing eroding with depositional transects where burial Brady soil has significantly higher EC values compared to the other soils (Fig2. D), and there was also a significant difference in EC at different soils layers (Table 2).

2.3.2 Carbon and Nitrogen

Modern soil layers in both the eroding and depositional transects had a higher concentration of organic carbon and nitrogen compared to the Brady soil layers. Organic carbon concentration ranged from 1.2% to 0.4% for the modern soils and 0.71% to 0.34% in the Brady soils. With depth, we observed a sharp decline in carbon concentrations in the burial transect but not in the eroding transect (Figure 3 C). Brady soil in the erosional transect, which was located at shallower depths of up to 1.5 m, had a higher concentration

of C compared to the Brady soil located along the burial transect, which was found below 1.5 m depth. There was no significant difference in TOC% in Brady and modern soils present in the erosional transect (Fig. 6 C). Total N (TN%) concentration followed a very similar pattern to organic carbon, where there was large variability in soil TN% concentration in topsoil layers. Still, the variability was reduced, and soil total N concentration dropped significantly with depth (Figure 3 D). Modern soils have significantly higher TN% compared to the Brady soils in both burial and erosional transects (Fig. 6 D). The C: N ratios were uniformly low, ranging from 7.5 to 12 (Figure 5 A). In erosional transects, Brady soil had a higher C: N ratio (Fig. 7 C) than the modern soils suggesting that the historic sources of SOM in the buried layers had a higher C: N ratio or more likely because burial of C in the Brady soil limits the extent of decomposition induced transformation of SOM composition in deep soil layers. The observed differences were also statistically significant between the groups modern lower to Brady upper ($p = <0.001$) and between Brady upper-modern upper ($p = 0.01$) at the soil layers (Table 2).

2.3.3 Stable isotope compositions

Landform (also mentioned as transect) had a significant effect on the $\delta^{13}C$ values of soils collected from Brady and modern soil layers. The $\delta^{13}C$ values for Brady soil at eroding and depositional transect were more depleted than those measured from modern soil layers (Figure 3. A). But there was no statistically significant difference in $\delta^{13}C$ among erosional modern, erosional Brady, and burial Brady soils (Figure 6. A). At different soil layers, $\delta^{13}C$ values were significantly different between the groups Brady lower- modern lower and Brady lower- modern upper ($p<0.001$) (Table 2). The stable isotope composition of nitrogen values showed different patterns at the burial vs. eroding transects, where the deeper Brady soils in the burial transect consistently had lower $\delta^{15}N$ values compared to the modern layer, but the opposite was true at the erosional transect (Figure 3. B). Modern soil's $\delta^{15}N$ values were significantly different from the Brady soils in both erosional and burial transect (Fig. 6 B). The $\delta^{13}C$ of all the soils we analyzed ranged from -21 ‰ to -17 ‰, suggesting mixed C3 and C4 plant sources for soil organic matter (Figure 4). Burial transect modern soil is mostly characterized by C4 plant-derived SOC. In contrast, Brady soil is characterized by a mixture of C3 and C4 plant-derived SOC reflecting the vegetation shift from C3 to C4 plants that occurred during the formation of the Brady soil (Marin-spiotta et al., 2014). We found that burial modern soil has an average of 73% C4-plant derived SOC and 27% of C3-plant derived SOC, whereas Brady soil has an average of 52% C4 and 48% of C3 plant-derived SOC. C3 plant-derived SOC (~48%) was highest in the burial transect Brady soil layer (Figure 4). We observed a statistically significant low C3 plant source of SOC in the burial transect modern soil (fig. 7 A) and significantly high C4 derived SOC in the modern soil (Fig. 7 B) of the same transect suggesting either topsoil removal or incorporation of newer SOC into the Brady soil in the erosional transect due to the shallower depth as the C4 plant roots reach the shallow depth and bring newer SOC into these soils. Among the soil layers, Brady lower-modern lower and Brady lower-modern upper, C3, and C4 derived SOC was also significantly different (Table 2).

2.3.4 Composition of soil organic matter

Baseline corrected DRIFT peak areas under the C-H and C=C regions differed significantly by landform for both the Brady and modern soils (Figure 7. D). We observed no significant differences in the abundance of simple plant-derived SOM functional group (C-H) across all transects, except between the groups' burial Brady-

burial modern (p=0.03) due to landform (transect) variability and among the groups' Brady lower- modern upper (p=0.01) and modern lower- modern upper (p=0.01) due to soil layer variability, suggesting common modern composition of plant-derived SOM in the modern soil layers (Table.2). We found that the abundance of the more complex plant-derived organic matter (C=C) was only significantly different between the groups' burial Brady- burial modern (p=0.03), burial modern- erosional Brady (p=0.003) due to the difference in transect and between groups Brady upper- modern upper (p=0.008) due to the variability in soil layers (Table. 2). The abundance of the microbially derived organic matter (C = O) increased with depth compared to the aliphatic (C-H) compound. We used a ratio of peak areas under simple plant-derived SOM and complex plant-derived SOM (C-H: C=C) to infer the extent of SOM transformation that occurs with exposure of buried SOM with erosion. As the depth of the exposure decreases with erosion, the C-H: C=C ratio decreases to the point where there is no statistically significant difference when comparing the Brady layer in the erosional transect with the modern soil layers in erosional and transect (Figure 7.D; Table. 2). The amount of potentially labile, simple plant-derived aliphatic (C-H) SOM was highest in the modern layers across the erosional transect and plant-derived complex aromatic compound (C=C) increased with the depth ((Figure 5. B; Figure 7.D).

2.3.5 Radiocarbon concentrations

We used radiocarbon concentrations in the soil to infer the mean residence times of SOC in the buried vs. modern layers and the impact that erosional exposure of SOM in buried soils has on its stability. The SOC in the Brady soil at both the burial and erosional transects is consistently older (i.e., has lower Fraction Modern (FM) values) than SOC in modern layers indicating retention of old carbon and/or dilution of modern SOC's radiocarbon signature by the input of new photosynthate (Figure 5 C). The FM of SOC in the Brady soil was older with depth. We found a significant difference in the FM values among the groups' burial Brady- burial modern ($p<0.001$) and burial Brady- erosional modern (p=0.009), but no significant difference between the group's erosional modern-erosional Brady (Table 2) provides evidence for the vulnerability of buried SOC with erosional exposure to near-surface environments in the erosional transect, where we found higher FM values compared to the Brady soil in the erosional transect compared to the burial transect.

The bulk SOC turnover time calculated using equation 5 showed significant differences between the modern and Brady soil layers. The turnover time of SOC in the modern soil layers ranged from 415 years to a maximum of 2000yrs, while the turnover time of SOC in the buried Brady soil layers was up to an order of magnitude higher (Fig. 8 A). Across both the erosional and burial transects, we noticed a consistent trend where exposure of the buried SOC by erosion causes a significant reduction in its stability (i.e., turnover time). Where the turnover time of SOC in the deepest Brady soil layer at 5.5 m was more than 23,000years compared to 5000 years in the shallowest Brady soil located at 0.2 m, below the soil surface, indicating less stabilization of the SOC in the erosional transect.

2.4 Discussion

Determining the composition and stability of SOM stored in buried soil layers and its susceptibility to loss under changing environmental conditions is critical for our ability to infer the contribution of C buried in paleosols to the contemporary and future cycling of carbon in the terrestrial ecosystem. Results from this study demonstrate that there is no

significant difference in the amount of C stored in the erosional transect Brady soils to the amount of C stored in erosional transect modern soils that they underlie. And important differences in not just composition but also the persistence of SOM are observed when the buried soil layers get exposed to near-surface environmental conditions by soil erosion. More alkaline pH value of the Brady soil indicates the presence of base cations which can help in organo-mineral association and strong aggregate formation that can ultimately help in SOC stabilization and can store easily decomposable labile SOM.

2.4.1 Differences in SOM composition between buried and modern soil layers

The nature and composition of SOM are a function of the type of biomass the SOM is derived from and decomposition-related transformations that occur after the OM enters the soil system. In our study site, we observed a decrease in bulk soil TOC (%) with depth in burial and erosional transects (Fig. 3 C). But, when comparing Brady soil layers buried at different depths, we observed no significant increase in TOC with erosional exposure of the buried layer (i.e., for more shallow depths) (Figure 3. C). The soil TN (%) showed a similar trend of TOC for the decrease with depth, but erosional transects Brady soil had higher N concentration compared to the burial transect Brady soil suggesting either higher input or retention of soil N in the shallower Brady and modern soils, compared to deeply buried Brady soil layers (Figure 3. D) confirming that geomorphology of the landscape and erosional redistribution of organic matter rich topsoils can have important implications for biogeochemical cycling of the essential elements (Berhe et al., 2018). Enrichment of soil $\delta^{15}N$ can result from several factors such as NH_4^- adsorption on a clay surface, plant root NO_3^- efflux, N loss through gas, soil trophic interaction, and $\delta^{15}N$ fractionation during mineralization in addition to decomposition. Low $\delta^{15}N$ content of illuvial N and NO_3^- immobilization below the plant rooting zone can also produce lower $\delta^{15}N$ values of bulk soils in the sub-soil horizon (Nadelhoffer and Fry, 1994). Lower C: N ratio of modern SOM in the Brady soil layers at both eroding and burial transects, compared to modern SOM, suggests that OM near the soil surface experiences more decomposition-induced transformation of SOM composition compared to SOM in buried soil layers (Figure 5 A) but low $\delta^{15}N$ values of the Brady SOM, compared to modern in the burial but not the eroding transects, suggest that exposure to near-surface conditions either a shift in the $\delta^{15}N$ values of the source OM in the eroding transect and/or incorporation of newer and relatively less transformed SOM (depleted $d^{15}N$ values) (Berhe and Torn, 2017; Perakis et al. 2015, Kramer et al., 2003).

Our findings demonstrate that the plant source of SOM (Fig. 4) gets more mixed with the proximity of the analyzed soil depths to the near-surface environment. Generally, in well-aerated environments where C3 is the dominant vegetation, $\delta^{13}C$ values of the SOC generally range from -20‰ to -37‰, compared to environments dominated by C4 plants where $\delta^{13}C$ values of the SOC range from -16‰ to -19‰ (Nordet, et al., 2002). Increase in $\delta^{13}C$ values of SOC along with depth is associated with- preferential preservation, microbial decomposition, plant species variation, relocation of old organic carbon, and change in plant water use (Nadelhoffer and Fry, 1988; Balesdent et al., 1993; Connin et al., 2001). Taken together, the findings of less enriched $\delta^{15}N$ values in the Brady soil likely suggest the presence of less decomposed, either old or newly stored SOM in the buried soils. At the same time, the depletion in the $\delta^{13}C$ and $\delta^{15}N$values in the Brady soil

(upper to lower layer) can be also explained due to the new leachate OM accumulation either from the plant root or bioturbation (Hobbie & Ouimette, 2009).

We found that deep Brady soil OM is dominantly derived from C3 vegetation, but SOM from more shallow depths of both modern soils and Brady soils indicates a mixing of C3 and C4 sources in SOM (Figure 4). This is consistent with the results from previous studies from the same area that documented a vegetation shift (from C3 to C4) during the time of the Brady soil's formation (Marin-Spiotta et al., 2014; Woodburn et al., 2017). Currently, vegetation at the study site is a mixture of C3 and C4 along with the warming and drying conditions that the area experienced during the late Pleistocene to the early Holocene (Jacobs and Mason, 2004; Johnson and Willey, 2000; Mason et al., 2008). Brady soil was formed during the late Pleistocene when summer precipitation was low due to -low subtropical airflow, warmer environment, increased seasonality, and high summer temperature that favored C3 plants to dominate the area (Cordova et al., 2011). Another study (Marin-Spiotta et al., 2014) also found a high concentration of charred or pyrogenic matter in SOM of the Brady soil, which they linked to the C4 grasses that dominated during the warmer and drier climates during the time the Brady soil formed and the accompanying high degree of wind erosion and loess deposition in the study area. Our stable isotope results showed that where C3 vegetation was replaced by C4 vegetation showed 4-15% of C4 carbon enrichment at 50-100cm deep of the soil layer after 30 years, indicating a low turnover of subsoil carbon (Collins et al., 1999). On average, 47% and 59% of C4 plant-derived SOC were found in burial and erosional Brady lower soil layers, respectively, while we found up to 60% of C4 plant-derived SOC in the shallowest Brady soil at the erosional transect (~0.2m) suggesting that most of the SOC we measured is derived from the current perennial grasses. During soil sampling, we also noticed visible burrows in the soil profiles suggesting physical mixing of modern and Brady soil layers (Woodburn et al., 2017), which likely explains the presence of a higher proportion of C4 plant-derived SOC in the Brady soil. Incorporating new, presumably labile SOC into the Brady layers can have important implications for the fate of the previously buried SOC, as the new SOC can prime old SOC and render it more vulnerable to loss (Guenet et al., 2012).

We used DRIFT-FTIR to detect the presence of distinct SOM functional groups due to inherent differences based on the source of the SOM and/or differential processing of SOM during decomposition and other abiotic transformations (ex. photooxidation) (Kaiser et al., 2005; Leue et al., 2010; Kögel-Knabner, 1997; Tatzber et al., 2007). As discussed in Hall et al. (2018), the relative abundance of aliphatic to aromatic functional groups (C-H: C=C ratio) generally decreases with increasing decomposition along with the soil depth. Ratios of C=C/C=O (1500-1550/ 1570-1710) and C=C/COO (1500-1550/ 1360-1450) are used as indexes for the increased transformation of SOM (i.e, relative accumulation of oxygen-containing functional groups) during decomposition (Chefetz et al., 1998; Ding et al., 2002). Our soil's C=C/COO and C=C/C=O ratio indicated that oxygen-containing groups increased as we went from modern upper to Brady lower soils for all transects and depth except erosional D (~0.2m). This indicates the presence of less microbially decomposed compounds in the erosional transect shallowest Brady soils. Further, the relative decrease in C-H groups compared to other peak areas (C=O, C=C, COO) suggests more decomposed SOM (Ryals et al., 2014; Fissore et al., 2017), thus suggesting that accumulated SOM is considerably altered by microbial decomposition. Previously, in the same study system, Marin-Spiotta et al. (2014) found less polysaccharide and lignin compared to aliphatic carbon, which suggests an alteration in plant OM and protection of C by soil minerals in the subsoil.

2.4.2 Effect of erosional exposure of the formerly buried soil layers on its composition and persistence

The fraction modern ($F^{14}C$) values of SOC in the shallow, modern soil layers were all near 1, indicating the presence of newer, actively cycling SOC in the topsoil layers, compared to SOC in the Brady soil layers that were considerably older and slower cycling (up to 23,000 yrs turnover rate (Figure 8 B). The turnover time for SOC in modern soils ranged from 415 (±128) to 2034 (±1048) years. In both erosional and burial transects, the turnover time increased with depth reaching maximum of 15723 (±893.68) yrs in the eroding transect and 23217 (±758.08) yrs in the burial transect. The turnover time of SOM in the modern upper soil layer in the burial transect (0-30cm) was 384.34 years shorter than that of the modern upper layer (0-30cm) in the erosional transect, suggesting that the topsoil layer in the erosional transect has eroded out exposing the old SOM that was in deeper soil layers. Berhe et al. (2012) study at Tennessee valley, in an annual grassland watershed also found that SOM protection is more effective in the lowest lying poorly drained landform compared to the well-drained upper shoulder landform.

SOC turnover time for all the Brady soil present in both the burial and erosional transects is long due to moisture limitation in that depth of the soil and a higher proportion of fine soil particles (Szymanski et al., 2022 in preparation). Previous studies in the same area showed that the Brady soil has more silt and clay content compared to the overlying modern soils. In contrast, clay content was highest at burial Brady A (~5.5m) depth (Szymanski, 2021). Our turnover time data shows that this same layer with the highest silt and clay content also had the highest turnover time of SOM (~23,000 years) compared to even the other Brady soils located in shallower soil depths (Szymanski, 2021). As the clay and silt content decreases along with increasing exposure of the Brady soils (Szymanski, 2021) at different depths and transects, the turnover time of the SOM also decreases.

Overall, our findings demonstrate that the Brady soils at the erosional transect had the youngest SOC compared to the burial transect. Brady soil contains a relatively high % SOC. Still, we saw clear evidence that SOM in the erosional transect Brady soils was younger compared to the burial transect suggesting loss of older SOC and/or incorporation of newer SOC. Further, we infer that the SOM in the Brady soils buried in shallow depths may be potentially vulnerable to lose via erosion, disruption of aggregates during wetting in near-surface environments, priming, and associated phenomenon.

2.5 Conclusion

Our results show that the buried Brady soils store more than half C compared to the modern soil layers. The composition of SOM in the Brady soil suggests that it is made up of less transformed (marked by an abundance of aliphatic functional groups) and older (i.e., stabilized) SOM compared to modern soil layers suggesting that burial is an important mechanism for SOM storage and stabilization. However, we also found evidence demonstrating that exposure of the buried soil layers to near-surface environmental conditions by soil erosion is rendering the previously stabilized SOM vulnerable to lose. More alkaline pH value of the Brady soil indicates the presence of base cations which can help in organo-mineral association and strong aggregate formation, which can help in SOC stabilization and can store easily decomposable labile

SOM. $\delta^{13}C$ data indicated the dominance of C4 vegetation-derived SOM in both burial and erosional transect. Isotopic mass balance data indicated Burial Brady soil has the highest percentage of C3 plant-derived SOM and is significantly different from all other soil groups. Burial transect Brady soil showed a depleted trend in $\delta^{13}C$ values as we went from upper Brady to lower Brady at all the depth categories. This may be explained either by the accumulation of ^{13}C depleted charred material or by the presence of Ca and kaolinite that can increase the stability of the aggregate by providing physical and chemical protection where labile organic matter can persist longer. More alkaline pH value of the Brady soil indicates the presence of base cations which can help in organo-mineral association and strong aggregate formation, which can help in SOC stabilization and can store easily decomposable labile SOM. Bulk soil's $\delta^{13}C$ data indicate the dominance of C4 vegetation-derived SOM in burial and erosional transects. Isotopic mass balance data indicated that Burial Brady soil has the highest percentage of C3 plant-derived SOM and is significantly different from all other soil groups. Burial transect Brady soil showed a depleted trend in $\delta^{13}C$ values as we went from upper Brady to lower Brady at all the depth categories. This may be explained either by the accumulation of ^{13}C depleted charred material or by the presence of Ca and kaolinite that can increase the stability of the aggregate by providing physical and chemical protection where labile organic matter can persist longer. Another reason can be the vegetation shift from C3 to C4 plants during Brady soil formation. The majority of the Brady soils were enriched in low C: N values depleted $\delta^{13}C$ and $\delta^{15}N$ values which indicate less decomposed SOM which might be present at that depth due to mineral-organic matter association. Burial transect modern soil has the shortest turnover time as projected by the $F^{14}C$ values near 1. Although it is uncommon to see ~415 years turnover time for modern soils, but we have to remember that the modern upper soils were sampled from 0-30cm depth which can include some previously stabilized SOC due to the unavailability of oxygen, and microbial biomass within this depth. Brady soil turnover time decreased as we moved from deeper to shallower depth in both burial and erosional transect. This might indicate that there is a difference in SOM stabilization mechanism in burial vs erosional modern soils.

2.6 Reference

Alcantara, V., Don, A., Vesterdal, L., Well, R., and Nieder, R. (2017). Stability of Buried Carbon in Deep-Ploughed Forest and Cropland Soils- Implications for Carbon Stock. Scientific Reports, July 14, 2017. 7: 5511, DOI:10.1038/s41598-017-05501-y.

Balesdent, J., Girardin, C., and Mariotti, A. (1993). Site-Related $d^{13}C$ of Tree Leaves and Soil Organic Matter in a Temperate Forest. Ecology, 74(6), 1713-1721.

Bender, M. M. (1971). Variations in the 13C/12C ratios of plants in relation to the pathway of photosynthetic carbon dioxide fixation. Phytochemistry, 10(6), 1239-1244.

Berhe, A. A., Harte, J., Harden, J. W., and Torn, M. S. (2007). The significance of the erosion-induced terrestrial carbon sink. Bioscience, 57, 337-346, https://doi.org/10.1641/B570408

Berhe, A. A., Harden, J. W., Torn, M. S., Kleber, M., Burton, S. D., and Harte, J. (2012). Persistence of soil organic matter in eroding versus depositional landform positions. J. Geophys. Res., 117, G02019, doi:10.1029/2011JG001790.

Berhe, A. A., and Torn, M. S. (2017). Erosional redistribution of topsoil controls soil nitrogen dynamics. Biogeochemistry, 132(1), 37-54.

Berhe, A. A., Barnes, R. T., Six, J., and Marin-Spiotta, E. (2018). Role of soil erosion in biogeochemical cycling of essential elements: carbon, nitrogen, and phosphorus. Annu. Rev. Earth Planet. Sci, 46(1), 521-548.

Bellamy, P. H., Loveland, P. I., Bradley, I. R., Lark, M. R., and Kirk, G. J. D. (2005). Carbon losses from all soils across England and Wales 1978-2003. Nature, 437, 245-248.

Chaopricha, N. T., and Marin-Spiotta, E. (2014). Soil Burial Contributes to Deep Soil Organic Carbon Storage. Soil Biology and Biogeochemistry, 56, 251-264, https://doi.org/10.1016/j.soilbio.2013.11.011.

Chefetz, B., Chen, Y., Hadar, Y., and Hatcher, P. G. (1998). Characterization of dissolved organic matter extracted from composted municipal solid waste. Soil Science Society of America Journal, 62(2), 326-332.

Collins, H. P., Christenson, D. R., Blevins, R. L., Bundy, L. G., Dick, W. A., Huggins, D. R., and Paul, E. A. (1999). Soil carbon dynamics in corn-based agroecosystems: Results from carbon-13 natural abundance. Soil Science Society of America Journal, 63(3), 584-591.

Connin, S. L., Feng, X., and Virginia, R. A. (2001). Isotopic discrimination during long-term decomposition in an arid land ecosystem. Soil Biology and Biochemistry, 33(1), 41-51.

Cordova, C. E., Johnson, W. C., Mandel, R. D., and Palmer, M. W. (2011). Late Quaternary environmental change inferred from phytoliths and other soil-related proxies: case studies from the central and southern Great Plains, USA. Catena, 85(2), 87-108.

D'Elia, A. H., Liles, G. C., Viers, J. H., and Smart, D. R. (2017). Deep carbon storage potential of buried floodplain soils. Scientific reports, 7(1), 1-7.

Ding, G., Novak, J. M., Amarasiriwardena, D., Hunt, P. G., and Xing, B. (2002). Soil organic matter characteristics as affected by tillage management. Soil Science Society of America Journal, 66(2), 421-429.

Gao, X., Huang, R., Li, J., Wang, C., Lan, T., Li, Q., Deng, O., Tao, Q., and Zeng, M. (2020). Temperature induces soil organic carbon mineralization in urban park green spaces, Chengdu, southwestern China: Effects of planting years and vegetation types. Urban Forestry & Urban Greening, 54, 126761.

Guenet, B., Juarez, S., Bardoux, G., Abbadie, L., and Chenu, C. (2012). Evidence that stable C is as vulnerable to priming effect as is more labile C in soil. Soil Biology and Biochemistry, 52, 43-48.

Effects of planting years and vegetation types. Urban Forestry & Urban Greening,54, 2020, 126761, ISSN 1618-8667, https://doi.org/10.1016/j.ufug.2020.126761.

Fissore, C., Dalzell, B. J., Berhe, A. A., Voegtle, M., Evans, M., and Wu, A. (2017). Influence of topography on soil organic carbon dynamics in a Southern California grassland. Catena, 149, 140-149.

Gaudinski, J. B., Trumbore, S. E., Davidson, E. A., and Zheng, S. (2000). Soil carbon cycling in a temperate forest: radiocarbon-based estimates of residence times, sequestration rates and partitioning of fluxes. Biogeochemistry, 51(1), 33-69.

Gaudinski, J. B., Torn, M. S., Riley, W. J., Dawson, T. E., Joslin, J. D., and Majdi, H. (2010). Measuring and modeling the spectrum of fine-root turnover times in three forests using isotopes, minirhizotrons, and the Radix model. Global Biogeochemical Cycles, 24(3).

Hall, S. J., Berhe, A. A., and Thompson, A. (2018). Order from disorder: do soil organic matter composition and turnover co-vary with iron phase crystallinity?. Biogeochemistry, 140(1), 93-110.

Hobbie, E. A., and Ouimette, A. P. (2009). Controls of nitrogen isotope patterns in soil profiles. Biogeochemistry, 95(2), 355-371.

Hoffmann, T., Schlummer, M., Verstraeten, G., and Notebaert, B. (2013). Significance of sediment and carbon storage on hillslopes and floodplains. Global Biogeochem. Cy, 27, 22013.

Jacobs, P. M., and Mason, J. A. (2004). Pedology of soils in thick Holocene loess, Nebraska, USA, Revista Mexicana de Ciencias Geológicas, 21(1), 54-70

Jacobs, P.M. and Mason, J.A. (2007). Late Quaternary climate change, loess sedimentation, and soil profile development in the central Great Plains: A pedosedimentary model. Geological Society of merica Bulletin 119:462. doi: 10.1130/B25868.1

Jiang, L., Ma, X., Song, Y., Gao, S., Ren, J., Zhang, H., and Wang, X. (2022). Warming-induced labile carbon change soil organic carbon mineralization and microbial abundance in a northern peatland. Microorganisms, 10(7), 1329. https://doi.org/10.3390/microorganisms10071329

Jickells, T. D., An, Z.S., Andersen, K. K., Baker, A.R., Bergametti, G., Brooks, N., Cao, J. J., Boyd, P.W., Duce, R. A., Hunter, K. A., Kawahata, H., Kubilay, N., laRoche, J., Liss, P. S., Mahowald, Prospero, J. M., Ridgwell, A. J., Tegen, L., and Torres, R. (2005). Global iron connections between desert dust, ocean biogeochemistry, and climate. Science, 308 (5718)

Jobbagy, E. G., and R. B. Jackson (2000), The vertical distribution of soil organic carbon and its relation to climate and vegetation. Ecological Applications,10(2),423–436, https://doi.org/10.1890/1051-0761(2000)010[0423:TVDOSO]2.0.CO;2

Johnson, D. L. 1998. Paleosols are buried soils. Quaternary international, 51,52:7

Johnson, W.C., and Willey, K.L. (2000). Isotopic and rock magnetic expression of environmental changes at the Pleistocene-Holocene transition in the central Great Plains. Quaternary International, 67,89-106.

Johnson, W. C., Willey, K. L., Mason, J. A., and May, D. W. (2007). Stratigraphy and environmental reconstruction at the middle Wisconsinan Gilman Canyon formation type locality, Buzzard's Roost, southwestern Nebraska, USA. Quaternary Research, 67(3), 474-486.

Kaiser, M., R. H. Ellerbrock and H. H. Gerke (2005), Cation exchange capacity and composition of soluble soil organic matter fractions, Soil science society of America journal, 72:1278-1285

Kramer, M. G., Sollins, P., Sletten, R. S., and Swart, P. K. (2003). N isotope fractionation and measures of organic matter alteration during decomposition. Ecology, 84(8), 2021-2025.

Kögel-Knabner, I. (1997). 13C and 15N NMR spectroscopy as a tool in soil organic matter studies. Geoderma, 80(3-4), 243-270.

Lal, R., Iivari, T., & Kimble, J. M. (2003). Soil degradation in the United States: extent, severity, and trends. CRC Press.

Lal, R. (2008). Carbon sequestration. Philosophical Transactions of the Royal Society B: Biological Sciences, 363(1492), 815-830.

Leopold, M., Völkel, J., Dethier, D., Huber, J., and Steffens, M. (2011). Characteristics of a paleosol and its implication for the Critical Zone development, Rocky Mountain Front Range of Colorado, USA. Applied Geochemistry, 26, S72-S75.

Leue, M., Ellerbrock, R. H., and Gerke, H. H. (2010). DRIFT mapping of organic matter composition at intact soil aggregate surfaces. Vadose Zone Journal, 9(2), 317-324.

Le Quéré, C., R. M. Andrew, P. Friedlingstein, S. Sitch, J. Hauck, J. Pongratz, P. A. Pickers, J. I. Korsbakken, G. P. Peters, J. G. Canadell, A. Arneth, V. K. Arora, L. Barbero, A. Bastos, L. Bopp, F. Chevallier, L. P. Chini, P. Ciais, S. C. Doney, T. Gkritzalis, D. S. Goll, I. Harris, V. Haverd, F. M. Hoffman, M. Hoppema, R. A. Houghton, G. Hurtt, T. Ilyina, A. K. Jain, T. Johannessen, C. D. Jones, E. Kato, R. F. Keeling, K. K. Goldewijk, P. Landschützer, N. Lefèvre, S. Lienert, Z. Liu, D. Lombardozzi, N. Metzl, D. R. Munro, J. E. M. S. Nabel, S. Nakaoka, C. Neill, A. Olsen, T. Ono, P. Patra, A. Peregon, W. Peters, P. Peylin, B. Pfeil, D. Pierrot, B. Poulter, G. Rehder, L. Resplandy, E. Robertson, M. Rocher, C. Rödenbeck, U. Schuster, J. Schwinger, R. Séférian, I. Skjelvan, T. Steinhoff, A. Sutton, P. P. Tans, H. Tian, B. Tilbrook, F. N. Tubiello, I. T. van der Laan-Luijkx, G. R. van der Werf, N. Viovy, A. P. Walker, A. J. Wiltshire, R. Wright, S. Zaehle, and B. Zheng (2018).

Global Carbon Budget 2018, Earth Syst. Sci. Data, 10, 2141–2194, https://doi.org/10.5194/essd-10-2141-2018.

Mason, J.A., and Kuzila, M.S. (2000). Episodic Holocene loess deposition in central Nebraska. Quaternary International ,67:119–131.

Mason, J. A., Jacobs, P. M., Greene, R. S., and Nettleton, W. D. (2003). Sedimentary aggregates in the Peoria Loess of Nebraska, USA. Catena, 53(4), 377-397.

Mason, J. A., Miao, X., Hanson, P. R., Johnson, W. C., Jacobs, P. M., and Goble, R. J. (2008). Loess record of the Pleistocene–Holocene transition on the northern and central Great Plains, USA. Quaternary Science Reviews, 27(17-18), 1772-1783.

Marin-Spiotta, E., Chadwick, O. A., Kramer, M., and Carbone, M. S. (2011). Carbon delivery to deep mineral horizons in Hawaiian rain forest soils. Journal of Geophysical Research: Biogeosciences, 116(G3).

Marin-Spiotta, E., Chaopricha, N. T., Plante, A. F., Diefendorf, A. F., Muller, C. W., Grandy, A. S., and Mason, J. A. (2014). Long-term stabilization of deep soil carbon by fire and burial during early Holocene climate change. Nature Geoscience, May 25, 2014. DOI: 10.1038/NGEO2169

McDowell, T. (2020). Processes controlling soil hydrology and pedogenic carbonate formation in loess tablelands, Nebraska, USA (Doctoral dissertation).

McFarlane, K. J., Torn, M. S., Hanson, P. J., Porras, R. C., Swanston, C. W., Callaham, M. A., and Guilderson, T. P. (2013). Comparison of soil organic matter dynamics at five temperate deciduous forests with physical fractionation and radiocarbon measurements. Biogeochemistry, 112(1), 457-476.

Natelhoffer, K. J., & Fry, B. (1988). Controls on natural nitrogen-15 and carbon-13 abundances in forest soil organic matter. Soil Science Society of America Journal, 52(6), 1633-1640.

Nadelhoffer K J, Fry B (1994) Nitrogen isotope studies in forest ecosystems. In: Lajtha K, Michner R (eds) Stable isotopes in ecology. Blackwell, Oxford, pp 22–44

Neff, J. C., Ballantyne, A. P., Farmer, G. L., Mahowald, N. M., Conroy, J. L., Landry, C. C., Overpeck, J. T., Painter, T. H., Lawrence, C. R., and Reynolds, R. L. (2008). Increasing eolian dust deposition in the western United States linked to human activity. Nature Geoscience, 1(3), 189-195.

Nordt, L. C., Boutton, T. W., Jacob, J. S., and Mandel, R. D. (2002). C4 plant productivity and climate-CO_2 variations in south-central Texas during the late Quaternary. Quaternary Research, 58(2), 182-188.

Perakis, S. S., Tepley, A. J., and Compton, J. E. (2015). Disturbance and topography shape nitrogen availability and δ15N over long-term forest succession. Ecosystems, 18(4), 573-588.

Rasse, D. P., Mulder, J., Moni, C., and Chenu, C. (2006). Carbon turnover kinetics with depth in a French loamy soil. Soil Science Society of America Journal, 70(6), 2097-2105.

Ryals, R., Kaiser, M., Torn, M. S., Berhe, A. A., and Silver, W. L. (2014). Impacts of organic matter amendments on carbon and nitrogen dynamics in grassland soils. Soil Biology and Biochemistry, 68, 52-61.

Reynolds, R., J. Belnap, M. Reheis, P. Lamothe, and F. Luiszer (2001), Aeolian dust in Colorado Plateau soils: nutrient inputs and recent change in source. Proc. Natl. Acad. Sci. USA 98, 7123–7127

Ruhe, R.V. (1983). Depositional environment of late Wisconsin loess in the midcontinental United States. In: Porter, S.C. (Ed.), Late-Quaternary Environments of the United States, Vol. 1, The Pleistocene. University of Minnesota Press, Minneapolis, pp. 130-137

Rumpel, C., and Kögel-Knabner, I. (2011). Deep soil organic matter—a key but poorly understood component of terrestrial C cycle. Plant Soil, 338**,** 143–158

Schmidt, M. W. I., Torn, M .S., Abiven, S., Dittmar, T., Guggenberger, G., Janssens, I. A., Kleber, M., Kogel-Knabner, I., Lehmann, D J., Manning, A. C., Nannipieri, P., Rasse, D. P., Weiner, S., and Trumbore, S. E. (2011). Persistence of soil organic matter as an ecosystem property, Nature, 478, 49-56, doi:10.1038/nature10386

Sankey, J. B., Germino, M. J., and Glenn, N. F. (2009). Aeolian sediment transport following wildfire in sagebrush steppe. Journal of Arid Environments, 73(10), 912-919.

Szymanski, L. M. (2021). Spatial distribution and long-time persistence of ancient carbon in buried soils and its vulnerability to landscape disturbance (Publication No. 28720040) [Doctoral dissertation, University of Wisconsin, Madison]. ProQuest Dissertations & Theses Global

Tabor, N. J., and Myers, T. S. (2015). Paleosols as indicators of paleoenvironment and paleoclimate. Annual Review of Earth and Planetary Sciences, 43(1), 333-361.

Tatzber, M., Stemmer, M., Spiegel, H., Katzlberger, C., Haberhauer, G., and Gerzabek, M. H. (2007). An alternative method to measure carbonate in soils by FT-IR spectroscopy. Environmental Chemistry Letters, 5(1), 9-12.

Torn, M. S., Lapenis, A. G., Timofeev, A., Fischer, M. L., Babikov, B. V., and Harden, J. W. (2002). Organic carbon and carbon isotopes in modern and 100-year-old-soil archives of the Russian steppe. Global Change Biology, 8(10), 941-953.

Torn, M. S., Swanston, C. W., Castanha, C., and Trumbore, S. E. (2009). Storage and turnover of organic matter in soil. Biophysico-chemical processes involving natural nonliving organic matter in environmental systems, 219-272.

Trumbore, S. (2000). Age of soil organic matter and soil respiration: radiocarbon constraints on belowground C dynamics. Ecological applications, 10(2), 399-411.

Vermeire, L. T., D. B.Wester, R.B. Mitchell, and S. D. Fuhlendorf (2005), Fire and grazing effects on wind erosion, soil water content, and soil temperature. J. Environ. Qual. 34, 1559–1565.

Woodburn, T., Johnson, W. C., Mason, J. A, Bozarth, S. R., and Halfen, A. F. (2017). Vegetation dynamics during the pleistocene- Holocene transition in the central great plains, USA. The Holocene, 27(1), 155-163.

Xu, W., Yuan, W., Cui, L., Ma, M., & Zhang, F. (2019). Responses of soil organic carbon decomposition to warming depend on the natural warming gradient. Geoderma, 343, 10-18.

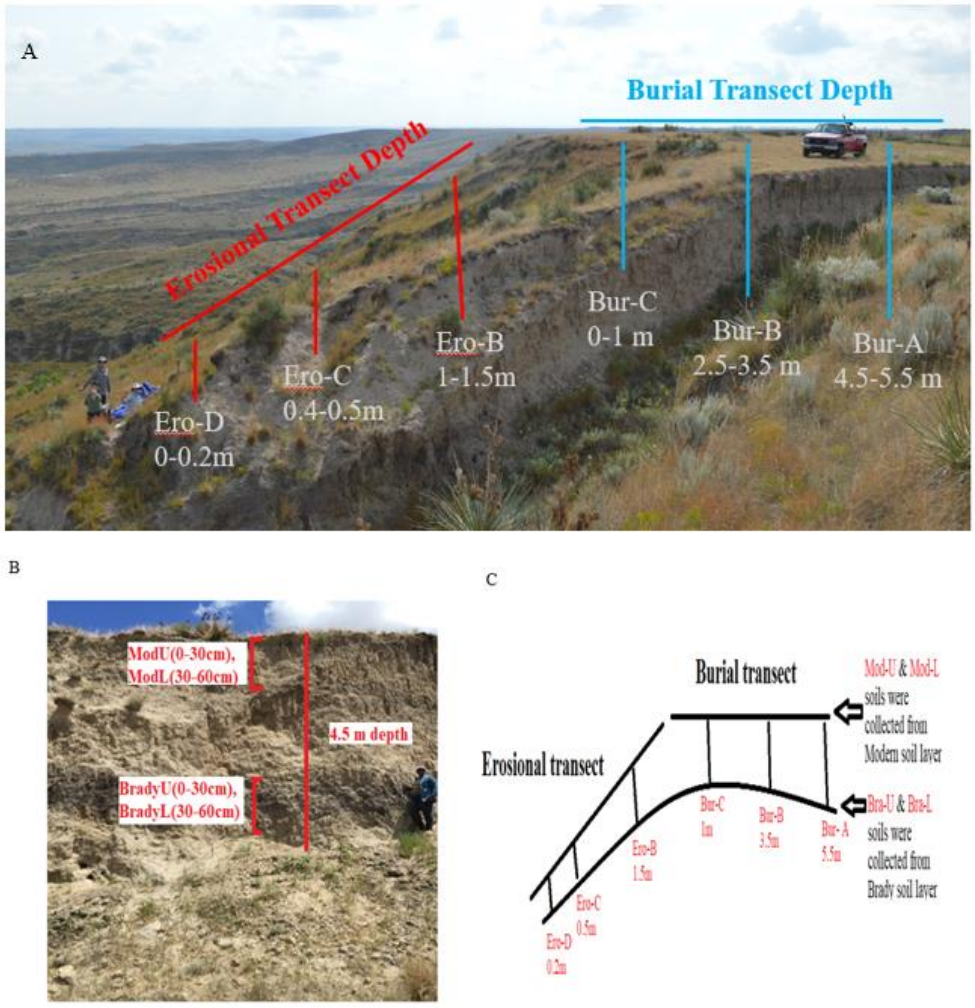

Figure 2-1 Schematic representation of sampling locations in the study system located in Nebraska. The depth of the Brady soil varies along topographic gradients, depending on whether one considers different layers of aeolian deposits the Brady soil was buried under originally (i.e., burial transect or depositional transect) vs. areas that are currently eroding (i.e., erosional). Pictures B and C is showing a detail of how the soil samples were collected from different depth categories.

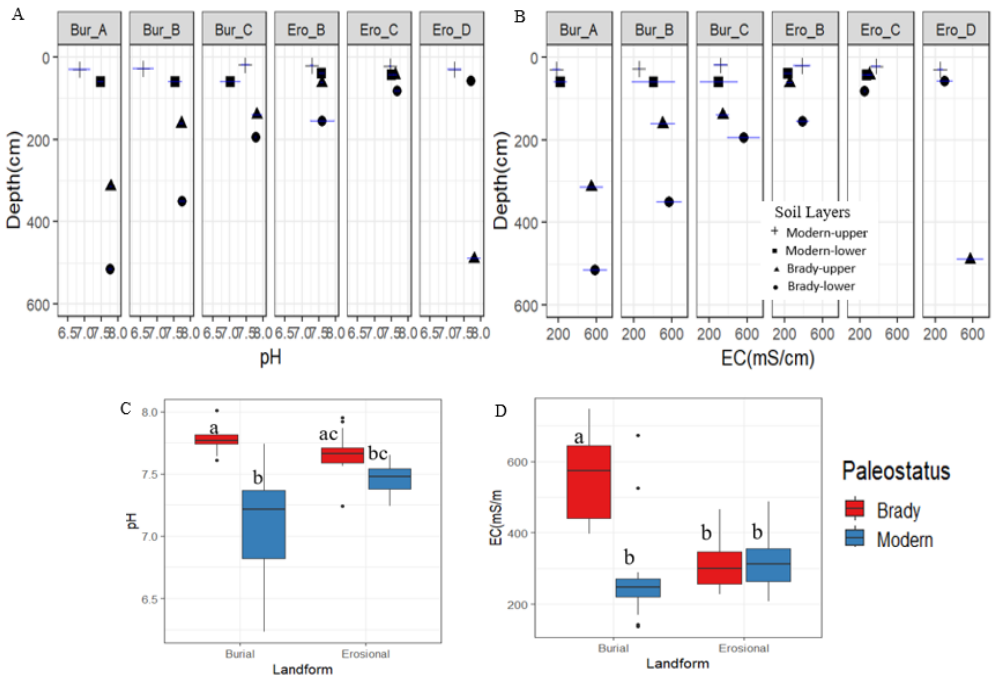

Figure 2-2 First 2 figures indicate the mean ± standard deviation of site triplicates of bulk soil pH(A) and EC (B) from burial/ depositional and erosional transect different depth categories. In our study, Brady soil was collected at Bur- A (~5.5m), Bur-B (~3m), Bur- and C (~1m) from burial/ depositional transect, and Ero-B (~1-1.5m), Ero-C (~0.5m) and Ero-D (~0.2m) from erosional transects. In the below 2 figures, Y-axis shows the values of pH (C) and EC (D), and the X-axis shows the transect from where the soil has been collected. To understand the variability of pH and EC at different soil transects, modern soils were combined depending on from which transect they have been collected, and Brady soils were combined depending on which transect they have been collected irrespective of depth category

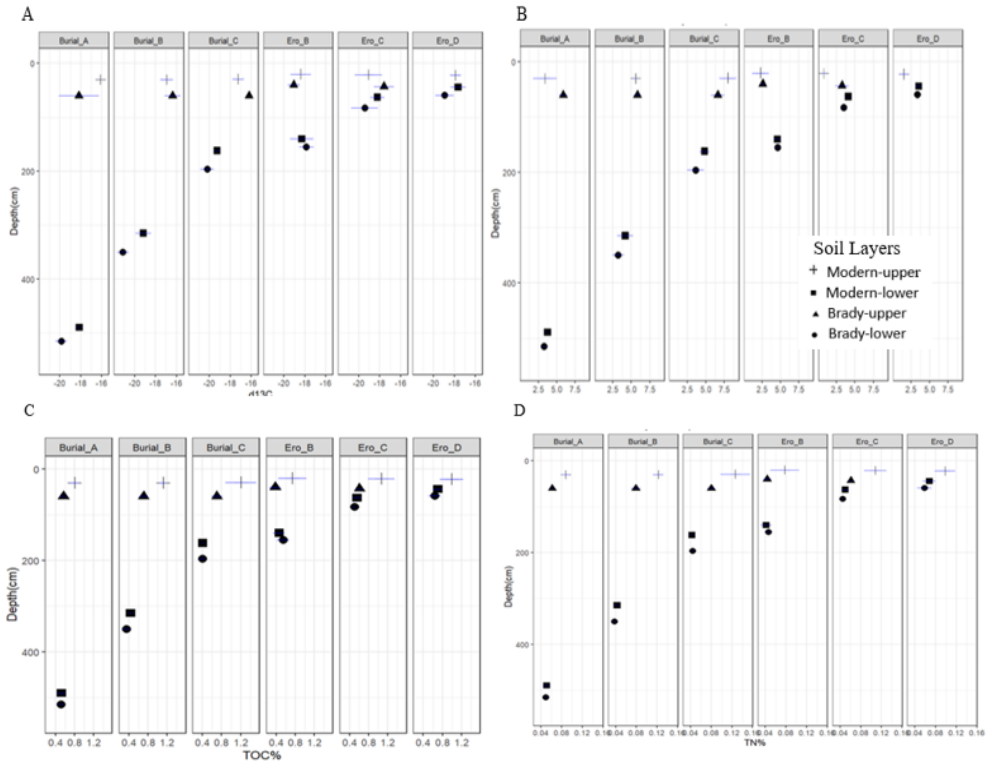

Figure 2-3 Reported figures indicate the mean ± standard deviation of site triplicates of bulk soil $\delta^{13}C$ (A), $\delta^{15}N$ (B), TOC% (C), and TN% (D) from burial/ depositional and erosional transect different depth categories. In our study, Brady soil was collected at Bur- A (~5.5m), Bur-B (~3m), Bur-and C (~1m) from burial/ depositional transect, and Ero-B (~1-1.5m), Ero-C (~0.5m) and Ero-D (~0.2m) from erosional transects.

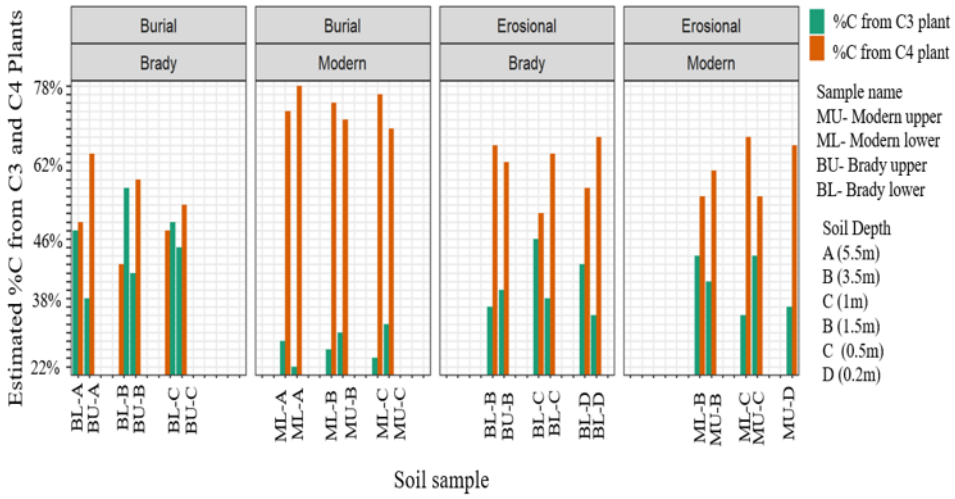

Figure 2-4 Reported Figure 4: Estimated percentage of organic carbon derived from C3 and C4 plants for each soil sample

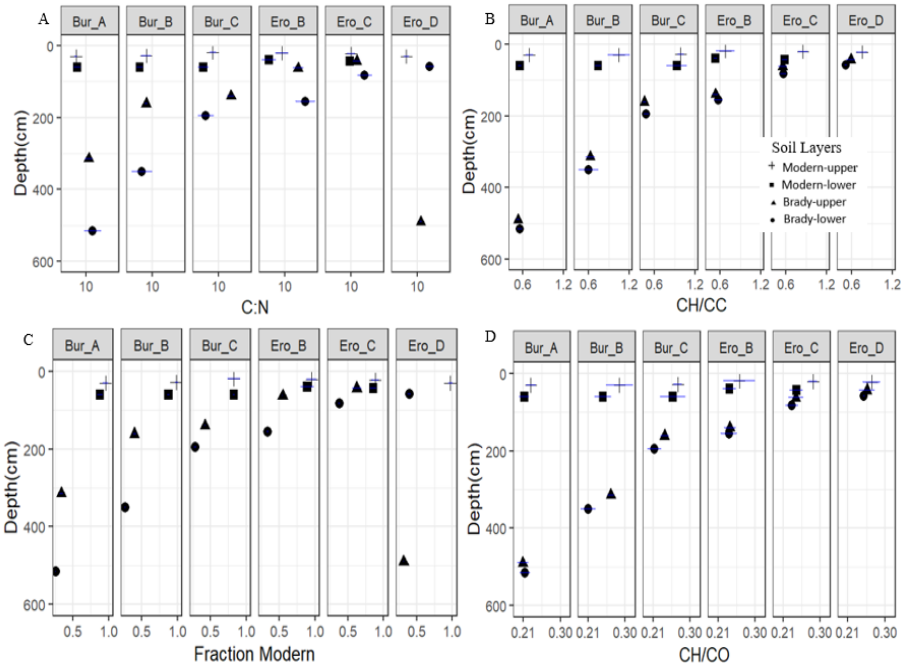

Figure 2-5 Reported figures indicate the mean ± standard deviation of site triplicates of bulk soil C:N (A), CH: CC (B), Fraction Modern (C) , and CH: CO (D) from burial/ depositional and erosional transect different depth categories. In our study, Brady soil was collected at Bur- A (~5.5m), Bur-B (~3m), Bur-and C (~1m) from burial/ depositional transect, and Ero-B (~1-1.5m), Ero-C (~0.5m) and Ero-D (~0.2m) from erosional transects.

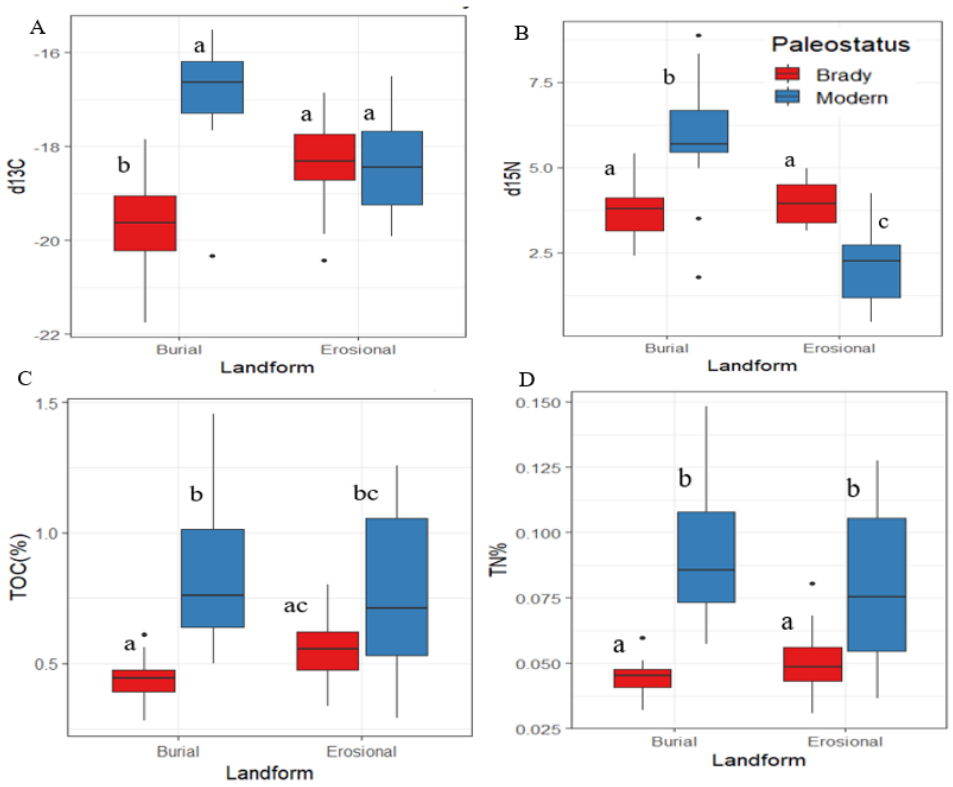

Figure 2-6 Reported these figures, Y-axis shows $\delta^{13}C$ values (A), $\delta^{15}N$ values (B), TOC% values (C), and TN% values (D) of bulk soils from burial/ depositional and erosional transect. Here, X axis are showing soil transect categories from where the soil has been collected. To understand soil-transect (burial- modern, burial- Brady, erosional-modern, erosional-Brady) variability, we combined the data of transect (burial vs erosional) with landform (modern vs Brady) where modern upper, modern lower soils were combined as modern burial or modern erosional depending on from which transect they were collected and Brady upper, Brady lower were combined into burial Brady and erosional Brady depending on the transect they were collected irrespective of depth category.

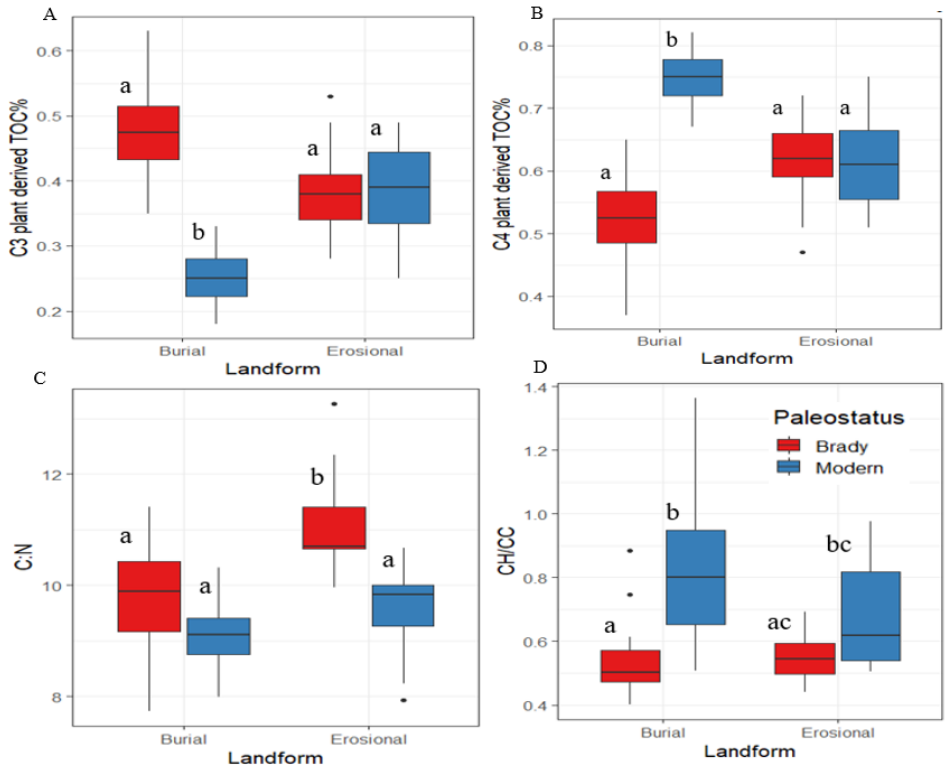

Figure 2-7 Reported these X axis showing SOM derived from C3% values (A), SOM derived from C4% values (B), C: N values (C) and aliphatic: aromatic (CH:CC) values (D) of bulk soils from burial and erosional transect. All Y axes are showing soil depth categories .To understand soil-landform-transect (burial- modern, burial- brady, erosional-modern, erosional-Brady) variability we combined the data of transect (burial vs erosional) with landform (modern vs Brady) where modern upper, modern lower soils were combined as modern burial or modern erosional depending on from which transect they were collected and Brady upper, Brady lower were combined into burial Brady and erosional Brady depending on the transect they were collected irrespective of depth category [A (~5.5m), B (~3m), and C (~1m) for burial sites and B (~1-1.5m), C (~0.5m) and D (~0.2m) for erosional sites]

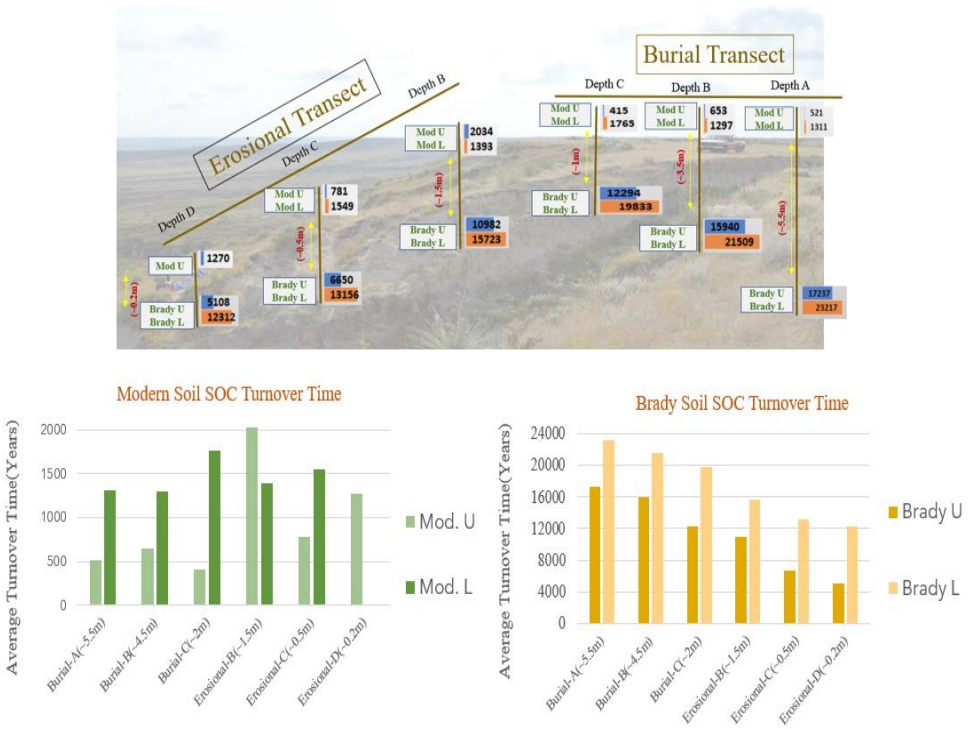

Figure 2-8 Turnover time of bulk soils found in modern and Brady soils (A). Figure (B) showing how does the turnover time change in upper soil layer to lower soils layer in modern vs Brady soils.

Table 2-1. DRIFT-FTIR peak assignment for soil SOM (Hall et al., 2018; Tatzber et al., 2007)

Compound	Wavenumber (cm^{1})	Vibration
Aliphatic	2898-2976 2839-2870	asymmetric stretch of C-H symmetric stretch of C-H
Amides, quinones, and ketones	1570-1710	C=O, C=C stretch of amides
Aromatic	1500-1550	C=C
Carboxylate	1360-1450	C-O(COO) stretch

Table 2-2. Adjusted p values of the analyzed parameters derived from the Kruskal-Wallis post-hock Dunn test. To determine the variability of soil physical and chemical data due to soil-landform-transect (burial- modern, burial- Brady, erosional-modern, erosional-Brady), we combined the data of transect (burial vs erosional) with landform (modern vs Brady) depending on the transect they were collected irrespective of different depth category of the Brady soils present in this site. For soil layer (upper vs lower) variability - all upper modern, all lower modern, all upper Brady, and all lower Brady were combined irrespective of transect and depth categories of Brady soils and made groups of upper modern, lower modern, upper Brady, and lower Brady

Landform Variability (n= 18)	pH	EC	$d^{13}C$	$d^{15}N$	%TN	%TOC	C:N	CH/CC	CH/CO	MOM	FM	C4	C3
Burial Brady-Burial Modern	<0.001	<0.001	<0.001	0.002	<0.001	<0.001	>0.1	<0.001	>0.1	0.007	<0.001	<0.001	<0.001
Burial Brady-Erosional Brady	>0.1	<0.001	0.087	n.s	n.s	>0.1	0.004	n.s	>0.1	>0.1	n.s	>0.1	>0.1
Burial Modern-Erosional Brady	<0.001	>0.1	0.005	0.015	<0.001	0.018	<0.001	0.001	n.s	>0.1	>0.1	<0.001	<0.001
Burial Brady-Erosional Modern	<0.001	<0.001	>0.1	0.02	<0.001	0.001	n.s	0.039	0.043	0.001	0.009	>0.1	>0.1
Burial Modern-Erosional Modern	n.s	>0.1	0.005	<0.001	>0.1	n.s	>0.1	>0.1	n.s	n.s	n.s	<0.001	<0.001
Erosional Brady-Erosional Modern	0.0247	n.s	n.s	0.004	0.05	>0.1	<0.001	>0.1	n.s	>0.1	>0.1	n.s	n.s
Soil-layer (n=18)													
Brady lower-Brady upper	n.s	n.s	>0.1	n.s	n.s	n.s	n.s	>0.1	n. s	n.s	0.026	>0.1	>0.1
Brady lower-Modern lower	0.002	0.049	0.0002	>0.1	0.026	>0.1	0.005	n.s	n.s	0.006	n.s	<0.001	<0.001
Brady upper-Modern lower	0.003	0.015	>0.1	n.s	>0.1	>0.1	<0.001	n.s	>0.1	0.029	>0.1	0.047	0.047

Landform Variability (n= 18)	pH	EC	$d^{13}C$	$d^{15}N$	%TN	%TOC	C:N	CH/CC	CH/CO	MOM	FM	C4	C3
Brady lower-Modern upper	<0.001	0.03	<0.001	n.s	<0.001	<0.001	0.073	0.003	>0.1	0.087	<0.001	<0.001	<0.001
Brady upper-Modern upper	<0.001	0.089	>0.1	>0.1	<0.001	<0.001	0.014	>0.1	0.008	>0.1	n.s	>0.1	>0.1
Modern lower-Modern upper	>0.1	n.s	n.s	>0.1	0.043	0.009	n.s	>0.1	n.s	n.s	0.029	n.s	n.s

Table 2-3. Soil EC, pH, TOC%, TC%, TN%, $\delta^{13}C$, $\delta^{15}N$ and TOC: N data from modern and Brady soil samples collected from three replicate transects of burial and erosional landform with decreasing depth to the Brady.

Landform	Paleostatus	SoilLayer	Depth to Brady(m)	pH	EC(dS/m)	TOC%	TC%	TN%	d13C ‰	d15N‰	C:N
Burial	Brady	L	5.5	7.8	4.6	0.53	0.66	0.05	-20.1	3.1	11.4
Burial	Brady	L	5.5	7.7	7.2	0.56	0.66	0.05	-19.3	3.7	11.1
Burial	Brady	L	5.5	7.8	5.9	0.45	0.59	0.05	-20.3	3.1	9.1
Burial	Brady	L	3.5	7.7	6.7	0.44	0.70	0.04	-20.7	2.6	10.8
Burial	Brady	L	3.5	7.7	4.2	0.30	0.37	0.04	-20.9	4.1	7.9
Burial	Brady	L	3.5	7.8	6.3	0.28	0.43	0.03	-21.8	2.9	8.7
Burial	Brady	L	1.5	7.8	7.5	0.44	0.74	0.04	-20.0	4.6	10.0
Burial	Brady	L	1.5	7.8	4.0	0.42	0.59	0.05	-19.7	3.9	9.0
Burial	Brady	L	1.5	7.8	5.5	0.32	0.61	0.04	-20.9	2.4	7.7
Eros.	Brady	L	1.5	8.0	3.5	0.43	0.63	0.04	-18.3	4.9	10.6
Eros.	Brady	L	1.5	7.6	3.6	0.68	0.77	0.05	-17.3	4.5	13.3
Eros.	Brady	L	1.5	7.2	4.7	0.53	0.69	0.05	-18.0	4.5	11.3
Eros.	Brady	L	0.5	7.7	2.4	0.48	0.74	0.04	-19.9	3.3	10.7
Eros.	Brady	L	0.5	7.6	2.6	0.52	0.59	0.04	-20.4	3.4	12.4
Eros.	Brady	L	0.5	7.8	2.6	0.49	0.68	0.05	-18.0	3.7	10.4
Eros.	Brady	L	0.2	7.7	3.6	0.56	0.82	0.05	-19.6	3.4	11.4
Eros.	Brady	L	0.2	7.7	2.4	0.73	1.11	0.07	-18.3	3.3	10.7
Burial	Brady	U	5.5	7.8	4.3	0.47	0.58	0.05	-18.3	3.6	10.2
Burial	Brady	U	5.5	7.6	7.1	0.61	0.92	0.06	-18.3	3.7	10.2
Burial	Brady	U	5.5	8.0	5.6	0.50	0.63	0.05	-17.9	4.0	10.5
Burial	Brady	U	3.5	7.8	6.0	0.48	0.63	0.05	-18.5	3.3	9.9
Burial	Brady	U	3.5	7.7	4.1	0.44	0.55	0.04	-19.9	5.4	10.9
Burial	Brady	U	3.5	7.8	6.3	0.39	0.64	0.04	-19.1	3.8	9.9
Burial	Brady	U	1.5	7.8	6.5	0.38	0.83	0.04	-19.6	5.3	9.7
Burial	Brady	U	1.5	7.8	4.0	0.40	0.79	0.04	-19.0	5.2	9.5
Burial	Brady	U	1.5	7.6	4.7	0.43	0.68	0.05	-19.2	4.1	9.3
Eros.	Brady	U	1.5	7.9	3.1	0.34	0.87	0.03	-19.6	4.1	10.9
Eros.	Brady	U	1.5	7.7	3.0	0.58	0.75	0.05	-17.7	5.0	11.5
Eros.	Brady	U	1.5	7.9	4.2	0.46	0.66	0.04	-17.6	4.7	10.7
Eros.	Brady	U	0.5	7.6	2.4	0.62	0.88	0.05	-18.7	4.2	12.0
Eros.	Brady	U	0.5	7.6	2.9	0.60	0.83	0.06	-18.5	3.9	10.7
Eros.	Brady	U	0.5	7.7	2.3	0.45	0.69	0.04	-17.5	4.2	10.7
Eros.	Brady	U	0.2	7.6	3.2	0.69	1.07	0.07	-18.3	3.1	10.4
Eros.	Brady	U	0.2	7.7	3.2	0.62	0.87	0.06	-17.7	3.9	11.1
Eros.	Brady	L	0.2	7.6	2.6	0.80	1.06	0.08	-16.9	3.6	10.0

Landform	Paleostatus	SoilLayer	Depth to Brady(m)	pH	EC(dS/m)	TOC%	TC%	TN%	d13C ‰	d15N‰	C:N
Burial	Modern	L	5.5	7.4	1.4	0.62	0.73	0.07	-16.8	5.8	9.4
Burial	Modern	L	5.5	7.5	2.4	0.60	0.81	0.06	-20.3	6.5	9.7
Burial	Modern	L	5.5	7.5	2.8	0.50	0.68	0.06	-17.4	5.4	8.7
Burial	Modern	L	3.5	7.7	6.7	0.70	0.76	0.07	-16.6	6.3	9.4
Burial	Modern	L	3.5	7.6	2.9	0.80	0.92	0.09	-15.5	5.6	9.0
Burial	Modern	L	3.5	7.3	2.6	0.61	0.67	0.07	-17.0	5.5	8.4
Burial	Modern	L	1.5	7.4	5.3	0.73	0.74	0.08	-16.2	7.2	8.6
Burial	Modern	L	1.5	6.8	1.4	0.57	0.58	0.07	-16.1	5.6	8.0
Burial	Modern	L	1.5	6.9	2.4	0.77	0.80	0.08	-16.3	7.0	9.5
Eros.	Modern	L	1.5	7.7	2.1	0.35	0.74	0.04	-19.6	2.5	8.2
Eros.	Modern	L	1.5	7.6	2.1	0.29	0.61	0.04	-18.5	2.3	7.9
Eros.	Modern	L	1.5	7.5	2.8	0.51	0.93	0.05	-19.2	3.0	9.8
Eros.	Modern	L	0.5	7.6	3.0	0.67	0.90	0.07	-18.0	3.0	10.1
Eros.	Modern	L	0.5	7.4	2.9	0.59	0.84	0.06	-18.3	2.5	10.0
Eros.	Modern	L	0.5	7.5	2.1	0.55	0.91	0.06	-16.5	4.2	9.6
Burial	Modern	U	5.5	7.0	2.2	0.91	0.96	0.10	-16.1	3.5	9.4
Burial	Modern	U	5.5	7.4	2.5	0.75	0.91	0.09	-16.2	1.8	8.7
Burial	Modern	U	5.5	7.3	2.8	0.74	0.90	0.08	-16.0	5.0	9.1
Burial	Modern	U	3.5	7.0	1.7	1.05	1.09	0.11	-17.6	5.3	9.4
Burial	Modern	U	3.5	7.1	2.2	1.11	1.21	0.12	-16.4	5.6	9.1
Burial	Modern	U	3.5	6.5	1.4	1.19	1.28	0.13	-16.9	5.9	9.0
Burial	Modern	U	1.5	6.8	2.5	1.21	1.33	0.14	-17.7	8.9	8.9
Burial	Modern	U	1.5	6.2	2.5	0.87	0.88	0.09	-17.4	6.7	9.3
Burial	Modern	U	1.5	6.8	2.6	1.46	1.53	0.15	-16.7	8.3	10.3
Eros.	Modern	U	1.5	7.5	3.3	0.71	1.05	0.08	-19.3	2.0	9.1
Eros.	Modern	U	1.5	7.6	2.4	0.46	0.82	0.05	-17.3	3.5	9.4
Eros.	Modern	U	1.5	7.3	3.8	1.05	1.19	0.10	-18.6	1.3	10.0
Eros.	Modern	U	0.5	7.2	3.5	1.26	1.41	0.13	-19.9	1.0	9.8
Eros.	Modern	U	0.5	7.4	3.1	0.75	1.19	0.08	-19.7	0.5	8.8
Eros.	Modern	U	0.5	7.3	4.9	1.19	1.30	0.11	-17.6	0.8	10.7
Eros.	Modern	U	0.2	7.5	4.2	1.19	1.32	0.11	-17.5	1.1	10.5
Eros.	Modern	U	0.2	7.5	3.4	0.72	1.04	0.08	-17.8	2.2	9.5
Eros.	Modern	U	0.2	7.5	3.6	1.07	1.29	0.11	-18.5	1.3	10.0

Table 2-4. Soil organic matter functional group data of C-H, C=C, C=O, COO, ratio of C-H/C=C, C-H/C=O and fraction modern (Fm) and turnover time (ToT)of modern and Brady soil samples collected from three replicate transects of burial and erosional landform with decreasing depth to the Brady.

Landform	Paleostatus	Soil Layer	Depth to Brady(m)	C-H	C=C	C=O	COO	C-H/C=C	C-H/C=O	Fm	ToT(Yr)
Burial	Brady	L	5.5	15.91	80.57	32.37	61.02	0.49	0.20	0.25	24732
Burial	Brady	L	5.5	12.39	60.26	21.89	47.10	0.57	0.21	0.26	22410.8
Burial	Brady	L	5.5	14.46	60.50	23.82	46.59	0.61	0.24	0.26	22507.9
Burial	Brady	L	3.5	11.90	61.62	24.42	50.88	0.49	0.19	0.27	21407.7
Burial	Brady	L	3.5	14.25	57.66	16.11	40.55	0.88	0.25	0.29	20120.2
Burial	Brady	L	3.5	11.04	57.65	26.54	48.32	0.42	0.19	0.26	23000.1
Burial	Brady	L	1.5	13.38	72.39	31.65	58.47	0.42	0.18	0.31	17545.9
Burial	Brady	L	1.5	13.31	63.28	28.74	52.34	0.46	0.21	0.30	18948.3
Burial	Brady	L	1.5	14.03	57.46	24.94	46.92	0.56	0.24	0.26	23005.5
Eros.	Brady	L	1.5	15.59	73.95	32.47	58.29	0.48	0.21	0.34	15418.5
Eros.	Brady	L	1.5	17.29	63.28	25.13	46.18	0.69	0.27	0.36	14350.4
Eros.	Brady	L	1.5	15.18	67.21	27.40	51.84	0.55	0.23	0.32	17400.9
Eros.	Brady	L	0.5	16.33	68.12	30.70	53.96	0.53	0.24	0.36	14314.2
Eros.	Brady	L	0.5	13.99	69.25	27.69	55.30	0.51	0.20	0.38	13388.8
Eros.	Brady	L	0.5	16.23	64.15	24.61	49.38	0.66	0.25	0.41	11763.6
Eros.	Brady	L	0.2	14.72	59.48	29.62	48.80	0.50	0.25	0.37	13491
Eros.	Brady	L	0.2	16.71	66.71	31.42	52.45	0.53	0.25	0.42	11132
Burial	Brady	U	5.5	14.11	75.59	29.60	56.44	0.48	0.19	0.32	17666
Burial	Brady	U	5.5	13.65	65.14	25.25	50.32	0.54	0.21	0.32	17461.7
Burial	Brady	U	5.5	15.12	65.07	26.39	48.04	0.57	0.23	0.33	16584.2
Burial	Brady	U	3.5	16.74	61.02	27.30	47.34	0.61	0.27	0.38	13051.3
Burial	Brady	U	3.5	15.06	55.56	20.14	43.03	0.75	0.27	0.33	16502.2
Burial	Brady	U	3.5	14.22	56.81	27.70	46.55	0.51	0.25	0.31	18268
Burial	Brady	U	1.5	14.10	63.19	35.09	52.43	0.40	0.22	0.40	11918.1
Burial	Brady	U	1.5	15.22	59.31	31.13	48.76	0.49	0.26	0.36	14430.4
Burial	Brady	U	1.5	13.69	58.46	29.02	47.54	0.47	0.23	0.43	10533.7
Eros.	Brady	U	1.5	16.08	74.66	34.02	58.63	0.47	0.22	0.43	10863.5
Eros.	Brady	U	1.5	16.52	63.99	27.98	50.69	0.59	0.26	0.42	11154.2
Eros.	Brady	U	1.5	17.39	71.38	31.95	54.73	0.54	0.24	0.42	10929.7
Eros.	Brady	U	0.5	16.04	77.77	36.32	59.66	0.44	0.21	0.55	6704.05
Eros.	Brady	U	0.5	17.44	65.22	26.54	46.84	0.66	0.27	0.56	6361.38
Eros.	Brady	U	0.5	15.87	63.43	28.10	48.80	0.56	0.25	0.54	6884.01
Eros.	Brady	U	0.2	15.93	70.47	33.16	56.81	0.48	0.23	0.59	5584
Eros.	Brady	U	0.2	16.85	67.02	28.42	50.66	0.59	0.25	0.54	6871

Landform	Paleostatus	Soil Layer	Depth to Bedr(m)	C-H	C=C	C=O	COO	C-H/C=C	C-H/C=O	Fm	ToT(Yr)
Eros.	Brady	L	0.2	18.53	63.59	26.73	46.51	0.69	0.29	0.74	2869
Burial	Modern	L	5.5	19.89	86.02	33.53	61.15	0.59	0.23	0.90	1093
Burial	Modern	L	5.5	17.77	93.08	35.03	60.70	0.51	0.19	0.94	718.69
Burial	Modern	L	5.5	19.76	91.15	34.76	55.21	0.57	0.22	0.80	2121.11
Burial	Modern	L	3.5	16.98	80.25	26.02	56.46	0.65	0.21	0.90	1009.07
Burial	Modern	L	3.5	21.21	74.94	26.65	51.33	0.80	0.28	0.87	1282.99
Burial	Modern	L	3.5	22.96	94.57	29.72	60.54	0.77	0.24	0.84	1598.91
Burial	Modern	L	1.5	18.68	69.02	19.41	46.75	0.96	0.27	0.84	1657.21
Burial	Modern	L	1.5	17.21	85.94	26.25	59.13	0.66	0.20	0.80	2125.09
Burial	Modern	L	1.5	19.60	64.58	16.67	41.49	1.18	0.30	0.85	1512.48
Eros.	Modern	L	1.5	17.70	86.20	34.62	58.76	0.51	0.21	1.02	241.45
Eros.	Modern	L	1.5	18.33	71.42	31.46	52.31	0.58	0.26	0.72	3259.61
Eros.	Modern	L	1.5	16.14	64.32	31.96	46.16	0.51	0.25	0.94	679.28
Eros.	Modern	L	0.5	18.40	85.38	36.03	55.85	0.51	0.22	0.81	1984.2
Eros.	Modern	L	0.5	20.26	83.92	30.51	57.18	0.66	0.24	0.96	585.78
Eros.	Modern	L	0.5	19.68	72.64	33.75	52.03	0.58	0.27	0.80	2076.36
Burial	Modern	U	5.5	22.54	89.18	28.04	61.80	0.80	0.25	1.03	255
Burial	Modern	U	5.5	18.55	87.44	28.12	58.42	0.66	0.21	0.92	834.04
Burial	Modern	U	5.5	17.48	78.89	28.29	52.29	0.62	0.22	0.97	474.39
Burial	Modern	U	3.5	18.14	71.62	20.13	47.29	0.90	0.25	0.99	395.94
Burial	Modern	U	3.5	21.80	85.73	25.35	56.30	0.86	0.25	0.87	1270.18
Burial	Modern	U	3.5	26.23	74.89	19.26	41.34	1.36	0.35	1.01	293.1
Burial	Modern	U	1.5	18.56	64.62	17.23	42.34	1.08	0.29	1.00	317.83
Burial	Modern	U	1.5	18.19	72.52	19.53	46.71	0.93	0.25	0.94	669.03
Burial	Modern	U	1.5	24.48	90.16	25.62	56.59	0.96	0.27	1.02	259
Eros.	Modern	U	1.5	18.09	83.45	34.60	54.98	0.52	0.22	0.84	1625.26
Eros.	Modern	U	1.5	16.65	72.43	29.85	49.83	0.56	0.23	0.67	4018.74
Eros.	Modern	U	1.5	25.69	76.17	27.10	48.58	0.95	0.34	0.97	458.08
Eros.	Modern	U	0.5	23.20	78.15	23.76	51.40	0.98	0.30	1.05	163.02
Eros.	Modern	U	0.5	23.58	90.00	32.85	57.58	0.72	0.26	0.82	1849.89
Eros.	Modern	U	0.5	24.28	84.01	28.17	53.83	0.86	0.29	1.00	330.31
Eros.	Modern	U	0.2	23.03	84.64	29.68	53.19	0.78	0.27	0.95	655
Eros.	Modern	U	0.2	20.09	87.14	32.46	55.18	0.62	0.23	0.79	2183
Eros.	Modern	U	0.2	19.42	64.83	22.34	44.30	0.87	0.30	0.91	973

Chapter 3.
Soil organic matter stabilization by polyvalent cations in a buried alkaline soil

Abstract

Large stocks of soil organic matter (SOM) can be found in deep paleosols or buried soil layers. The residence time of subsoil SOM is typically longer compared to the topsoil partly due to the disconnection from near-surface environmental conditions that may favor decomposition. As the largest carbon reservoir in terrestrial ecosystems, it is crucial to understand soil C dynamics better to predict its sensitivity to climate change. SOM continuously cycled and transformed belowground; however, their vulnerability can be altered by the presence of minerals capable of stabilizing even simple organic compounds from loss due to microbial degradation or dissolution. The rationale for this study was-that the controls on carbon (C) dynamics in subsoil might be different from topsoil because subsoil has more mineral and polyvalent cations compared to topsoil. Therefore, the stability of the SOM in deeper soil will be more prone to forming organomineral complexes by cation bridging. In this study, our objective was to understand -to what extent the mechanism of SOM stabilization in buried soil vs modern soils can be explained by the soil's physical and chemical properties as a function of paleostatus (buried vs modern) and landform. The study site is in Nebraska, Great Plains, where climate-driven varying rates of loess deposition during the late Pleistocene and Holocene resulted in sequences of paleosols in thick loess deposits. The Brady paleosol here is buried up to 6m below the surface soil. The landform of the study site is dissected by gullies here which presents an interesting case study to understand the dynamics of sub-SOM and topo sequence position. We sampled along the catena to understand the spatial variability in the different depths of Brady soil total organic carbon and the mechanism of soil organic carbon (SOC) protection that contributes to the long-term persistence of organic matter in soils. Our finding indicated higher pH, EC, total inorganic carbon (TIC), and lower TOC in the buried Brady soils compared to the modern soils in the depositional landform might have provided the SOC stabilization through the formation of aggregates or organo-mineral complexes through cation bridging or cementation or by the action of all playing together. Modern soils present in the depositional transect don't have the extra layer of protection by cementation. Erosional landform modern and Brady soils were not significantly different in pH, EC, TOC%, and TIC%, and the mechanism of stabilization can be organo-mineral complexation and aggregate formation. Due to that, Brady soils present in erosional landforms can be as vulnerable as modern soils.

3.1 Introduction

3.1.1 Stability of Soil Organic Matter (SOM) at different depths of the soil layer

Retention of SOM belowground increases its persistence through chemical and physical mechanisms. Sorption of OM is facilitated by electrostatic attraction directly between organo-mineral surfaces or bridged by cations, while occlusion of OM within micro aggregates creates physical means for persistence. Many mechanisms responsible for the mineral association of SOM increase their persistence by decreasing OM bioavailability to decomposers (Sollins et al.,1996; Rowley et al.,2018). The stability of the SOC depends on the chemical properties of the soil, such as mineral fractions, cations in the soil, structure of the soil matrix, and mineral surface that are capable of adsorbing organic materials which lead to stabilization of soil carbon compounds due to organomineral interaction. SOM stabilization can occur by physical occlusion through forming microaggregate with silt and clay. Eventually, macroaggregates will form in the presence of silt, clay, and microaggregates. Biological mechanism influences macroaggregate stabilization by roots, fungi, microorganisms, and extracellular substances. This difference in structural stability, porosity, and hydrophilicity determines the stability of the aggregate occluded SOC in the soil (Six et al., 2004). Microaggregate provides longer stabilization to the occluded SOM compared to the macroaggregate occluded SOC. In general, the degree of protection against decomposition decreases from chemical to physical mechanisms of protection (Six et al., 2004).

Deep-buried soils, which is a previous topsoil, can store significantly more carbon (C) than what would exist at such depths only from root inputs and leach from upper horizons alone (Marin-Spiotta et al., 2014; Marin-Spiotta et al., 2011). Although SOC plays an important role in soil carbon dynamics, most studies focus on the distribution along the top 10-20 cm of the soil profile, as sampling is restricted to the top layer of the soil (Grand et al., 2011). Homann et al. (2005) reported that more than half of the C stock is below 20 cm of the ground. This indicates that subsoil C should be distinguished from topsoil C dynamics as they differ from each other (Salome et al. 2010). Carbon-to-nitrogen ratios play an important role in determining SOM decomposition. High C: N ratio hampers the mineralization of SOM due to the deficiency in nitrogen (N) for microbial decomposition, while lower values of the C: N ratio with depth show a higher degree of transformation of SOM (Norris et al., 2011). Mineral-associated organic matter's C: N ratio is generally lower, and less variable compared to the mineral-free organic matter, as soil N is retained by the microbial mineralization-immobilization process in contrast with the catabolic loss of C (Paul and Clarks, 1996).

3.1.2 Role of pH, cations, and minerals in SOC stabilization

Soil pH can change the solubility of dissolved organic matter (DOM) and stabilization of the DOM due to the presence of exchangeable base cations and metal oxides that have a pH-dependent surface charge. It has been noted that organic matter solubility increases along with the increase in pH due to the increase of negatively charged components in both organic matters and in the soil (Andersson et al., 2000; Kalbitz et al., 2000; Oste et al., 2002). So, higher DOM loss is positively correlated with pH (Oste et al., 2002). In an acidic environment- Al^{+3}, Fe^{+3}, their mineral forms and cementation by Fe oxides play key roles in SOC stabilization. But, where the soil pH is above 6, Ca^{+2} plays an important role in SOC stabilization (Rowley et al., 2018; Zhao et al., 2017). When the soil pH is

higher than 8.3, Ca^{+2} starts to precipitate as $CaCO_3$ (Rowley et al., 2018), and beyond pH 9.5, the soil may become highly concentrated with Na^{+}, which reduces the sorption and weakens the stabilization of SOC (Lindsey, 1979).

Calcium makes up 2.94% of the upper continental crust providing alkalinity to the soil (Rowley et al., 2018). Alkaline cations (divalent) can play an important role in SOC stabilization by bridging between negatively charged particles of the organic molecule or organic molecule to a mineral, and thus the microbial activity to decompose the soil becomes slower (Whittinghill and Hobbie, 2012; Grunewald et al., 2006; Wedephol, 1995; Rowley et al., 2018). Ca^{+2} bridging has a positive effect on soil as it provides long-term soil structural stability (Six et al., 2004), which in turn can help in the accumulation of total organic carbon (TOC) due to intramacroaggregate physical protection (Briedis et al., 2012). Due to a high point of zero charge, $CaCO_3$ acts as an effective adsorbent (Suzuki, 2002). There have been several research on potential $CaCO_3$-SOC adsorption interaction on dissolved organic carbon (DOC) (Jin and Zimmerman, 2010; Lee et al., 2005), but how the occurrence of $CaCO_3$ positively affects the stabilization of SOC on buried aeolian soils is lesser known. Ca^{+2} has larger residence time compared to the monovalent cations and is a good flocculating agent for a natural system for outer sphere bridging (Rowley et al. 2018) and can also form an inner-sphere complex with oxygen(O)- bearing ligands (Sposito, 2008). In the presence of Ca^{+2} and CO_3^{-2} or HCO_3^{-} ions, pedogenic calcite precipitate from the soil solution and the source of carbonate and bicarbonate anions as the CO_2 dissolute in the water, thus the calcite precipitation depends on the concentration of calcium, pH of the soil, CO_2 pressure in the soil air and microbial activity (Falsone et al., 2010). Pedogenic carbonate remains in the soil until the soil solution becomes completely saturated with calcite and is generally found in arid, semiarid, and Mediterranean regions and thus can stabilize a large amount of SOC.

Along with the percentage of clay, clay mineralogy plays an important role in aggregate stability and dispersion. For example, 1:1 clay mineral, such as kaolinite-dominated stability is attributed due to the binding capacity of the minerals, but the aggregate stability in 2:1 dominated clay mineral soil depends on polyvalent metal-organic complexes which form bridges between the negatively charged clay particle (Oades & Waters, 1991, Six et al., 2000). Wuddivira and Camps-roach (2007) indicated that the stability of the soil aggregate increase with increasing the clay content that is non-expanding, crystalline clays and less dispersive such as kaolinite, and their result found calcium in addition to organic matter, improved aggregation and increased soil's saturated hydraulic conductivity that is dominated by 1:1 clay mineral in the soils of Trinidad and Tobago.

The presence of polyvalent cations, metals, and reactive minerals have an influence on increased SOC stock (Oades and Waters, 1991; Zhao et al., 2017; Falsone et al., 2010; Fernandez-Ugalde et al., 2014; Grand and Lavkulich, 2011; Baldoc and Skjemstad, 2000; Minic et al., 2017; Whittinghill and Hobbie, 2012). Most of the research has focused on acidic soil environment where the interaction between SOC and aluminum (Al) or iron (Fe) play a major role in SOC stabilization, but fewer studies have been conducted on alkaline soils where calcium (Ca) plays a major role, as exchangeable Ca positively correlate with SOC concentration and its resistance to oxidation and by forming inner or outer sphere bridging with SOC. The presence of $CaCO_3$ in alkaline soil is very common, and it plays an important role in SOC stabilization by occlusion and aggregate formation in alkaline soils, but little is known about its role in stabilizing SOC in buried soils. Finally, the research objective was to understand to what extent SOM stabilization can be

explained in the presence of polyvalent cations and the effect of soil physical and chemical properties on SOC stabilization at two different landforms (erosional and depositional) dynamics in the Brady paleosol, deep loess (aeolian) deposit in Nebraska, USA, where climate has historically driven varying rates of loess deposition during the late Pleistocene and Holocene, burying soils up to 50m below the surface. Our objective was to understand 1) how the concentration and types of polyvalent cations differ in Brady paleosol and modern soils in depositional and erosional landforms, 2) does the relationship between SOC concentration and various polyvalent concentrations differ in depositional and erosional landform modern and Brady soils.

3.2 Materials and method

3.2.1 Site description

The study site is in the Great Plains in Wauneta, Nebraska, where the variation of climate-driven rates of loess deposition during the Late Pleistocene and Holocene resulted in sequences of buried soils (Johnson et al., 2007). The mean annual temperature (MAT) of this area is 9.7°C, mean annual precipitation (MAP) is 495 mm (seasonal). The aridity index class at the study site is considered semi-arid. The vegetation is mixed C3, C4, and short grass prairie. The land is cultivated where the topography permits and grazed in uncultivated land. The Brady soil was formed between cs. 13 to 10 kya and was buried by loess (Mason et al., 2008). In our study site, the modern soils are loess derived as well and classified as Mollisols (USDA).

Brady soil is a morphologically distinct stratigraphic and paleoenvironmental marker in the central Great Plains (Johnson and Willy, 2000). The paleosol was formed due to aeolian deposition, which has an important beneficial effect such as nutrient transportation to the terrestrial and aquatic systems (Sankey et al., 2009; Neff et al., 2008; Lal et al., 2003; Jickells et al., 2005; Reynolds et al., 2001). Jacobs and Mason (2004) found that the Brady soil has A, B, and C horizon morphology. The A horizon is very dark greyish brown, and the texture is invariably silt loam. A Mollisol study of the region characterized the dark color of the Brady soil A horizon to be from the clay-organic matter complexes (Jacobs and Mason, 2004). Yet the organic carbon chemistry in the Brady soil is not well studied. Most secondary calcium carbonates are present in the A horizon and some throughout the profile. Previous works have suggested that Brady soil was formed in a stable landscape (Mason and Kuzila, 2000) because of the reduction in the deposition rate (Jacobs and Mason, 2007). This paleosol is below younger Mollisol soil that formed from aeolian deposition as well but is connected to the current environmental factors. This provides a unique opportunity to test our objectives.

3.2.2 Field sampling

Soil samples were collected in the summer of 2016 and 2017. The samples were collected from the depositional and the erosional of the topo sequence. Three sampling plots were chosen in the depositional landform and another three in the erosional landform for a total of six sampling locations in the catena sequence. We collected 3 replicates from each landform and ensured the depth of the buried Brady paleosol was similar. Soil transects, sampling locations, and different depth categories of Brady soil were selected using information from prior research (Jacobs and Mason, 2004; Marin-Spiotta et al., 2014; Mason et al., 2008).

3.2.3 Soil sampling

To account for the differences in depth and increasing exposure of the Brady paleosol, we collected soils from 6 different plots (n=3) in the depositional and in the erosional (n=3) (Figure 1) regions. Soil samples from the Brady soil and overlying modern soils were collected from two different topographical region. Soils were collected from 6 different plots, where each plot had three replications. At the depositional site, Brady soil samples were collected from depths of ~5.5m(deepest), ~3m(intermediate), and ~1m(shallowest), whereas samples at the erosional site were collected from the depth of 1-1.5m(deepest), ~0.5m(intermediate) and ~0.2m(shallowest). Soils were sampled using Giddings's probe (Giddings Machine Company; Windsor, CO) in 10.2 or 8.9m sampling tubes for the depositional sampling while soil pits were dug at the erosional (see details in Szymanski et al., 2022, in preparation). For all the topographic positions, we sampled the top of 0-30 cm and 30-60 cm of the modern and paleosol profiles. For the intermediate and shallower depth at the erosional, samples were collected within 15-30 cm for the modern soils and Brady soils were collected below that. All the reported values presented in figures 2 (A, B), 3, 4, 5, and 8 are the mean of the three replicates of the 6 sequential depth categories of the continuum of buried to ~5.5 m, ~3m, ~1m and eroded to ~1.5m, ~0.5m, and ~0.2m for a total of 18 samples (core for the depositional and hand dug a pit for erosional landform) identified as either burial or erosional. Three soil samples were randomly taken from every six plots by carefully making sure the depth of the underlying Brady paleosol and soil cores according to the depth category were extruded into a zip-lock bag, sealed, and taken to the laboratory, where we air-dried the sample at the University of Wisconsin, Madison.

3.2.4 Laboratory analysis

3.2.4.1 Quantifying Soil Chemical and Physical processes

Soils were air-dried, then samples were sieved (< 2mm) to remove any plant materials and stones for the soil's physical and chemical analysis. Soils were analyzed for pH in a 1:2 slurry in deionized water, and 0.01M $CaCl_2$ (Thomas, 1996; Mason and Kuzila 2000), and soil electrical conductivity (EC) was measured in a 1:1 (soil: water) (Rhoades,1996). Total organic carbon (TOC%), total inorganic carbon (TIC%), and total nitrogen (TN%) were analyzed by using a 4010-elemental analyzer (Costech) that is interfaced with a ThermoFisher Delta V Plus isotope ratio mass spectrometer (IRMS) with Conflo IV interfaces at the stable isotope ecosystem laboratory of UC Merced (SIELO). The details of these analyses have been provided in Chapter 2, Sections 2.2 and 2.3, and in Szymanski, 2021. Percent TOC, TN, and TIC are reported as percent by weight.

3.2.4.2 Extraction of base cations

We used CEC by summation method. For this procedure, the soluble and rapidly exchangeable pools of base cations are extracted by leaching soil with NH4OAc (ammonium acetate), and their concentrations in the leachate are measured by inductively coupled plasma-optical emission spectroscopy (ICP-OES) at the environmental analytical lab (EAL) of UC Merced to get the cation concentration in ppm. Extraction of base cations Ca^{+2}, Mg^{+2}, Na^{+}, and K^{+} was done by weighing 2.0 g, air-dried, sieved soil in a 50ml centrifuge tube with 1 (M) NH_4OAc. A sample blank was also prepared with 1(M) NH4OAc. The pH of the ammonium acetate was adjusted to match the soil pH (~7-8.2) by using ammonium hydroxide. The centrifuge tube with soil and ammonium acetate was

placed on a shaker at room temperature and shacked for around 1.5 hours. After shaking, the samples were centrifuged at 6000rpm for 10 minutes, and the process was repeated until the supernatant was clear. The supernatant was analyzed by ICP-OES for Ca^{+2}, Mg^{+2}, Na^{+}, and K^{+} nutrients at UC Merced.

The exchangeable Ca, Mg, Na, and K were calculated by

$$\text{Exchangeable cation X } (mol_c/kg \text{ soil dry wt}) = \frac{(a-b)\times 20\times mcf}{10\times y\times s} \quad (3.1)$$

where X = Ca^{+2}, Mg^{+2}, Na^{+}, or K^{+}, a= concentration (ppm) of Ca^{+2}, Mg^{+2}, Na^{+}, or K in the extraction solution, b = concentration (ppm) of Ca^{+2}, Mg^{+2}, Na^{+}, or K in the blank, 20= amount of NH4OAc used, y = atomic weight of Ca, Mg, Na or K, s= mass of air-dried soil in g, mcf= moisture correlation factor, the difference in moisture content between air-dried and oven-dried soils calculated as

$$mcf = \frac{100 + \%\, moist}{100} \quad (3.2)$$

where % moist = $M_{water} / M_{oven\ dry\ soil}$. (M = mass of soil)

Finally, total exchangeable base cations ($cmol_c$/kg dry soil) were calculated as

$$\sum(Ca + Mg + Na + K) \quad (3.3)$$

We calculated the sodium adsorption ratio (SAR) by

$$SAR = \frac{Exchangable\ Na^{+1}}{\frac{Exchangable(Ca^{+2} + Mg^{+2})^{2/1}}{2}} \quad (3.4)$$

3.2.4.3 Soil particle size analysis

Soil particle size was determined by high-resolution particle size analysis by laser diffraction by using a Mastersizer 2000 particle size analyzer (Malvern Panalytical, Malvern, UK) (Jacobs and Mason 2007) at the University of Wisconsin, Madison. First, the soil samples were dispersed with 10ml of 50mg/L sodium- hexametaphosphate (Na-HMP) and sonicated by a 6m ultrasound. Clay contents were determined by wet sieving and pipette separation with H_2O_2 and sodium acetate buffer to remove the aggregation caused by organic matter and the presence of carbonate (Kilmer and Alexander 1949; Gee and Bauder 1986; Jacobs and Mason 2007). The details of this analysis have been given in Szymanski, 2021.

3.2.5 Statistical analysis

Samples were plotted to visually understand the variability of soil pH, EC, TOC%, TC%, TN%, and organic C to nitrogen (TOC: TN). We also plotted Ca^{+2}, Mg^{+2}, Na^{+}, and K^{+} ammonium acetate extractable concentrations and an exchangeable fraction of the same nutrient in a similar way. Linear regression analyses were plotted using the R package corrplot to visualize the correlation matrix to understand the pattern among variables.

To understand the variability in Modern vs Brady soil at depositional vs erosional positions, we combined upper and lower soil layers together. All upper modern and all lower modern soils were combined in the depositional position as well as in the erosional position of the study site. Similarly, all upper Brady and lower Brady soils were combined in these two landforms irrespective of the depth categories of Brady soils found in either topographical position. Finally, samples were grouped as Depositional Modern, Depositional Brady, Erosional Modern, and Erosional Brady to ease the complexity and to understand the variability across samples. All statistical tests were conducted using CRAN-R (version 3.5.1; R Development Core Team, 2017). To test for significant differences in the soil's physical and chemical properties, we used Kruskal-Wallis's test with an alpha = 0.05, followed by Dunn's post hoc test to determine pair-wise differences.

3.3 Results

3.3.1 Soil pH and Electrical Conductivity

Soil pH and Electrical Conductivity (EC) both increased along with the depth from modern to Brady soils in both depositional and erosional positions. The average pH of the depositional and erosional Brady soil was alkaline, around 7.73 (±0.14) and 7.68 (±0.13) for depositional and erosional landforms. But modern soils were nearer to neutral values, 7.1 (±0.41) and 7.4 (±0.12) for depositional and erosional, respectively. In the depositional landform, soil pH was significantly higher in the Brady soil than in the Modern. At the erosional landform, modern and Brady soil pH has no significant difference. Depositional landform Brady soil pH was significantly higher than the modern soils in both landforms (Figure 2. A). EC values ranged from 1.7 to 7.2 dS/m in these soils. The average EC was highest in depositional Brady soil, 5.58 dS/m (±1.2), and was lowest in the depositional modern soil, 2.67 dS/m (±1.32). Depositional landform Brady soil EC was significantly higher compared to the modern soils and erosional Brady soil (Figure 2. B). There was no significant difference in pH and EC between erosional modern and erosional Brady soils (Figure 2 A and B). The details of the pH and EC data are provided in Szymanski, 2021 and as well as in Chapter 1, section 3.1.

3.3.2 Soil texture

All modern and Brady soils present in the depositional and erosional landform are characterized as mostly silt loam soils (Figure 5), where depositional Brady soil has an average of 8.86% (±2.18) clay, followed by erosional Brady soils of 7.7% (±0.75), erosional modern soils 6.45% (±0.75), and depositional modern soils 6.43% (±0.99). The percentage of silt was highest in depositional Brady soils, an average of 58.89% (±4.19), whereas the sand content was highest in erosional modern soils, an average of 40.69% (±2.58). Silt percentages varied widely in depositional modern soils, 55% to 81%, while in the erosional modern soils, they were between 58% to 68% (Figure 5). Clay content was significantly higher in the Brady soils compared to the modern soils (Figure 4. A). The percentage of silt was significantly lower in erosional modern soils compared to the other soils (Figure 4. B), and the sand percentage was significantly low in depositional Brady soils compared to the other soils (Figure 4. C). The details of the soil texture have been provided in Szymanski, 2021.

3.3.3 Total organic Carbon (TOC%), total inorganic carbon (TIC%), total nitrogen (TN%) and TOC%: TN% ratio

The details of the soil elemental analysis have been provided in Szymanski, 2021. TOC% decreased along with the depth from modern to Brady soils in depositional and erosional landforms. On average depositional modern soil has the highest TOC% (0.85±0.26) and depositional Brady soil has the lowest TOC% (0.44±0.47). Organic carbon was significantly low in the depositional Brady soil compared to the modern soils (Figure 2. C). There was no significant difference in organic carbon percentage between erosional modern and erosional Brady soils. The average TIC% was lowest in depositional modern soils (0.08 ±0.06), and the highest TIC% was in erosional modern soils (0.28±0.11). TIC% was significantly lower in depositional modern soils, and there was no significant difference in TIC% among erosional modern, erosional Brady, and depositional modern soils (Figure 2. D). C: N ratio was significantly high in erosional Brady compared to other soils, and there was no significant difference in C: N ratio among depositional modern, depositional Brady, and erosional modern soils (Figure 2. F). More details of these data have been provided in Chapter 1, Section 3.2.

3.3.4 Base Cations

Among the base cations (Ca^{+2}, Mg^{+2}, $K^{+,}$ and Na^{+}), Ca^{+2} has the highest concentration in all soils ranging from 180 to 499.7 ppm. Total and exchangeable Ca^{+2} was significantly higher in erosional modern soils compared to the depositional modern soils, and there was no significant difference between the Brady soils (Figure 3. A). Ca^{+2} concentration was slightly lower in depositional modern soils compared to the other soils. Total Magnesium (Mg^{+2}) concentration ranged from 11 to 33 ppm in modern soils, and in Brady soils, the range was between 19 to 63.2 ppm. Exchangeable Mg^{+2} ranged from 0.9 to 5.1 ($cmol_c$/kg soil dry wt). On average, depositional Brady has the highest, and erosional modern has the lowest total Mg^{+2} and exchangeable Mg^{+2} (Figure 3. B). Total and exchangeable Mg^{+2} was significantly higher in depositional Brady compared to the modern soils. Erosional modern soils have significantly lower Mg^{+2} compared to the erosional Brady soils. K^{+} concentration ranged from 13 to 120 ppm and was significantly higher in the Brady soils compared to the modern soils, and there was no significant difference between the Brady and modern soils at burial and erosional landforms (Figure 3. C). The concentration of Na^{+} was not detectable in the majority of the modern soils, and it was significantly higher in depositional Brady soils compared to the erosional Brady soils. SAR values ranged from 0.02 to 0.28 in the Brady soils. The highest average SAR was noticed in depositional Brady soils, 0.12 (±0.09), followed by erosional Brady, 0.03 (±0.06). Exchangeable Na^{+} and Sar were significantly high in depositional Brady soils, and there was no significant difference in depositional modern, erosional modern, and erosional Brady soils (Figure 3. D and E).

3.4 Discussion

Brady soil present in the depositional landform has significantly lower TOC% and significantly higher pH and EC (Figure 2. A, B, C, and D). During the formation of the Brady soil, the loess deposition was slow, and in the presence of oxidizing environment, there might be an accumulation of more stable SOC (Jacobs and Mason 2004). Brady soil and modern soils differ in physical and chemical properties (Figures 2, 3, 4, and 6), and Brady soil characteristics follow Jacobs and Mason's (2004, 2007) research on the Great Plains area. We found significantly higher clay content in the Brady soil compared to the

modern soils (Figure 4. A), which indicated the pedogenesis and transportation of the loess material (Jacobs and Mason 2007). The mineral present in the soils plays a dominant role in aggregate formation. A study of clay mineralogy of this area by Szymanski (2021) indicated that the shallowest depth Brady soil in erosional landform has significantly less kaolinite compared to the modern soils. The study also reported the illite to kaolinite ratio, which indicates that weathering of the soil didn't differ among the Brady soils present at different depths and modern soils at the two different landforms.

A study by Jacobs and Mason (2007) on a similar site of the Nebraska Great Plains also indicated that the clay mineralogy of the Brady subsoil was similar to the Peoria loess, whereas the upper Brady was alike to the Bigness loess. Overall, the clay percentage was significantly higher in the Brady soils compared to the modern soils, whereas silt content was relatively high in both erosional and depositional landforms (Figure 4. B). Silicate plays an essential role in micro aggregate formation by bonding with a free primary particle and plays a key role in SOC storage (Six et al., 2004). We also know that OM has a high affinity to bind with clay and silt-size mineral particles (Kleber et al., 2015) and hence makes them more stable against microbial decomposition. A study by Szymanski (2021) on the same landforms and the soils indicated that the modern soil has larger SOC associated with macro and micro aggregate occluded POM ($Ag\&M_{>53}$), but in the Brady soil, >90% of the SOC is associated with <53 mineral-associated fractions and aggregate ($M\&Ag_{<53}$). This contrast with the observation by Bischoff et al. (2018) in the semiarid areas of Siberian steep soils, which depicted <10% SOC in the particulate organic matter (POM) and the presence of >90% SOC in mineral bound fraction. This finding indicated that mineral-associated SOC is the dominant stabilization mechanism for Brady soils.

SOC stabilization capability of the polyvalent cations shifts from Al to Fe to Ca as soil pH moves from acidic to alkaline (Rowley et al., 2018). Low or higher pH has a different capability of SOC stabilization as the polyvalent cation activity depends on them (Clarholm and Skyllberg, 2013; Rowley et al., 2018). At the lower pH, the SOC stabilization mechanism is dominant by Al and Fe, but as the pH increases, the dominant SOC stabilization becomes occlusion by aggregate either for a short or long time, depending on the mineral properties of the soil (Rowley et al., 2018). Since our soil pH ranged from neutral to alkaline, we assumed our SOC stabilization will depend on polyvalent cation Ca^{+2} (Kayler et al., 2011; Rowley et al., 2018).

Salt-affected soils can be classified depending on the EC (dS/m) and sodium adsorption ratio (SAR). When the EC< 4 dS/m and the SAR<13, the soil is classified as none, and when the EC> 4 dS/m and SAR < 13, the soil is saline, and in both these conditions, the soil's physical conditions will be flocculated (US salinity laboratory staff, 1954). For all the modern soils and erosional landform Brady soils, the EC <4 dS/m and SAR <13. Brady soil present in the depositional landform has an EC of >4 dS/m and SAR < 13, which makes them saline soil. All of our soils fall into the category of flocculated and clay flocculation is one of the main reasons for soil aggregate formation (Dexter, 1988). This indicates that our study area soils might be stabilized due to the clay flocculation.

In saline soils, common cations are Ca^{+2}, Mg^{+2}, $Na^{+,}$ and $K^{+,}$ which play an essential role in SOC adsorption by dispersion and flocculation. Depositional Brady soil has significantly high exchangeable Na^{+}, and it is significantly positively correlated with TOC% (Figure 7). OM coated with Na^{+} has higher solubility compared to OM coated with Ca^{+2}, and high exchangeable Na^{+} can cause the dispersion of soil particles (Nelson and Oades 1998). The potential for the dispersion of K^{+} ions is also low compared to Na^{+}.

Clay dispersion causes soil physical property dispersion which can occur in depositional Brady soils, and SOC will become more susceptible to microbial decomposition in appropriate environments. With an increase in SAR, the desorption of OM from clay increases, but a rise in EC along with a high proportion of divalent cations can counterbalance the Na^{+} dispersion effect by flocculation (Mavie et al., 2012; Setia et al., 2014). However, the depositional Brady soils have a higher Sar value compared to the modern soil's high EC (Figure 2. B), and the presence of divalent cations (Ca^{+2} and Mg^{+2}) (Figure 3. A and B) probably can overrule the Na^{+} dispersion effect but in erosional landform Brady soil, this might not be the case.

The presence of Ca^{+2} has a positive effect on soil structure stability through aggregate formation (Peterson 1947). TOC% and TIC% are significantly positively correlated with Ca^{+2} in erosional Brady soils (Figure 7). We think this positive correlation is due to the cementation by $CaCO_3$ (Wuddivira and Camps-Roah 2007) on the aggregates present in these soils and also because of the flocculation due to Ca^{+2} which might be coming from the weathering of $CaCO_3$. This observation tells us that Ca^{+2} might be the major cation playing an important role in SOC stabilization through flocculation, inclusion (envelopment of SOC with a mineral), cementation of the aggregate, or co-occurring all these processes together. TOC% is significantly negatively correlated with Ca^{+2}, and TIC% correlation with Ca^{+2} is marginally significant in depositional modern soil (Figure 7). This indicates that most of the TOC% present in these soils is organic carbon (Figure. 2. C), and other carbons present in these soils are inorganic carbon, containing $CaCO_3$. We saw significantly higher TIC% in depositional Brady, erosional modern, and erosional Brady soils compared to depositional modern soil (Figure 2.D). The high amount of inorganic carbon indicates a possibility of cementation, which decrease the porosity (Falsone et al., 2010) and hence greater potential for higher stability. But we have to remember that the presence of plant roots can increase the dissolution rate of $CaCO_3$ by producing large quantities of CO_2 and H^{+}, which can increase the level of exchangeable Ca^{+2} (Qadir et al., 2005) and make the previously stable SOC susceptible to decomposition. Our data showed a higher exchangeable Mg^{+2}, $Na^{+,}$ and K^{+} in the Brady soils in both depositional and erosional landforms (Figure 3. B, C, and D), which is in a deeper sub-surface horizon compared to the modern soils. The polyvalent cations can reach deeper soils by leaching, and that might be the case for these cations. Since the exchangeable Ca^{+2} was similar in erosional modern, erosional Brady, and depositional Brady soil, this indicates flocculation and complexation in the presence of clay and organic acid prevented their transportation to the subsoil horizon (Rowley et al., 2018).

Exchangeable Mg^{+2} decreased along with the depth of Brady soil in depositional landforms but remain similar in erosional landforms. But exchangeable Ca^{+2} decreased along with the depth in erosional landform and didn't change in depositional landform. This decline can be attributed to Na^{+}, which replaces Ca^{+2} and Mg^{+2} and causes the loss of exchangeable Ca^{+2} and Mg^{+2} (Sing, 2016). There was no exchangeable Na^{+} available for the erosional modern soils. Bertrand et al. (2007) and Yang et al. (2016) have shown that there is a positive correlation between exchangeable Ca and SOC which can be explained as increasing the SOC concentration replaces also increases the cation exchange capacity (CEC) of the soil (Rowley et al. 2018) as it increases the net primary productivity (NPP) in above and belowground biomass (Briedis et al. 2012).

SOC can get stabilized by physical separation or by sorption on minerals through cation bridging. Microaggregate formation is the most known process for physical stabilization, which has been demonstrated by several researchers (Virto et al., 2008, 2010) due to

reduced porosity (Denef et al., 2004) which ultimately helps the SOC to stay occluded within. The aggregate formation can involve electrostatic flocculation of 2-20 µm size particles (Ghezzehei et al., 2011) which then can get bound by cementing agents (Falsone et al., 2010). SOC stabilization by chemical sorption includes OM adsorbing on minerals such as phyllosilicates through polyvalent cation bridging. The presence of specific reactive miners has a positive correlation with SOC stock (Baldock and Skjemstad, 2000). An increase in polyvalent cations increases soil aggregation by flocculation (Bronick and Lal 2005) and cementation (Zhao et al., 2017; Falsone et al., 2010), which might be the case for depositional Brady, erosional modern, and erosional Brady soils as they all have higher base CEC (Figure 3. F) compared to the depositional modern soils. SOC complexation with a mineral generally has an older ^{14}C age compared to other pools (Kleber et al., 2011). We have observed that Brady soils present in the deeper soil layers have higher turnover times compared to the modern soils (Chapter 2), indicating that adsorption of SOC by polyvalent cations plays a major role in SOC stabilization in these soils.

Our results suggested that the physiochemical properties play a critical role in predicting SOC stabilization. A study by Lehman and Kleber (2015) has also revealed that spatial inaccessibility (organo-mineral complexation) of the substrate to the microbes is a major control for SOC storage. When the SOC gets occluded inside an aggregate or gets attached to the mineral through-mineral sorption, microbial enzyme gets restricted to impede the SOC decomposition (Six et al., 2006), which restrict the diffusion of oxygen. The presence of Ca^{+} and Mg^{+2} can restrict SOC availability by flocculating and binding SOC to clay surfaces by cation bridging in neutral to alkaline soils (Rowley et al., 2018). SOC can be stabilized by an outer-sphere or inner-sphere complex (Sposito 2008), and they both interact together to stabilize the SOC over a medium to an extended period (Rowley et al., 2018). Due to the high pH and less aridity in the deeper soil and modern soil compaction from the top, cation bridging with the Ca^{+} tended to be the major contributor to SOC stabilization in these soils. Our results suggest SOC stabilization mechanism is linked to the soil particle distribution (clay%, silt%, sand%) and organo-mineral complexation is controlling the SOC stabilization at modern and Brady soils. Since the soil physio-chemical properties are different in depositional vs erosional landforms Brady and modern soils, we see that the stabilization mechanism is also different. Loss of exchangeable Ca^{+2} and Mg^{+2} weakens the aggregate protection and mineral-SOC association, which can make the SOC vulnerable to microbial decomposition (Yao et al., 2022). A further study on the plant and microbial community will better forecast the soil C stability in these soils.

3.5 Conclusion

The relative importance of chemical and physical storage is not consistent in modern and Brady soils present in different landforms. Our study suggests high content of polyvalent cations present in these soils is large enough to promote the flocculation of the organic matter with minerals. It can provide organo-mineral complexes for SOC stabilization. With our study in this area soil, we found that the potential mechanism of stabilization of the SOC is different in Depositional Brady soils and overlying modern soils as they have different concentrations of polyvalent cations. Depositional Brady soils have high inorganic carbon present along with the polyvalent cations. This combination can provide SOC stabilization by aggregation, along with cation bridging and cementation. But in depositional modern soils, due to less inorganic carbon and a high amount of organic

carbon, this protection mechanism can primarily come from organo-mineral complexes due to cation bridging and aggregation. In the erosional landform, we didn't find much variability in TIC% between modern and Brady soils, which indicates that the stability for both of these soils can be attributed to the formation of aggregate formation, organo-mineral complexes, and cementation. Brady soils present in the deeper horizon of the depositional landform have a greater potential for stabilization due to the added effect of cementation on top of the aggregate formation and organo-mineral complexation due to the compaction from the top. But soils in the shallower sub-surface can be more prone to dissolution if they come in contact with the modern environment due to erosion and chemical dissolution by precipitation and wind. Our soils have a pH range of 7.1 to 7.8, which indicates that high pH can help in OM ionization which can increase its dissolution and increase its potential organic carbon loss (Pathak and Rao 1998). The stability of the SOC in the calcareous soils can be altered with moisture gradient as the presence of moisture can increase microbial activity. The consequences can result in a decrease in pH and the dissolution of calcium carbonate that previously cemented and occluded SOC from microbes. TOC% was negatively correlated with pH for all of our soils because high pH has limited nutrient availability. We noticed that pH can be a master variable in SOC stabilization as it regulates which cation will play the major role in the stabilization mechanism, and we also noticed pH is negatively correlated with TOC%, as it affects the biological activity too and prevents more TOC% accumulation. We believe the accumulation of Na^{+} in the Brady soils is due to the mobilization of the salt, either naturally or by previous irrigation practices on the study site. High Ca^{+2} content might have played an important role in SOC stabilization in these soils through cation bridging by exchangeable Ca^{+2}, as it is more stable compared to monovalent cations, and thus Ca^{+2} is a good flocculating agent of the natural systems. SOC can get stabilized by Ca^{+2} by binding with high molecular weight organic compounds. The amount of silt present in these soils plays a role in TOC% stabilization. Formation of the aggregate promotes long-term carbon sequestration by physically protecting the SOM inside the aggregate from microbial decomposition and action of cementation on top of the aggregates can protect SOM longer than an aggregate without cementation.

3.6 Reference

Andersson, S., Nilsson, S. I. and Saetre, P. (2000). Leaching of dissolved organic carbon (DOC) and dissolved organic nitrogen (DON) in mor humus as affected by temperature and pH. Soil Biol Biochem, 32**,**1–10.

Baldock, J. A. and Skjemstad, J. O. (2000). Role of the soil matrix and minerals in protecting natural organic materials against biological attack. Org Geochem., 31(7–8),697–710.

Bertrand, I., Delfosse, O., and Mary, B. (2007). Carbon and nitrogen mineralization in acidic, limed and calcareous agricultural soils: apparent and actual effects. Soil Biol Biochem, 39(1), 276–288

Briedis, C., Sa´, J. Cd. M., Caires, E. F., Navarro, J. dF., Inagaki, T. M., Boer, A., Neto, C. Q., Ferreira Ad. O., Canalli, L. B. and Santos, J. Bd. (2012). Soil organic matter pools and carbon-protection mechanisms in aggregate classes influenced by surface liming in a no-till system. Geoderma, 170,80–88.

Bronick, C.J. and Lal, R. (2005). Soil structure and management: a review. Geoderma, 124,3–22

Clarholm, M., and Skyllberg, U. (2013). Translocation of metals by trees and fungi regulates pH, soil organic matter turnover and nitrogen availability in acidic forest soils. Soil Biol Biochem, 63,142–153

Denef, K., Six, J., Merckx, R., and Paustian, K. (2004). Carbon sequestration in microaggregates of no-tillage soils with different clay mineralogy. Soil Sci Soc Am J, 68(6),1935–1944

Dexter, A. R. (1988). Advances in characterization of soil structure. Soil and Tillage Research 11(3),199–238

Ferna´ndez-Ugalde, O., Virto, I., Barre´, P., Apesteguı´a, M., Enrique, A., Imaz, M. J. and Bescansa, P. (2014). Mechanisms of macroaggregate stabilization by carbonates: implications for organic matter protection in semi-arid calcareous soils. Soil Res.**,** 52(2),180–192.

Falsone, G., Catoni, M. and Bonifacio, E. (2010). Effects of calcite on the soil porous structure: natural and experimental conditions. Agrochimica, 54(1),1–12.

Gee, G.W., and Bauder, J.W. (1986). Particle-size analysis, in Klute, A., ed., Methods of soil analysis: Part 1: Madison, Wisconsin. American Society of Agronomy, 383-411.

Ghezzehei T. A (2011). Soil structure. In: Huang PA, Li Y, Sumner ME (eds) Handbook of soil sciences. CRC Press, Boca Raton,1–18

Grand, S. and Lavkulich, L. M. (2011). Depth distribution and predictors of soil organic carbon in Podzols of a forested watershed in southwestern Canada. Soil Sci., 176(4),164–174.

Gru¨newald, G., Kaiser, K., Jahn, R. and Guggenberger, G. (2006). Organic matter stabilization in young calcareous soils as revealed by density fractionation and analysis of lignin derived constituents. Org Geochem., 37(11),1573–1589.

Homann, P. S, Harmon M., Remillard S., and Smithwick E. A. H. (2005). What the soil reveals: Potential total ecosystem C stores of the Pacific Northwest region, U.S.A. For. Ecol. Manag., 220,270Y283.

Jacobs, P. M., and Mason, J. A. (2004). Pedology of soils in thick Holocene loess, Nebraska, USA, Revista Mexicana de Ciencias Geológicas,21(1) , 54-70

Jacobs, P.M. and Mason, J.A. (2007). Late Quaternary climate change, loess sedimentation, and soil profile development in the central Great Plains: A pedosedimentary model. Geological Society of America Bulletin, 119, 462. doi: 10.1130/B25868.1.

Jickells, T. D., An, Z.S., Andersen, K. K., Baker, A.R., Bergametti, G., Brooks, N., Cao, J. J., Boyd, P.W., Duce, R. A., Hunter, K. A., Kawahata, H., Kubilay, N., laRoche, J., Liss, P. S., Mahowald, Prospero, J. M., Ridgwell, A. J., Tegen, L., and Torres, R.

(2005). Global iron connections between desert dust, ocean biogeochemistry, and climate. Science, 308 (5718)

Jin, J., and Zimmerman, A. R. (2010). Abiotic interactions of natural dissolved organic matter and carbonate aquifer rock. Appl Geochem, 25(3), 472–484

Johnson, W.C., and Willey, K.L. (2000). Isotopic and rock magnetic expression of environmental changes at the Pleistocene-Holocene transition in the central Great Plains. Quaternary International, 67,89-106.

Johnson, W. C., Willey, K. L., Mason, J. A., and May, D. W. (2007), Stratigraphy and environmental reconstruction at the middle Wisconsinan Gilman Canyon formation type locality, Buzzard's Roost, southwestern /Nebraska, USA. Quaternary research,67, 474-486, https://doi.org/10.1016/j.yqres.2007.01.011

Kalbitz, K., Solinger, S., Park, J. H., Michalzik, B. and Matzner, E. (2000). Controls on the dynamics of dissolved organic matter in soils: a review. Soil Sci.**,** 165, 277–304

Kayler, Z. E., Kaiser, M., Gessler, A., Ellerbrock, R. H, Sommer, M. (2011). Application of delta C-13 and delta N-15 isotopic signatures of organic matter fractions sequentially separated from adjacent arable and forest soils to identify carbon stabilization mechanisms. Biogeosciences, 8(10), 2895– 2906

Kilmer, V.J., and Alexander, L.T. (1949). Methods of making mechanical analysis of soils: Soil Science, 68,15–24.

Kleber, M., Nico, P., Plante, A., Filley, T., and Kramer, M. (2011). Old and stable soil organic matter is not necessarily chemically recalcitrant: implication for modeling concepts and temperature sensitivity. Global change biology, 17, 1097-1107. https://doi.org/10.1111/j.1365-2486.2010.02278.x

Kleber, M., Eusterhues, K., Keiluweit, M., Mikutta, C., Mikutta, R., and Nico, P. S. (2015). Chapter One - Mineral–Organic Associations: Formation, Properties, and Relevance in Soil Environments,130, 1-140

Lal, R., Sobecki, T. M., Livari, T., and Kimble, J. M. (2003). Soil Degradation in the United States: Extent, Severity, and Trends. Lewis Publisher, Boca Raton, Florida

Lee, Y. J., Elzinga, E. J. and Reeder, R. J. (2005). Cu (II) adsorption at the calcite–water interface in the presence of natural organic matter: kinetic studies and molecular-scale characterization. Geochim Cosmochim Acta, 69(1), 49–61

Lindsay, W.L., (1979). Chemical Equilibria in Soils. Wiley, New York

Mason, J.A., and Kuzila, M.S. (2000). Episodic Holocene loess deposition in central Nebraska.

Quaternary International, 67,119–131.

Mason, J. A., Miao, X., Hanson, P. R., Jhonson, W.C., Jacob, P. M., and Goble, R. J. (2008). Loess record of the Pleistocene-Holocene transition on the northern and

central Great Plains, USA. Quaternary science review, 37,947-950, https://doi.org/10.1016/j.quascirev.2008.07.004

Marin-Spiotta, E., Chadwick, O. A., Kramer, M., and Carbone, M. S. (2011). Carbon delivery to deep mineral horizons in Hawaiian rain forest soils. Journal of geophysical research,116, G03011, doi:10.1029/2010JG001587.

Marin-Spiotta, E., Chaopricha, N. T., Plante, A. F., Diefendorf, A. F., Muller, C. W., Grandy, A. S., and Mason, J. A. (2014). Long-term Stabilization of Deep Soil Carbon by Fire and Burial During Early Holocene Climate Change. Nature Geoscience, May 25, 2014. DOI: 10.1038/NGEO2169

Mason, J. A., Miao, X., Hanson, P. R., Jhonson, W. C., Jacob, P. M. and Goble, R. J. (2008) Loess record of the Pleistocene-Holocene transition on the northern and central Great Plains, USA. Quaternary science review, 37, 947-950.

Mavi, M. S., Sanderman, J., Chittleborough, D. J., Cox, J. W., and Marschner, P. (2012). Sorption of dissolved organic matter in salt-affected soils: effect of salinity, sodicity and texture. Sci Total Environ, 435,337–344

Minick, K. J, Fisk, M. C., and Groffman, P. M. (2017). Soil Ca alters processes contributing to C and N retention in the Oa/A horizon of a northern hardwood forest. Biogeochemistry, 132,343–357

Neff, J. C., Ballantyne, A. P., Famer, G. L., Mahowald, N. M., Conroy, J. L., Landry, C. C., Overpeck, J. T., Painter, T. H., Lawrence, C. R., and Reynolds R. L. (2008). Increasing eolian dust deposition in the western United States linked to human activity. Nature – Geosciences. doi:10.1038/ngeo133.

Nelson, P., Baldock, J., and Oades, J. (1998). Changes in dispersible clay content, organic carbon content, and electrolyte composition following incubation of sodic soil. Soil Res, 36,883–897

Norris, C. E., Quideau, S. A., Bhatti, J. S. and Wasylishen, R. E. (2011). Soil carbon stabilization in jack pine stands along the Boreal Forest Transect Case Study. Glob. Chang. Biol.**,** 17, 480Y494.

Oades, J. and Waters, A. (1991). Aggregate hierarchy in soils. Soil Res, 29(6), 815–828.

Oste, L. A., Temminghoff, E. J. M. and Van Riemsdijk, W. H. (2002). Solid solution partitioning of organic matter in soils as influenced by an increase in pH or Ca concentration. Environ Sci Technol, 36, 208–214. doi:10.1021/es0100571.

Paul, E. A. and Clarks F. E. (1996). Soil microbiology and biochemistry. Academic Press, San Diego.

Peterson, J. B. (1947). Calcium linkage, a mechanism in soil granulation. Soil Sci Soc Am J, 12, 29–34

Reynolds, R., Belnap, J., Reheis, M., Lamothe, P., and Luiszer, F. (2001). Aeolian dust in Colorado Plateau soils: nutrient inputs and recent change in source. Proc. Natl. Acad. Sci. USA 98, 7123–7127

Rhoades, J. D. (1996). Salinity: Electrical conductivity and total dissolved solids. Methods of soil analysis: Part 3 Chemical methods, 5, 417-435.

Ruhe, R.V. (1983). Depositional environment of late Wisconsin loess in the midcontinental United States. In: Porter, S.C. (Ed.), Late-Quaternary Environments of the United States, Vol. 1, The Pleistocene. University of Minnesota Press, Minneapolis, pp. 130-137

Rowley, M. C., Grand, S. and Verrecchia, E. P. (2018). Calcium-Mediated stabilization of soil organic carbon. Biogeochemistry, 17, 27-49.

Salome´, C., Nunan, N., Pouteau, V., Lerch, T. Z. and Chenu, C. (2010). Carbon dynamics in topsoil and in subsoil may be controlled by different regulatory mechanisms. Glob. Chang. Biol.**,** 16, 416Y426.

Salinity Laboratory Staff US (1954) Diagnosis and improvement of saline and alkali soils. USDA Agriculture Handbook 60. United States Salinity Laboratory, Washington, 160p

Sankey, J. B., Germino, M. J., and Glenn, N. F. (2009). Aeolian sediment transport following wildfire in sagebrush steppe. Journal of arid environments,73, 912-919.

Setie, R., Rengasamy, P., and Marschner, P.(2014). Effect of mono and divalent cation on sorption of water extractable organic carbon and microbial activity. Biol Fertile Soils, 50,727-734.

Singh, M., Sarkar, B., Biswas, B., Churchman, J., and Bolan, N. S. (2016). Adsorption-desorption behavior of dissolved organic carbon by soil clay fractions of varying mineralogy. Geoderma, 280, 47-56, ISSN 0016-7061, https://doi.org/10.1016/j.geoderma.2016.06.005.

Six, J., Elliot, E.T. and Paustian, K. (2000). Soil structure and organic matter. II. A normalized stability index and effect of mineralogy. Soil Science Society of America Journal, 64, 1042–1049.

Six, J., Bossuyt, H., Degryze, S. and Denef, K. (2004). Review: A history of research on the link between (micro)aggregates, soil biota, and soil organic matter dynamics. Soil and tillage research, 79, 7–31.

Soil Science Soil Survey Laboratory Methods Manual. 1996. USDA.

Sollins, P., Homann ,P., and Caldwell, B. A. (1996). Stabilization and destabilization of soil organic matter: mechanisms and controls. Geoderma, 74(1–2), 65–105

Sposito, G. (2008) The chemistry of soils. *Oxford University Press, Oxford*.

Suzuki, S. (2002) Black tea adsorption on calcium carbonate: a new application to chalk powder for brown powder materials. Colloids Surf A., 202(1), 81–91.

Szymanski, L. M. (2021). *Spatial distribution and long-time persistence of ancient carbon in buried soils and its vulnerability to landscape disturbance* (Publication No. 28720040) [Doctoral dissertation, University of Wisconsin, Madison]. ProQuest Dissertations & Theses Global

Thomas, G. W. (1996). Soil pH and soil acidity. Methods of soil analysis: part 3 chemical methods, 5, 475-490.

Virto, I., Barre, P., and Chenu, C. (2008). Microaggregation and organic matter storage at the silt-size scale. Geoderma, 146(1–2), 326– 335

Virto, I., Moni, C., Swanston, C., and Chenu, C. (2010). Turnover of intra and extra-aggregate organic matter at the silt-size scale. Geoderma, 156(1–2),1–10

Whittinghill, K. A., Hobbie, S. E. (2012). Effects of pH and calcium on soil organic matter dynamics in Alaskan tundra. Biogeochemistry, 111(1–3), 569–581.

Wuddivira, M. N. and Camps-Roach, G. (2007). Effects of organic matter and calcium on soil structural stability. European journal of soil science, 58, 722–727

Yang, S., Cammeraat, E., Jansen, B., Cerli, C., and Kalbitz, K. (2016). Organic carbon stabilization of soils formed on acidic and calcareous bedrocks in Neotropical alpine grassland, Peru. EGU General Assembly 2016, held 17-22 April, 2016 in Vienna, Austria

Yao, Y., Chen, J., Li, F., Sun, M., Yang, X., Wang, G., Ma, J., and Sun W. (2022). Exchangeable Ca2+ content and soil aggregate stability control the soil organic carbon content in degraded Horqin grassland. Ecological Indicators, 134,108507,

Zhao, J., Chen, S., Hu, R. and Li, Y. (2017). Aggregate stability and size distribution of red soils under different land uses integrally regulated by soil organic matter, and iron and aluminum oxides. Soil Tillage Res., 16, 73–79.

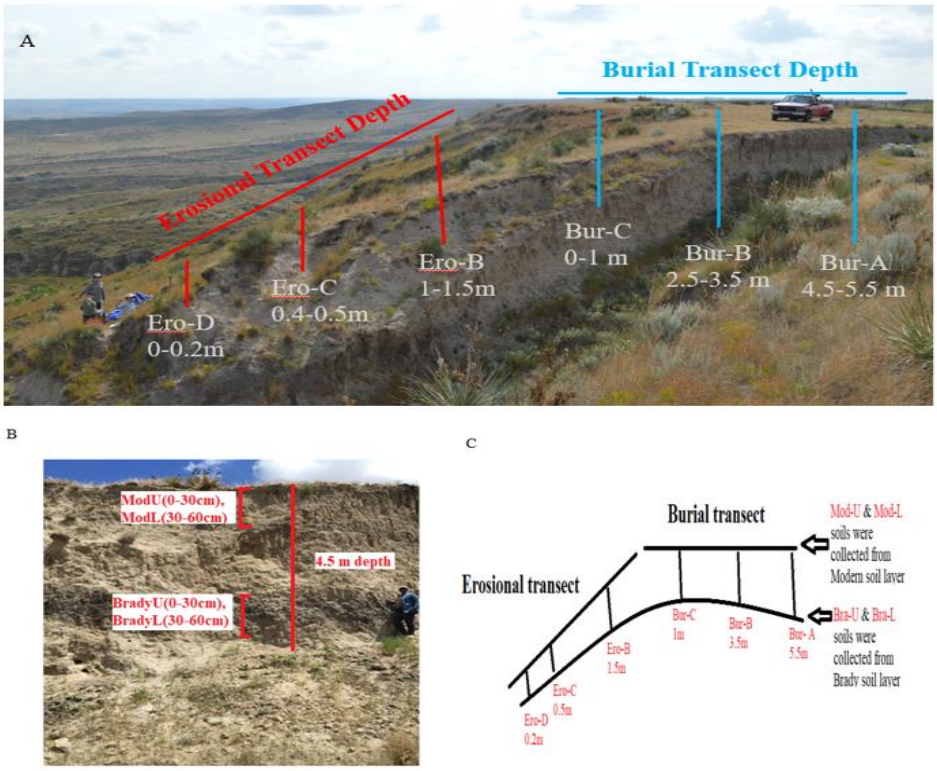

Figure 3-1 Schematic representation of sampling locations in the study system located in Nebraska. The depth of the Brady soil varies along topographic gradients, depending on whether one considers different layers of aeolian deposits the Brady soil was buried under originally (i.e., burial transect or depositional transect) vs. areas that are currently eroding (i.e., erosional). Pictures B and C is showing a detail of how the soil samples were collected from different depth categories.

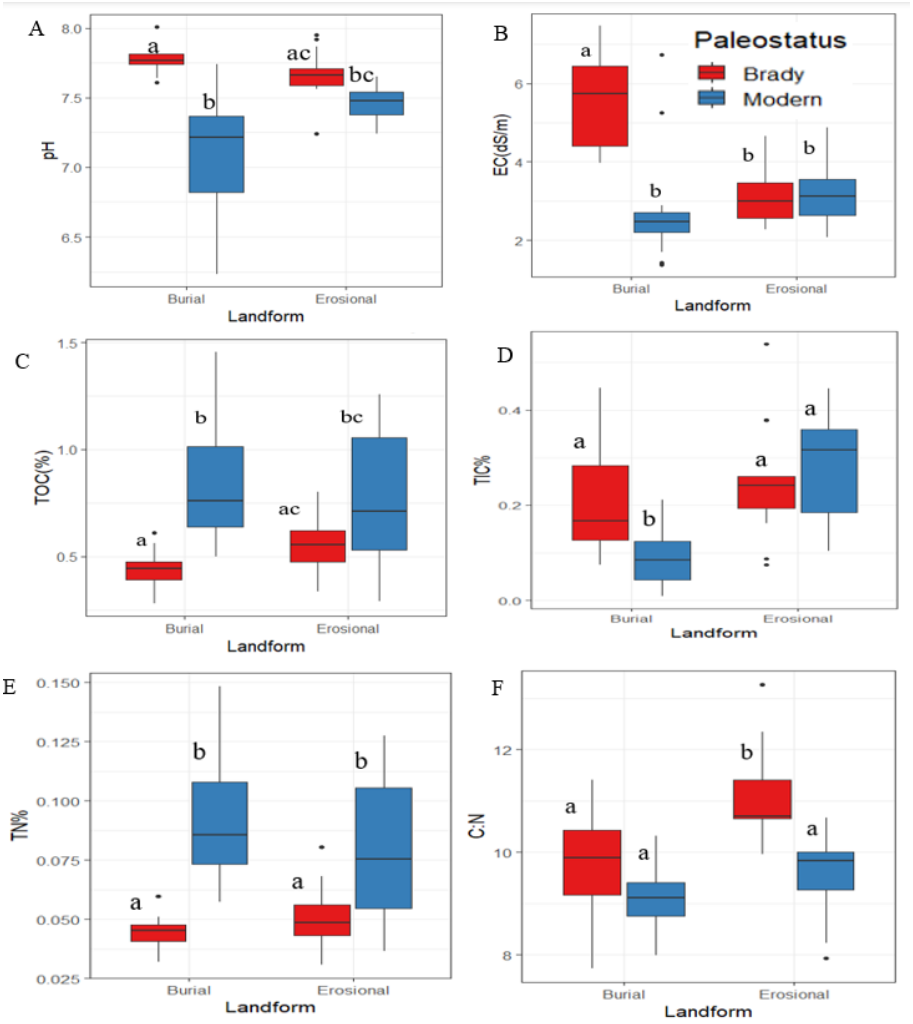

Figure 3-2 In these figures, Y-axis shows the values of pH (A) EC (B), total organic carbon (TOC%) (C), total inorganic carbon (TIC%) (D), total nitrogen (%) (E), and total organic carbon: total nitrogen (C: N) (F). The X-axis shows the paleostatus from where the soil has been collected. To understand the variability of pH, EC, TOC%, TIC%, TN%, and C: N at different soil transects/ landforms (burial vs. erosional) and paleostatus (modern vs. Brady), modern soils and Brady soils were combined depending on from which paleostatus and transect they have been collected. Brady soils were combined depending on which transect/landform they have been collected irrespective of depth category.

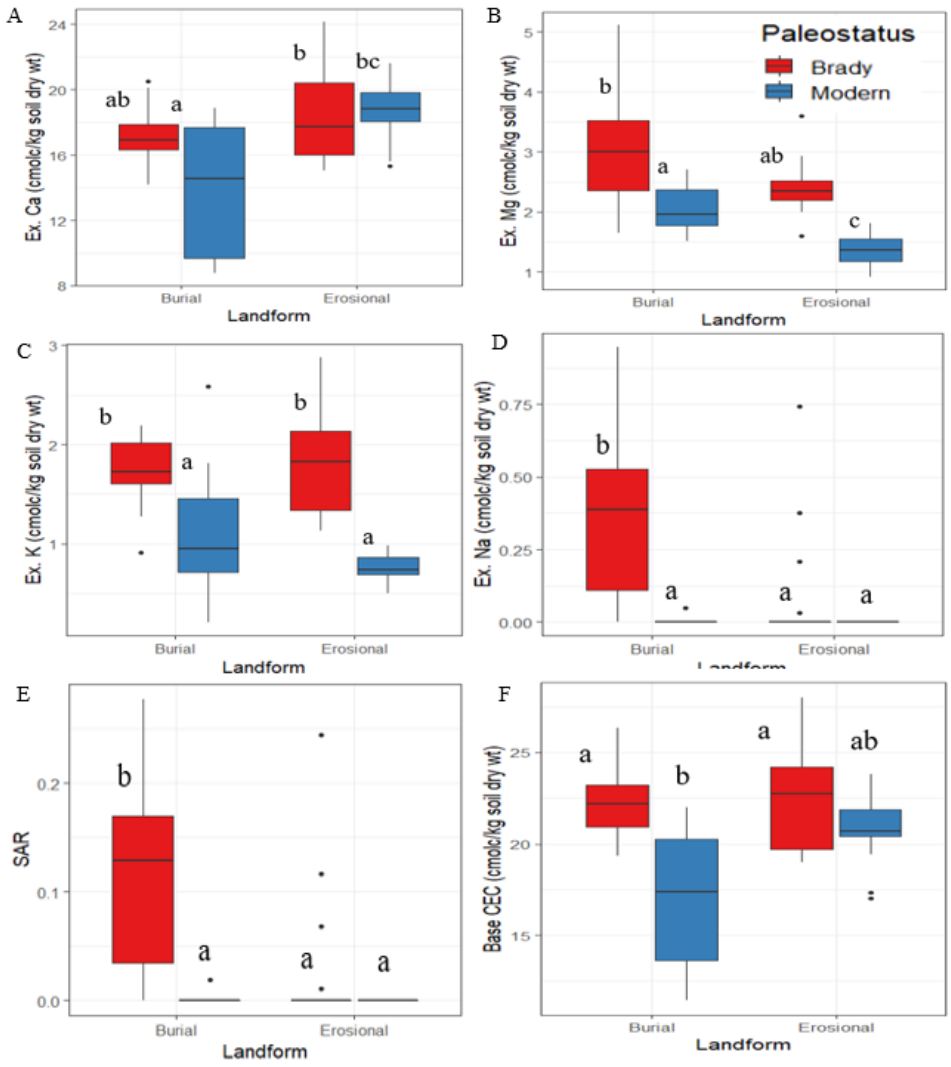

Figure 3-3 In these figures, Y-axis shows the values of exchangeable Ca (A), exchangeable Mg (B), exchangeable K (C), exchangeable Na (D), SAR (E), and base cation exchange capacity (CEC) (F). The values of the y-axis are in $cmol_c$/kg soil dry wt for exchangeable Ca, Mg, Na, and K. The X-axis shows the paleostatus from where the soil has been collected. To understand the variability of exchangeable Ca, Mg, Na, and K at different soil transects/landforms (burial vs. erosional) and paleostatus (modern vs. Brady), modern soils and Brady soils were combined depending on which paleostatus they have been collected. Brady soils were combined depending on which paleostatus and transect/landform they have been collected, irrespective of depth category.

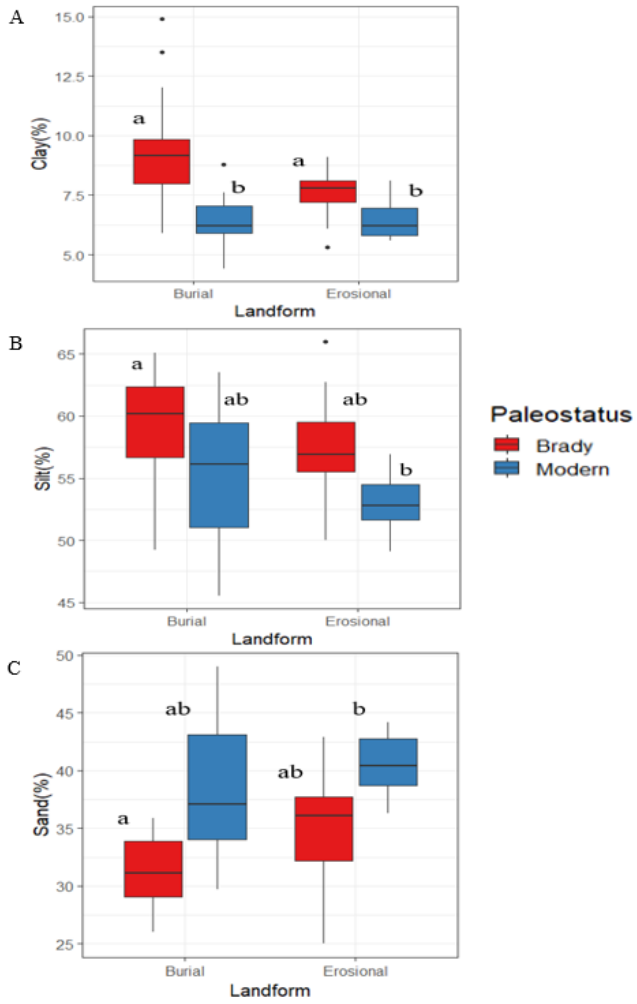

Figure 3-4 In these figures, Y-axis shows the values of exchangeable clay percentage (A), silt percentage (B), and sand percentage(C). To understand the variability of clay, silt, and sand at different soil transects/landform (burial vs erosional) and paleostatus (modern vs Brady), modern soils and Brady soils were combined depending on from which paleostatus and transect they have been collected. Brady soils were combined depending on which transect/landform they have been collected irrespective of depth category.

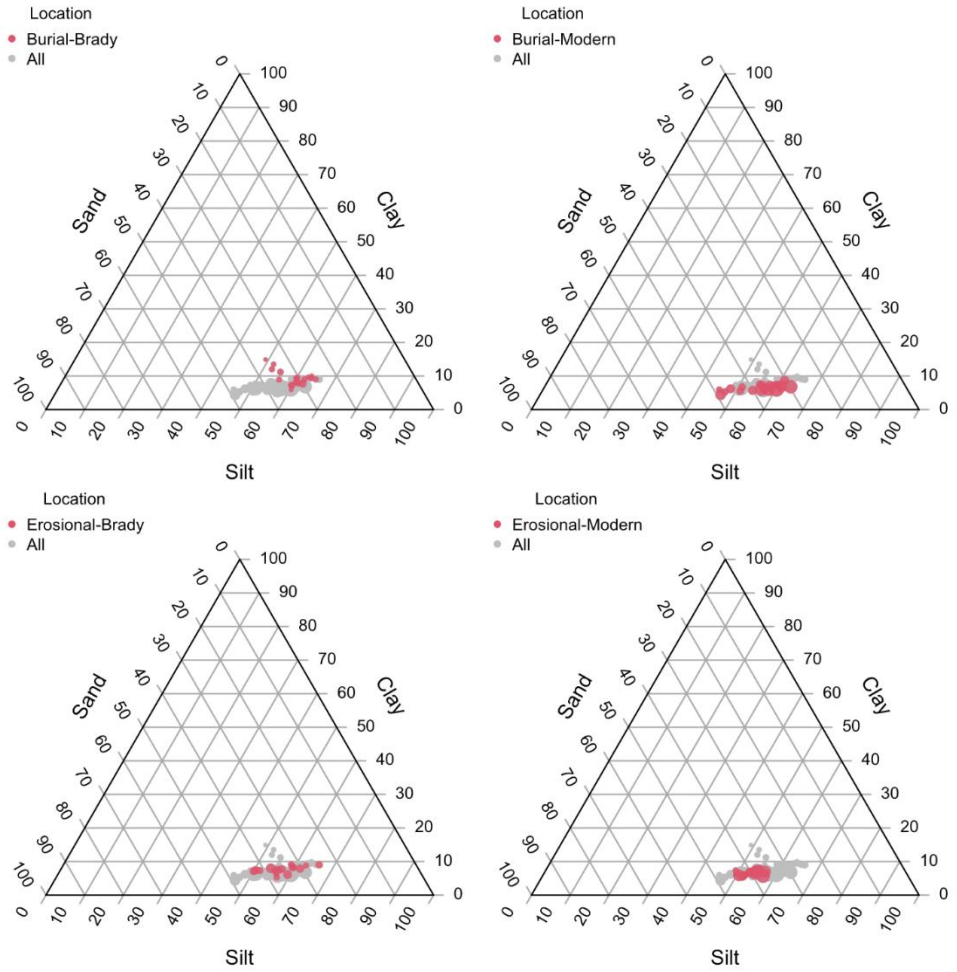

Figure 3-5 Soils showing the texture class. The red color shows the soils present in the landform (Depositional or erosional) and paleostatus (Brady or modern), while the grey color shows all the other soils. To understand the variability of texture at different soil transects/landforms (burial vs. erosional) and paleostatus (modern vs Brady), modern soils and Brady soils were combined depending on which paleostatus and transect/landform they were collected. Brady soils were combined depending on which transect/landform they have been collected, irrespective of depth category

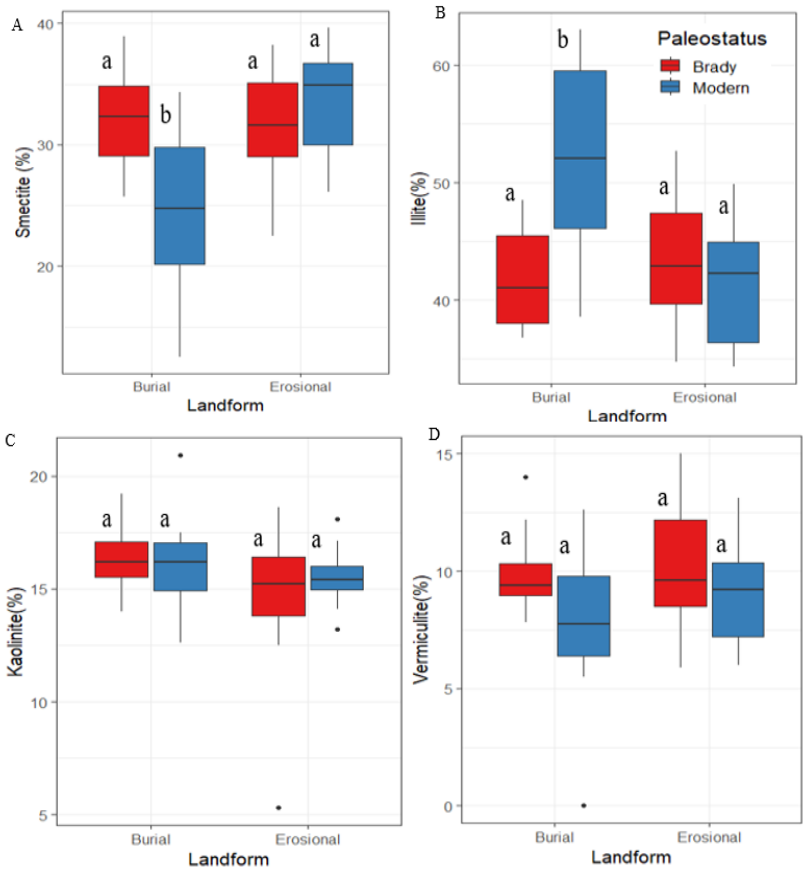

Figure 3-6 In these figures, Y-axis shows the values of exchangeable smectite (A), illite (B), kaolinite (C), and vermiculite (D). The values of the y-axis are in percentage. The X-axis shows the paleostatus from where the soil has been collected. To understand the variability of smectite, illite, kaolinite, and vermiculite of these soils, modern soils and Brady soils were combined depending on which paleostatus (modern vs Brady) and transect/landform (burial vs erosional) they were collected. Brady soils were combined depending on which transect/landform (burial vs erosional) they have been collected irrespective of depth category.

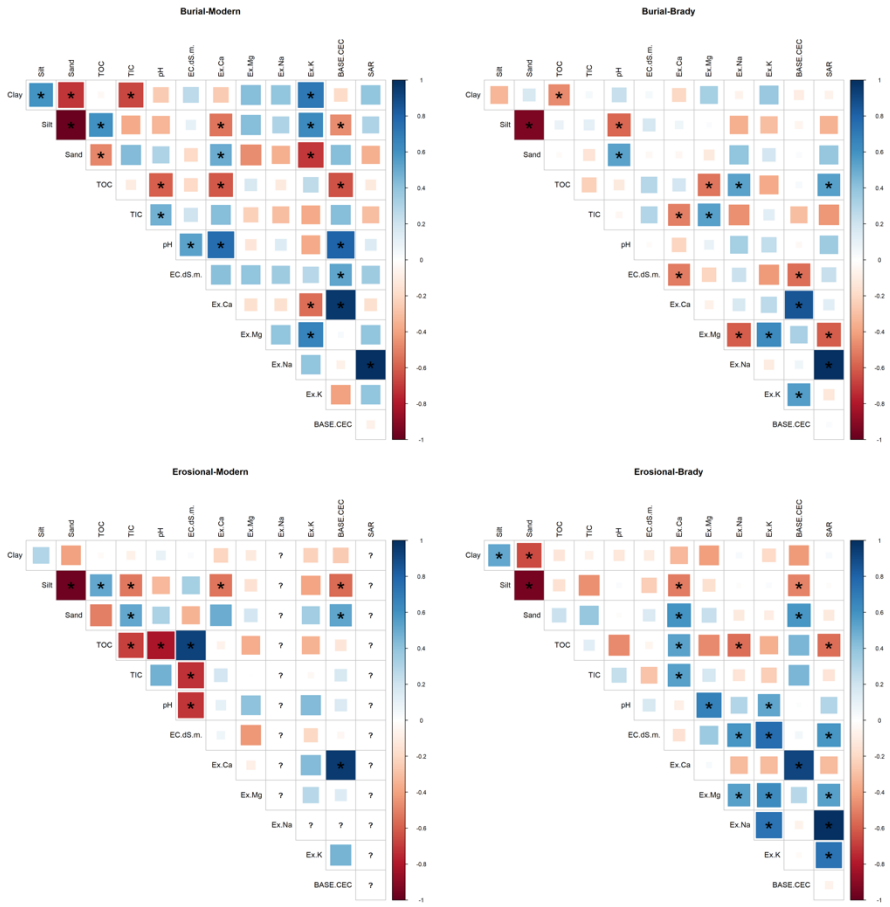

Figure 3-7 Spearman's correlation coefficient matrix divided into four different groups. To understand correlations of these soils, modern soils and Brady soils were combined depending on from which paleostatus (modern vs Brady) and transect/landform (burial vs erosional) they were collected. Brady soils were combined depending on which transect/landform (burial vs erosional) they have been collected irrespective of depth category. The value of positive (blue) and negative (red) and the correlation coefficient as variation in rectangle size. Asterix signs were added if the correlation coefficients are significant (α =0.05).

Table 3-1. Bulk soil texture, total organic carbon (TOC%), total inorganic carbon (TIC%), pH and electrical conductivity data of modern and Brady soils collected from burial and erosional landform at 6 different depth categories. In this table, L= lower layer of soil and U= upper layer of the soil.

Landform	Paleostatus	Soil Layer	Depth to Brady(m)	Clay	Silt	Sand	TOC%	TIC%	pH	EC(dS/m)
Burial	Brady	L	5.5	7.2	59.9	32.8	0.53	0.13	7.8	4.6
Burial	Brady	L	5.5	7.9	61.2	30.9	0.56	0.10	7.7	7.2
Burial	Brady	L	5.5	12	52.3	35.7	0.45	0.13	7.8	5.9
Burial	Brady	L	3.5	9	62.2	28.8	0.44	0.26	7.7	6.7
Burial	Brady	L	3.5	9.7	62.8	27.5	0.30	0.07	7.7	4.2
Burial	Brady	L	3.5	14.9	49.2	35.9	0.28	0.15	7.8	6.3
Burial	Brady	L	1.5	9.3	63.7	27	0.44	0.29	7.8	7.5
Burial	Brady	L	1.5	9.4	59.9	30.7	0.42	0.18	7.8	4.0
Burial	Brady	L	1.5	5.9	60.3	33.8	0.32	0.29	7.8	5.5
Eros.	Brady	L	1.5	8.8	62.7	28.5	0.43	0.20	8.0	3.5
Eros.	Brady	L	1.5	7.9	61.6	30.5	0.68	0.09	7.6	3.6
Eros.	Brady	L	1.5	7.2	55.5	37.3	0.53	0.16	7.2	4.7
Eros.	Brady	L	0.5	9.1	58.7	32.1	0.48	0.26	7.7	2.4
Eros.	Brady	L	0.5	8.1	59.7	32.2	0.52	0.07	7.6	2.6
Eros.	Brady	L	0.5	5.3	56.9	37.7	0.49	0.20	7.8	2.6
Eros.	Brady	L	0.2	7.3	51.5	41.2	0.56	0.26	7.7	3.6
Eros.	Brady	L	0.2	6.1	59.3	34.6	0.73	0.38	7.7	2.4
Burial	Brady	U	5.5	7.3	59.6	33.1	0.47	0.11	7.8	4.3
Burial	Brady	U	5.5	7.7	62.4	30	0.61	0.31	7.6	7.1
Burial	Brady	U	5.5	11.2	54.9	33.9	0.50	0.13	8.0	5.6
Burial	Brady	U	3.5	8.2	60.4	31.4	0.48	0.16	7.8	6.0
Burial	Brady	U	3.5	9	65.1	26	0.44	0.11	7.7	4.1
Burial	Brady	U	3.5	13.5	52	34.6	0.39	0.26	7.8	6.3
Burial	Brady	U	1.5	9.9	63.6	26.5	0.38	0.45	7.8	6.5
Burial	Brady	U	1.5	9.6	60.1	30.3	0.40	0.39	7.8	4.0
Burial	Brady	U	1.5	8.9	55.7	35.4	0.43	0.26	7.6	4.7
Eros.	Brady	U	1.5	8	55.7	36.3	0.34	0.54	7.9	3.1
Eros.	Brady	U	1.5	9	66	25	0.58	0.16	7.7	3.0
Eros.	Brady	U	1.5	7.3	56.6	36.1	0.46	0.19	7.9	4.2
Eros.	Brady	U	0.5	8.3	59.5	32.3	0.62	0.26	7.6	2.4
Eros.	Brady	U	0.5	7.8	57	35.2	0.60	0.23	7.6	2.9
Eros.	Brady	U	0.5	6.4	56.2	37.4	0.45	0.24	7.7	2.3
Eros.	Brady	U	0.2	7.4	50.4	42.1	0.69	0.38	7.6	3.2
Eros.	Brady	U	0.2	7.1	50	42.9	0.62	0.24	7.7	3.2

Landform	Paleostatus	Soil Layer	Depth to Brady(m)	Clay	Silt	Sand	TOC %	TIC %	pH	EC(dS/m)
Eros.	Brady	L	0.2	8	54	37.9	0.80	0.25	7.6	2.6
Burial	Modern	L	5.5	5.5	51.1	43.4	0.62	0.11	7.4	1.4
Burial	Modern	L	5.5	5.3	47.3	47.5	0.60	0.21	7.5	2.4
Burial	Modern	L	5.5	5.9	45.5	48.6	0.50	0.18	7.5	2.8
Burial	Modern	L	3.5	7.3	59.9	32.9	0.70	0.06	7.7	6.7
Burial	Modern	L	3.5	6.2	57	36.8	0.80	0.11	7.6	2.9
Burial	Modern	L	3.5	6.7	51	42.3	0.61	0.06	7.3	2.6
Burial	Modern	L	1.5	8.8	60.9	30.3	0.73	0.01	7.4	5.3
Burial	Modern	L	1.5	7.6	55.1	37.3	0.57	0.01	6.8	1.4
Burial	Modern	L	1.5	7.2	56	36.8	0.77	0.03	6.9	2.4
Eros.	Modern	L	1.5	6.2	49.6	44.2	0.35	0.39	7.7	2.1
Eros.	Modern	L	1.5	5.7	52	42.3	0.29	0.32	7.6	2.1
Eros.	Modern	L	1.5	7.3	49.1	43.7	0.51	0.43	7.5	2.8
Eros.	Modern	L	0.5	6.8	52.8	40.4	0.67	0.23	7.6	3.0
Eros.	Modern	L	0.5	6	52.1	42	0.59	0.26	7.4	2.9
Eros.	Modern	L	0.5	8.1	54.7	37.1	0.55	0.36	7.5	2.1
Burial	Modern	U	5.5	4.4	46.6	49	0.91	0.05	7.0	2.2
Burial	Modern	U	5.5	5.7	54.2	40.1	0.75	0.15	7.4	2.5
Burial	Modern	U	5.5	6.2	48.3	45.5	0.74	0.16	7.3	2.8
Burial	Modern	U	3.5	6.9	61	32.1	1.05	0.04	7.0	1.7
Burial	Modern	U	3.5	5.9	58.2	35.9	1.11	0.10	7.1	2.2
Burial	Modern	U	3.5	6	56.3	37.7	1.19	0.10	6.5	1.4
Burial	Modern	U	1.5	6.8	63.5	29.7	1.21	0.13	6.8	2.5
Burial	Modern	U	1.5	7.1	58	34.9	0.87	0.01	6.2	2.5
Burial	Modern	U	1.5	6.2	60.1	33.7	1.46	0.07	6.8	2.6
Eros.	Modern	U	1.5	5.7	51.7	42.7	0.71	0.34	7.5	3.3
Eros.	Modern	U	1.5	6.2	53.5	40.4	0.46	0.36	7.6	2.4
Eros.	Modern	U	1.5	5.9	50.6	43.5	1.05	0.14	7.3	3.8
Eros.	Modern	U	0.5	5.7	56.9	37.5	1.26	0.15	7.2	3.5
Eros.	Modern	U	0.5	5.6	51.6	42.8	0.75	0.44	7.4	3.1
Eros.	Modern	U	0.5	7	54.6	38.4	1.19	0.10	7.3	4.9
Eros.	Modern	U	0.2	6.6	54.4	39	1.19	0.14	7.5	4.2
Eros.	Modern	U	0.2	6.9	53	40.1	0.72	0.32	7.5	3.4
Eros.	Modern	U	0.2	7	56.7	36.3	1.07	0.22	7.5	3.6

Table 3-2. Bulk soil base cation exchange concentration data for modern and Brady soils collected from burial and erosional landform at 6 different depth categories. In this table, L= lower layer of soil and U= upper layer of the soil.

Landform	Paleostatus	Soil Layer	Depth to Brady(m)	Ex.Ca	Ex.Mg	Ex.Na	Ex.K	Base CEC	SAR
Burial	Brady	L	5.5	16.30	1.78	0.46	1.28	19.81	0.15
Burial	Brady	L	5.5	19.23	2.08	0.49	1.44	23.24	0.15
Burial	Brady	L	5.5	17.00	2.31	0.53	1.71	21.55	0.17
Burial	Brady	L	3.5	16.68	2.72	0.79	1.65	21.85	0.25
Burial	Brady	L	3.5	17.95	2.51	0.21	1.49	22.16	0.07
Burial	Brady	L	3.5	14.92	2.82	0.38	1.67	19.79	0.13
Burial	Brady	L	1.5	14.98	4.06	0.08	1.59	20.70	0.03
Burial	Brady	L	1.5	16.85	4.59	0.08	2.02	23.53	0.02
Burial	Brady	L	1.5	17.66	3.51	0.19	1.84	23.20	0.06
Eros.	Brady	L	1.5	17.91	2.93	0.38	2.88	24.10	0.12
Eros.	Brady	L	1.5	15.37	2.00	NA	1.91	19.25	0.00
Eros.	Brady	L	1.5	16.01	2.44	0.74	2.47	21.66	0.24
Eros.	Brady	L	0.5	16.23	2.13	NA	1.18	19.38	0.00
Eros.	Brady	L	0.5	15.99	2.20	NA	1.33	19.40	0.00
Eros.	Brady	L	0.5	17.75	3.60	NA	1.80	23.00	0.00
Eros.	Brady	L	0.2	18.48	2.52	NA	1.83	22.76	0.00
Eros.	Brady	L	0.2	21.10	2.52	NA	1.83	25.33	0.00
Burial	Brady	U	5.5	17.72	2.21	0.60	1.74	22.26	0.19
Burial	Brady	U	5.5	16.38	1.65	0.39	0.91	19.33	0.13
Burial	Brady	U	5.5	20.12	3.24	0.95	2.04	26.34	0.28
Burial	Brady	U	3.5	16.74	3.04	0.82	1.70	22.31	0.26
Burial	Brady	U	3.5	20.50	2.97	0.36	2.18	26.01	0.11
Burial	Brady	U	3.5	16.13	3.28	0.51	2.19	22.11	0.16
Burial	Brady	U	1.5	14.19	3.57	0.00	1.88	19.33	0.00
Burial	Brady	U	1.5	18.22	5.11	0.00	2.00	25.29	0.00
Burial	Brady	U	1.5	17.10	3.53	0.08	2.04	22.75	0.03
Eros.	Brady	U	1.5	15.76	2.63	0.03	2.16	20.59	0.01
Eros.	Brady	U	1.5	15.06	2.22	0.00	1.83	19.00	0.00
Eros.	Brady	U	1.5	16.17	2.54	0.21	2.75	21.66	0.07
Eros.	Brady	U	0.5	19.38	2.25	0.00	1.25	22.88	0.00
Eros.	Brady	U	0.5	20.42	2.16	0.00	1.64	24.23	0.00
Eros.	Brady	U	0.5	16.29	2.23	0.00	1.34	19.71	0.00
Eros.	Brady	U	0.2	24.16	2.35	0.00	1.47	27.98	0.00
Eros.	Brady	U	0.2	21.90	2.44	0.00	2.14	26.47	0.00
Eros.	Brady	L	0.2	21.62	1.60	0.00	1.13	24.21	0.00

Landform	Paleostatus	Soil Layer	Depth to Brady(m)	Ex.Ca	Ex.Mg	Ex.Na	Ex.K	Base CEC	SAR
Burial	Modern	L	5.5	16.81	1.75	0.00	0.49	19.05	0.00
Burial	Modern	L	5.5	17.59	1.52	0.00	0.63	19.73	0.00
Burial	Modern	L	5.5	17.12	2.16	0.00	1.07	20.34	0.00
Burial	Modern	L	3.5	17.73	1.88	0.00	0.79	20.40	0.00
Burial	Modern	L	3.5	18.04	2.48	0.00	1.49	22.01	0.00
Burial	Modern	L	3.5	18.89	2.03	0.00	0.78	21.70	0.00
Burial	Modern	L	1.5	10.43	2.71	0.05	2.58	15.77	0.02
Burial	Modern	L	1.5	14.03	2.43	0.00	1.12	17.58	0.00
Burial	Modern	L	1.5	9.43	1.66	0.00	1.36	12.45	0.00
Eros.	Modern	L	1.5	18.09	1.63	0.00	0.83	20.55	0.00
Eros.	Modern	L	1.5	18.00	1.67	0.00	0.98	20.66	0.00
Eros.	Modern	L	1.5	19.77	1.31	0.00	0.73	21.82	0.00
Eros.	Modern	L	0.5	19.89	1.81	0.00	0.78	22.49	0.00
Eros.	Modern	L	0.5	18.83	1.36	0.00	0.86	21.05	0.00
Eros.	Modern	L	0.5	18.41	1.55	0.00	0.73	20.70	0.00
Burial	Modern	U	5.5	15.03	1.89	0.00	0.21	17.13	0.00
Burial	Modern	U	5.5	17.94	1.52	0.00	0.46	19.92	0.00
Burial	Modern	U	5.5	18.10	1.93	0.00	0.70	20.72	0.00
Burial	Modern	U	3.5	11.39	1.84	0.00	0.89	14.11	0.00
Burial	Modern	U	3.5	11.25	2.19	0.00	0.77	14.21	0.00
Burial	Modern	U	3.5	8.75	1.66	0.00	1.02	11.43	0.00
Burial	Modern	U	1.5	9.06	2.59	0.00	1.81	13.46	0.00
Burial	Modern	U	1.5	8.78	2.00	0.00	1.70	12.47	0.00
Burial	Modern	U	1.5	9.05	2.51	0.00	1.66	13.09	0.00
Eros.	Modern	U	1.5	21.17	1.53	0.00	0.89	23.59	0.00
Eros.	Modern	U	1.5	18.84	1.17	0.00	0.67	20.69	0.00
Eros.	Modern	U	1.5	21.61	1.35	0.00	0.87	23.83	0.00
Eros.	Modern	U	0.5	15.32	1.50	0.00	0.50	17.32	0.00
Eros.	Modern	U	0.5	19.99	1.20	0.00	0.71	21.90	0.00
Eros.	Modern	U	0.5	17.27	1.55	0.00	0.60	19.41	0.00
Eros.	Modern	U	0.2	19.36	1.14	0.00	0.74	21.24	0.00
Eros.	Modern	U	0.2	15.61	0.91	0.00	0.50	17.03	0.00
Eros.	Modern	U	0.2	18.47	1.09	0.00	0.88	20.28	0.00

Chapter 4.
Vulnerability of buried vs. modern soil organic matter to changes in water content: an attempt to infer the effect of changing precipitation patterns on SOM loss from paleosols

Abstract

Paleosols that are formed when the topsoil gets buried by lateral distribution of soil can store large quantities of soil organic matter (SOM) that may persistent over millennial timescales due to its detachment from the disturbances at the surface. We studied buried SOM dynamics in the Brady paleosol, a deep loess (aeolian) deposit in Nebraska, USA where climate has historically driven varying rates of loess deposition during the late Pleistocene and Holocene, burying soils up to 50 m below the surface. Soils were sampled along the burial and erosional transects at the depths from 0.2 to 4.2 m to understand the variability in physical and chemical composition of the soils in buried vs modern surface. We determined SOM composition using Fourier Transformed Infrared Spectroscopy (FTIR), total organic carbon, total nitrogen and other soil physio-chemical properties with SOM composition along with gradients from modern to buried soil layers in the Brady paleosol. Our data suggested, presence of less decomposed SOM in the buried layers and erosional landform shallower depth buried soil SOM are similar to the modern soils. We also determined the vulnerability of SOM by the addition of moisture. We added water to soil from the different transects and depths, at 60% pore space capacity in two different experimental set ups – repeated wet and drying cycles, and continuously wet. We found that erosional transect modern and Brady soils are more vulnerable to SOM decomposition in both continuous wet and wet-dry cycle. Our two-pool model fit indicated, slow cycling pool is dominant in these soils and burial transect Brady soil has the highest amount of slow cycling soil organic carbon (SOC) pool. Fast cycling pool of the Brady layers are faster than the modern counterpart indicating that the fast-cycling available SOC that was previously protected will decompose faster when brought to the modern environment.

4.1 Introduction

The subsoil environment is estimated to account for approximately half of the total global soil organic C (SOC) **(**Jobbágy & Jackson, 2000**).** Generally, the SOC that enters the deep soil horizons via (a) the transport of dissolved organic C (DOC), (b) movement of aboveground/root litter along root channels, or (c) through bioturbation is characterized by high mean residence times and low carbon-to-nitrogen (C/N) ratio, indicating that organic matter (OM) in deep soil horizons is highly processed **(**Rumpel & Kögel-Knabner, 2010**).** In comparison, ancient topsoils buried under aeolian, or alluvial deposits retain soil organic C that reflects the near-surface pedogenic conditions of the past environment, which may deviate significantly from the present conditions (Marin-Spiotta

et al., 2014). Although the total amount of C in soil buried during ancient and modern times is unknown, the frequency of landscape change and disturbance by various climatic, geologic, and anthropogenic events suggests that it is likely a significant pool (Marin-Spiotta et al., 2014; Chaopricha et al., 2014).

4.1.1 Stabilization of SOC in Subsurface Horizons

The subsurface horizons lack microbially favorable conditions of aeration, moisture, and fresh substrate inputs, so they can be suitable for preserving SOC for decades to centuries **(**Rumpel et al., 2012; Soong et al., 2021**).** Therefore, geomorphic processes that lead to the depositional of topsoil SOC may constitute a terrestrial sink for atmospheric CO_2 **(**Berhe et al., 2007; Stacy et al., 2015**).**

However, SOC buried in deep layers may become an active component in the global C cycle as the predicted warmer, wetter, and more extreme climate will lead to higher erosion rates and exposure of formerly buried layers to oxidizing near-surface environments **(**Fontaine et al., 2007**).** For example, after topsoil erosion, stable SOC from the buried paleosol can mix with the fresh labile plant residue and be subjected to a faster turnover rate **(**Doetterl et al., 2012**).** Similarly, sustained whole-soil warming can lead to a substantial loss of subsoil SOC and N stocks **(**Soong et al., 2021**).** In addition, road construction or changes in soil hydrology and plant rooting depths can reconnect buried SOC to conditions favorable for decomposition. In a rainfall manipulation study, Berhe et al. (2012) found that an increase in winter rainfall decreases the mineral-organic matter stabilization by Al and Fe oxides, indicating that changes in the timing of seasonal precipitation can destabilize old SOC.

The sensitivity of buried SOC to the changing environmental condition depends on the types of soil minerals present and the soil's response to the change in annual to decadal timescale **(**Harrison et al., 2011**).** Therefore, predicting the fate and vulnerability of buried SOC to climate change and landscape disturbance calls for an in-depth understanding of the mechanisms contributing to storage and turnover in these pools and their response to changing environmental conditions.

4.1.2 Study Goals

This study aimed to compare stoichiometric composition and sensitivity to precipitation of buried and modern soil organic matter (SOM) collected from erosional and depositional transects of a prominent paleosol (Brady soil) buried by loess between ca. 13 to 10 kya at different depths and landforms in the Central Great Plains, Nebraska. The guiding hypotheses of this study were (a) elevated moisture and near-surface aeration will initiate the decomposition of previously preserved in buried Brady soil, (b) buried SOM in the erosional transect is more vulnerable than the depositional transect as the shallower depth along with erosion allows mixing of new C with the SOC, and (c) high concentrations of pyrogenic SOC (Marin-Spiotta et al., 2014) in the buried SOM of the depositional transect renders it slower turnover rate.

In this study, we conducted a controlled in-situ experiment on soils from Wauneta, Nebraska, to understand the effect of different amounts of moisture and C mineralization from buried soil present at different depths vs modern soils collected from the top of these different depths buried soils. We choose two different landscapes as the amount of

SOC can vary spatially depending on the landscape and climate history, thus making it difficult to understand the effect of different moisture addition on soils from different landscapes. Our objective of this study was to understand CO_2 efflux to water addition in buried paleosol vs modern soils. By using a laboratory incubation, we tried to answer the following questions: What is the vulnerability of Brady soil SOM to the input of water? Are the Patterns of soil CO_2 efflux in response to dissimilar water addition (continuous wet vs wet-dry-rewet) events the same between the modern and Brady soil at erosional and depositional landforms? How does short-term pulse impact C release from Brady and modern soils?

4.2 Materials and Method

4.2.1 Site descriptions

Incubation soils used in this study were collected from the Wauneta, Nebraska, Great Plains, where climate-driven varying rates of loess deposition during the Late Pleistocene and Holocene resulted in sequences of buried soils in thick loess deposits (Johnson et al., 2007). The mean annual temperature of this area is 9.7°C, mean annual precipitation is 495 mm (seasonal). This area sees snowfall from October to April, and most of the rainfall occurs during the summer months with a mean temperature of 25.7°C (Woodburn et al., 2016; US Climate data). The vegetation is mixed C3, C4, and short grass prairie, and the land is cultivated where the topography permit and grazed where the topography doesn't. One especially prominent paleosol here, known as Brady soil, formed between cs. 13 to 10 kya and was buried by loess (Mason et al., 2008). Brady soil is a morphologically distinct stratigraphic and paleoenvironmental marker in the central great plains (c). Brady soil was formed due to aeolian deposition which has an important beneficial effect such as nutrient transportation to the terrestrial and aquatic system (Sankey et al., 2009; Neff et al., 2008; Lal et al., 2003; Jickells et al., 2005; Reynolds et al., 2001). Jacobs and Mason, (2004) study found that the Brady soil has A, B, and C horizon morphology. The A horizon is very dark greyish brown, and the texture is invariably silt loam. The dark color of the Brady soil A horizon is suggested coming from the biogeochemically stable clay-organic matter complexes (Jacobs and Mason, 2004) depending on a Mollisols study in that region, but the organic carbon chemistry in the Brady soil is not studied well. Secondary calcium carbonates are present in the A and other horizons of the Brady soil. Previous works have suggested that Brady soil was formed in a stable landscape (Mason and Kuzila, 2000), and it had time to form because of the reduction in the deposition rate (Jacobs and Mason, 2007). Here the modern soils are loess derived Mollisols.

Soil samples from the buried Brady soil and overlying modern soils were collected from two different topographical sequences- erosional and depositional landform in the summer of 2016 and 2017 to account for the differences in depth of depositional and increasing exposure of buried soils due to erosional processes and modern soil formation processes (Figure 1). The depositional (depositional) landform Brady soil samples were collected from depths of ~5.5m(A), ~3m(B), and ~1m(C), whereas the erosional Brady soil samples were collected from the depth of 1-1.5m(B), ~0.5m(C) and ~0.2m(D), where the letters-A, B, C, and D represent locations within the landform (see Figure 1. Soils were sampled using Giddings's probe (Giddings Machine Company; Windsor, CO) in 10.2 or 8.9m sampling tubes for the depositional landform and by digging pits for the erosional landform (see details in Szymanski et al., 2022, in preparation). For all the

locations, the sampled depths include Modern upper (0-30cm), and as soon as we hit the buried Brady layer Brady upper (0-30cm), soils were collected for this incubation study. All the reported soil physio-chemical property values are the mean of the three replicates of the 6 sequential depth categories of the continuum of buried to ~5.5 m, ~3m, ~1m, and eroded to ~1.5m, ~0.5m, and ~0.2m for a total of 18 sample locations identified as either depositional (depositional) or erosional. Soil landforms, sampling locations, and different depth categories of Brady soil were selected using information from prior research (Jacobs and Mason, 2004; Marin-Spiotta et al., 2014; Mason et al., 2008).

4.3 Soil chemical and physical properties

4.3.1 Soil pH and EC

Bulk soil pH was measured in a 1:2 (suspension: solution) slurry in deionized water and 0.01M $CaCl_2$ (Mason and Kuzila 2000), and soil electrical conductivity (EC) was measured in a 1:1 (soil: water) mixture by using a soil survey laboratory manual (1996) at University of Wisconsin, Madison. Detail of this experiment has been provided in Chapter 1, section 2.2.

4.3.2 Soil particle size analysis

Soil particle size was determined by high-resolution particle size analysis by laser diffraction by using a Mastersizer 2000 particle size analyzer (Malvern Panalytical, Malvern, UK) (Jacobs and Mason 2007) at the University of Wisconsin, Madison. First, the soil samples were dispersed with 10ml of 50mg/L sodium- hexametaphosphate (Na-HMP) and sonicated by a 6m ultrasound. Clay contents were determined by wet sieving and pipette separation with H_2O_2 and sodium acetate buffer to remove the aggregation caused by organic matter and the presence of carbonate (Kilmer and Alexander 1949; Gee and Bauder 1986; Jacobs and Mason 2007). The details of this analysis have been given in Szymanski (2021)

4.3.3 Bulk soil stable isotope, C and N concentrations

Before incubation, the bulk soils were analyzed for concentration of C, N, and $\delta^{13}C$, $\delta^{15}N$ isotopes. Approximately 70 (±0.5) mg of soil were weighed out into a tin capsule for N concentration and $\delta^{15}N$ analysis, whereas 10(±0.5) mg of soil were weighed out into a silver capsule, incubated with 12.1(M) hydrochloric acid (HCl) (Harrison et al., 2001) to remove the carbonate and hence got the organic C concentration and $\delta^{13}C$ values of the organic C. All the analyses were done at the Stable Isotope Ecosystems lab (SIELO), the University of California, Merced using a 4010-elemental analyzer (Costech) that is attached to a ThermoFisher Delta V Plus isotope ratio mass spectrometer (IRMS) with Conflo IV interfaces. The calibration curve was produced using- USGS 40 L-Glutamic Acid, USGS41a L-Glutamic Acid, EA sediment, and Costech Acetanilide to provide a corrected $\delta^{13}C_{VPDB}$ value. The details have been provided in Chapter 2.

4.3.4 Chemical composition of the bulk soil

Prior to the incubation, samples were analyzed for chemical composition by diffuse reflectance infrared fourier transform (DRIFT) spectroscopy under a vacuumed chamber by using a BrukerIFS 66v/S IR system (Ettlingen, Germany) equipped with a Praying Mantis DRIFT apparatus (Harrick Scientific Corporation, Ossining, NY) and background correction was carried out using OPUS-6.5 software. We recorded IR absorbances in the

mid-IR range (400 to 4000 cm^{-1}) at a resolution of 4 cm^{-1}. In all cases, 500 scans of the sample were recorded with a KBr background. Soil samples didn't need to be diluted to understand the variability of the soil organic compound. Baseline corrected DRIFT peak areas of three main functional groups: aliphatic (C-H), aromatic (C=C), and carboxylic (C= O) were selected based on previous research (Ellerbrock et al., 2004; Parikh et al., 2014; Ryals et al., 2014; Viscarra Rossel et al., 2016; Hall et al., 2018; Mainka et al., 2022). These groups indicate differences in chemical properties as described in Mainka et al., 2022 Table.1. Peak area 2898-2976 cm^{-1} and 2839-2870 cm^{-1} was attributed to aliphatic C-H (Parikh et al., 2014; Hall et al., 2018) and presented as simple plant-derived organic compounds (S-POM) (Mainka et al., 2022). Peak area 1500-1550 cm^{-1} represented as C=C aromatic compound (Parikh et al., 2014; Hall et al., 2018) and related to lignin-derived complex compound (C-POM) (Ryals et al., 2014; Mainka et al., 2022). Peak area 1660- 1580 cm^{-1} represented carboxylic C=O (Parikh et al., 2014) and was interpreted as microbially derived organic compounds (MOM) (Kögel-Knabner and Amelung, 2014; Mainka et al., 2022).

4.3.5 Incubation Experiments

4.3.5.1 Soil preparation

Soils used in continuous wet and drying-rewetting experiments were collected from modern soil upper surface (0-30cm) and Brady soil upper layer (0-30cm) as soon as we reached the different depths of Brady soil at depositional and erosional landforms. The study site has a midwestern climate indicating utmost differences between the seasons with less humid drier weather. The surface modern soil of the study site was silt loam in both depositional and erosional landforms. Brady soils were collected from ~5.5m, ~4.5m, and ~ 1.5m from the depositional landform, and ~1.5m, ~0.5m, and ~0.2m from the erosional landform were also silt loam. Soils were passed through a 2mm sieve, homogenized, and subsampled for incubation experiments. Finally, the soils were grounded on a SpexMill-8000D (SPEX SamplePrep; Metuchen, NJ) ball grinder at the University of Wisconsin, Madison. Here we did two different types of water addition experiment-continuous wet and drying-rewetting. To see only the effect of moisture on these soils, roots >2mm were removed by sieving and manually.

4.3.5.2 Experimental setup

The incubation experiment was conducted in 8oz mason jars. Previously homogenized three replicates of soils were subsampled and added to the mason jars to the equivalent of 30 (±0.5) g dry mass. After adding the soils into the jar with a predetermined amount of ultra-pure Milli-Q water, they were kept at room temperature. The average temperature was consistent at ~25˚C to match the average temperature of the soil in this area (https://cropwatch.unl.edu/soiltemperature). This area gets snow during the winter months and experiences seasonal fluctuation in moisture during the summer months. The mineralized fluxes associated with different soil moisture have the potential to impact the total annual C release. Soils were exposed to continuous wet and drying-rewetting treatment during a long-time experimental setting at room temperature (~25˚C). We choose room temperature for this experiment as the area generally has an average of 25.7˚ C during the summer rainy season when the soil experience most of the precipitation. The treatments were 1) continuous wet (moist at 60% WHC), where the moisture was kept constant throughout the experiment and 2) a wet-drying cycle in which soils were rewetted after the 7-day drying period (total 8 cycles). Each treatment group soil had 2 replicates. We also included soils with 5% WHC as control. The jars were equipped with

a lid that had a fitted rubber septum for headspace gas sample collection. Silicon gels were applied surrounding the septum surface to prevent any headspace gas loss during the experiment. For the continuous wet experiment, soils were kept at constant moisture of 60% WHC and jars were sealed until the sampling time. On average, soils lost 0.01ml/ day^{-1} of water per day, but the water loss ranged from 0.005ml/ day^{-1} to 0.02ml/ $_{day}^{-1}$ for the continuous wet experiment. Water was added to the soils after headspace gas collection to avoid the birch effect for the continuous wet experiment, and after every sampling, lids were kept open for an hour to equilibrate the jar CO_2 concentration with the ambient air CO_2 concentration. For the wet-dry experiment, soils were rewetted every 7-day by slowly adding deionized Milli-Q ultrapure water into the mason jar with a predetermined aliquot of water to bring the soils to 60% WHC. After adding the water, jars with soils were tied with a lid, and after 6 hours, evolved headspace gas samples were collected for the measurement of CO_2 concentration. After sample collection, soils were dried down to 5% WHC by removing the mason jar lids and keeping them in the incubator at ~25°C. The wet-drying data is presented here in days to compare with the continuous wet experiment.

4.3.5.3 Sampling schedule and evolved CO_2 analysis

For the continuous wet experiment, headspace gas for CO_2 analysis was collected on days 1, 3, 5, 7, 11, 16, 27, 55, 82,114, 151, and 225. For the continuous wet experiment, jar lids were kept open for one hour after each sampling to equilibrate the jar's air with the ambient air. To collect gas for the drying-rewetting experiment, jars were sealed for 6 hours after adding water, and headspace gas samples were collected to see the birch effect on days 1, 7, 21, 28, 35, 42, and 49. Control samples were also collected on these days for both experiments. The total incubation time for the continuous wet soils was 225 days, and for the drying-rewetting experiment soils, it was 56 days. Evolved CO_2 concentration of the soil samples for two different treatments and control was analyzed in a Shimadzu 2014 gas chromatograph (Kyoto, Japan) fitted with a thermal conductivity detector for CO_2 concentration at UC Merced and in an LI-830 CO_2 gas analyzer (IRGA, infrared gas analyzer) at LLNL.

4.4 Data analysis

Data are presented as mean ± standard error for soil pH, EC, $\delta^{13}C$, $\delta^{15}N$, C%, N%, C: N, silt%, clay%, sand%, C-POM, S-POM and MOM. Brady soils from 5.5m, 3.5m, and 1.5m at depositional landform and at 1.5m, 0.5m, and 1.2m at erosional landform were combined together to understand the effects of paleostatus (Brady vs modern) and landform (depositional vs erosional) on soil respiration, fraction modern values, pH, EC, $\delta^{13}C$, $\delta^{15}N$, %TOC, %TN, C: N, silt%, clay%, sand%, C-POM, S-POM, and MOM. To understand the differences in each soil type (i.e., paleostatus modern vs Brady) present at different landforms (depositional vs erosional), we combined the paleostatus with landform. We did Kruskal-Wallis's test to see any difference. All tests were followed by a Dunn's posthoc test to determine pair-wise significance differences using CRAN-R (version 3.5.1; R Development Core Team, 2017). Significance was determined at <0.05 unless otherwise noted.

Soil incubation data were presented as the replicate of two samples for the continuous wet and drying-wetting experiment and one sample for the control experiment. The

concentration of the CO_2 from the soils was corrected for g C and for the respiration per g soil with the below equation

$$\mu g\ \text{C-CO}_2 = \text{mmol air} \times \frac{\mu\text{mol CO}_2}{\text{mol air}} \times \frac{10^{-3}\ \text{mol air}}{\text{mmol air}} \times \frac{12\ \mu\text{g C}}{\mu\text{mol C}} \quad (1)$$

Here, we present cumulative respiration flux by summing the continuous wet fluxes throughout the time of incubation for the continuous wetting experiment. Finally, we fitted two-pool first-order decay models to the data

$$\mathrm{C}_{\mathrm{CO}_2}(t) = \mathrm{C}_0\left(f_\mathrm{f}\, e^{-k_\mathrm{f}\, t} + f_\mathrm{s}\, e^{-k_\mathrm{s}\, t}\right) \quad (2)$$

where $\mathrm{C}_{\mathrm{CO}_2}(t)$ is cumulative µg C of the incubated soil at day t, C_0 denotes TOC, $f_\mathrm{f} + f_s = 1$ denote the fast and slow cycling fractions of the TOC, respectively, and f_f and f_s are the corresponding decay rate constants. The model was fitted to the data using nonlinear least-squares fitting function "nlsLM (minpack.lm)" in R.

4.5 Results

4.5.1 Soil physiochemical properties

We saw an increase in the soil pH along with depth from modern soil to the buried Brady soil in both erosional and depositional landforms. Depositional modern soil has (an average of ~6.9±0.4) lower pH compared to the erosional modern (an average of ~7.4±0.1) soil. Depositional modern soil pH was significantly lower than depositional modern(p=0.00001) and Erosional Brady (p=0.0004). Depositional Brady soil pH was significantly different from erosional modern soil (p=0.006). Erosional modern soil pH was also significantly lower (p=0.008) from depositional Brady and marginally significant (p <0.1) from erosional Brady soil. EC was significantly low in depositional modern soils than in depositional Brady (p= <0.001) and erosional modern (p= 0.018), and depositional Brady has significantly higher EC than erosional Brady soil (p=0.005). A detail has also been provided in Chapter 1.

4.5.2 Soil particle size

Clay content was high in Brady soils compared to modern soils. Brady soil clay content in the depositional landform was an average of 9.6 % (± 1.9), and in the erosional landform, it was an average of 7.7% (±0.8), whereas, for the modern soils, it was an average of 6.1% (±0.8) and 6.29% (±0.6) for depositional and erosional landform respectively. Clay content was highest in the intermediate depth (~4.5m) of depositional landform Brady soil which was around 10.5%. Clay content was significantly higher in depositional Brady soils compared to depositional modern and erosional modern (p<0.001). There was no significant difference in clay content between depositional Brady and erosional Brady, but erosional Brady has significantly higher clay compared to depositional modern and erosional modern (p= 0.03)

Silt and sand content for the Brady and modern soils were almost similar. Brady soil had an average of 59.3% (±4.3) and 56.2% (± 4.8) of silt and 31.2 % (±3.4) and 35.6 % (± 5.0) of sand, considering that modern soils had an average of 56.24% (± 5.67) and 53.7% (±2.2) of silt and 37.6% (±6.3) and 39.0 % (±2.9) sand in depositional and erosional landform subsequently. Silt and sand content (%) was significantly higher in depositional

Brady soils compared to erosional modern, where the p-value was 0.04 and 0.002 for silt and sand consecutively. Finally, buried Brady soils and modern soils were characterized as silty loam in both depositional and erosional landforms, except one modern soil that was collected from the top of the ~5.5m Brady soil was characterized as sandy loam. A detail has also been provided by Szymanski (2021).

4.5.3 Elemental C, N, and isotopic Data

Total organic carbon (%) was higher in the modern soil and lower in the Brady soils, and we notice an exponential decrease while going from modern to Brady soils (Fig.2 a). Organic C (%) in the modern soil ranged between 0.74% to 1.2%, and for the Brady soil, the range was between 0.4% to 0.71%. We found a significantly higher organic C (%) depositional modern ($p=0.0001$) than depositional Brady, and there was no significant difference between erosional modern and erosional Brady soils.

Total nitrogen (N) (%) in the Brady soil ranged between 0.04% to 0.07%, and for the modern soils, these values were between 0.08% to 0.13%. Total N (%) was higher in the modern soil compared to the Brady soils in both depositional and erosional landforms. We found a significant difference in total N (%) among the groups' depositional Brady-depositional modern ($p=0.00008$), depositional modern- erosional Brady ($p=0.004$), and depositional Brady- erosional modern ($p=0.003$). The C: N ratio was higher as we went down from modern to Brady soil in the erosional landform, but the ratio remains similar in the depositional landform. For the Brady soil, the C: N ratio varied between 9 to 11, and for the modern soils, it was between the range of 9 to 10. We found a significantly higher C: N ratio in erosional Brady soil compared to depositional modern and erosional modern soil with a $p < 0.001$ and $p = 0.03$, respectively.

The $\delta^{13}C$ values were lower or depleted than those measured from modern soil layers, but erosional landform Brady soil stable $\delta^{13}C$ values were higher or enriched. Modern soil $\delta^{13}C$ values ranged between -16.1 ‰ to -19.1 ‰, and for the Brady soils, these values ranged between -17.6 ‰ to -19.3‰. We found a significant enrichment in $\delta^{13}C$ values for the depositional modern soils compared to depositional Brady ($p<0.001$) and erosional modern ($p=0.01$). In the erosional landform, the $\delta^{15}N$ values enriched as we went down from modern to Brady soils and these values decreased as we went from deeper to shallower Brady soils (Fig.2 c). The $\delta^{15}N$ values in the Brady soil ranged from 3.5‰ to 4.9‰, and for the modern soils, they ranged between 0.8‰ to 7.9‰. Depositional landform modern soil had higher $\delta^{15}N$ values compared to the erosional modern soils, and depositional Brady soils $\delta^{15}N$ values were depleted compared to the modern soil. We found significantly lower $\delta^{15}N$ values among the erosional modern soils compared to depositional Brady ($p=0.01$), depositional modern ($p<0.001$), and erosional Brady ($p=0.02$). A detail has also been provided in Chapter-1 and by Szymanski (2021).

4.5.4 DRIFT-FTIR data

DRIFT measurement showed distinguishing peaks of SOM interest in these soils. DRIFT peak area related to S-POM was significantly low in depositional Brady soils compared to depositional modern and erosional modern ($p <0.001$), whereas C-POM was significantly higher in erosional modern compared to depositional Brady ($p=0.038$), and MOM was significantly low in depositional Brady compared to depositional modern ($p=0.007$) and erosional modern($p=0.002$). This raised concern as C-POM might be sitting at Brady soil as undecomposed due to the absence of a proper environment. There

was no significant difference in S-POM, C-POM, and MOM between depositional Brady and erosional Brady soil.

4.5.5 Effects of continuous wetting on soil CO_2 efflux

In the continuous wet soil treatment group, erosional landform modern soil has the highest respiration averaging 35,945.37 µg C-CO_2 $gC^{-1,}$ compared to the depositional modern soil averaging 25,273 µg C-CO_2 gC^{-1} at the end of the 225 days. Among the Brady soils, erosional landform soil respiration was higher, averaging 22,580.22 µg C-CO_2 gC^{-1} compared to the depositional landform that respired 9,281.61 µg C-CO_2 gC^{-1} at the end of the 225 days incubation period. This trend was observed from the very first day of incubation. At the beginning of the experiment on days 1, 3, and 5, erosional landform modern soil collected from the top of the shallowest depth Brady soil (~0.2m) produced the highest cumulative µg CO_2 gC^{-1} compared to the other soils. Among the erosional and depositional Brady soils, the intermediate depth (~0.5m) Brady soil collected from the erosional landform emitted the highest cumulative CO_2 (33160.77 µg C-CO_2 gC^{-1}), and the deepest Brady soil collected from ~5.5m at depositional landform emitted the lowest cumulative CO_2 (4138.39 µg C-CO_2 gC^{-1}). By the end of the 225 days incubation period, the cumulative CO_2 flux of the erosional modern soil increased by ~16 fold, whereas depositional modern soil flux increased by ~13 fold compared to day 1. When the evolved CO_2 concentration was compared among different depths of the depositional landform Brady soil, CO_2 efflux followed the trend of shallowest depth > intermediate depth > deepest depth, but in the erosional landform, it was intermediate depth > shallowest depth > deepest depth. Among the depositional landform control soils (with 5% WHC), the shallowest depth Brady soil produced the highest CO_2, and modern soil collected from the top of intermediate depth Brady soil produced the least CO_2. Among the control soils in the erosional landform highest CO_2 was evolved in the intermediate depth (~0.5m) Brady soils, and the lowest CO_2 was evolved in the modern soil collected from the top of the shallowest depth Brady soil. Depositional modern soil emitted significantly higher CO_2 until 151 days and after that, there was no significant difference. Erosional modern has significantly higher evolved CO_2 compared to the depositional Bray soils ($p=0.005$) throughout the experiment. In the first 30 days of the incubation, erosional modern soils emitted significantly higher CO_2 compared to erosional Brady ($p=0.017$) and depositional Brady ($p=0.001$); depositional modern soils emitted significantly higher CO_2 compared to depositional Brady ($p=0.02$). Within the first two weeks of incubation, depositional modern soil accounted for ~38.5% of total cumulative respiration, and erosional modern soil accounted for ~31% of total cumulative respiration over the 225 days of incubation, while the erosional Brady accounted for ~17.5% and depositional Brady accounted for ~27% of the total cumulative respiration. A detail can be found in Table 2.

We fitted a first-order decay curve with the cumulative CO_2 data, and all data were the best fit by the two-pool decay function. This model was a significant predictor ($p < 0.05$) for most of the data except some erosional shallowest Brady, deepest Brady, and one depositional deepest Brady soil. In this 2-pool model, there was a large slow-cycling pool (>97%) (Figure4.a) and a much smaller fast-cycling pool where the decay constant of the slow-cycling pool is ~1000 fold slower compared to the fast-cycling pool. The cumulative respiration from the soils with 60% WHC continuous wet experiments was highest compared to the soil with control at 5%WHC. Depositional Brady soil emitted highest CO_2 concentration compared to other soils in the control with 5% WHC. Increasing soil moisture increase soil respiration and hence increase soil CO_2 production

up to a certain optimal level and then get reduced; that's what we see in our continuous wet experiment. The decline in the respiration rate over time indicates a decline in the decomposition rate. The decay constant (k) is significantly slower in the depositional Brady soils compared to the erosional modern soils, and the decay constant for the fast-cycling C-pool is much higher in erosional modern soils.

4.5.6 Effect of drying rewetting on soil CO_2 efflux

To calculate the soil respiration after rewetting, headspace gas was collected after 6 hours from each sample. In this experimental design, erosional modern soil respired more CO_2 compared to other soils. Among the Brady soils present in the depositional and erosional landform, the shallowest depth Brady soil at the erosional landform emitted the highest µg C-CO_2 $gC^{-1,}$ followed by the deepest Brady soil from the depositional landform at the end of 49day. At the end of the 49day with 8 wet-dry cycles, the overall respired CO_2 trend was erosional modern > erosional Brady > depositional modern > depositional Brady. Depositional Brady soil accounted for a decrease of ~58% in total respiration, followed by erosional Brady with ~56% of the total decrease in respiration over the 49 days of incubation, while the depositional modern accounted for ~31%, and erosional modern accounted for ~39.5% of the total respiration decrease. Experiment with 60%WHC, CO_2 efflux was higher compared to the control with 5%WHC (Figure 7). In control soils, depositional Brady evolved the highest CO_2 throughout the experiment.

Over the period of the laboratory incubation with drying-rewetting experiments, the overall rate of CO_2 efflux was highest in the erosional modern soils, followed by erosional Brady, depositional modern, and depositional Brady soil. Rewetting the dry soil constantly produces large fluxes where the largest pulses are produced on the first day and declined over time; at the end of the 49 days, the largest, 1170.13 and 1064.83 µg C-CO_2 gC^{-1} pulse was produced in the erosional modern and erosional Brady soils respectively, but depositional Brady soils produced 742.80 µg C-CO_2 gC^{-1} pulse. This support our hypothesis that buried soil, which does not experience a regular wet-dry cycle, present in the erosional landform, will have more microbial stress, and the SOC present there will be more susceptible to C-mineralization. This can be related to the presence of the higher labile compound in the erosional Brady soil due to the shallower depth and effect of priming by plat roots or bioturbation. But at the end of 49 days, there was no significant difference in evolved CO_2 between depositional or erosional soils. We see a significantly high evolved CO2 from erosional modern soil compared to depositional Brady soil till cycle day28, and after that, the significance disappears. On wet-dry cycle day 42, we noticed significantly high CO_2 from erosional Brady soil compared to the depositional Brady soils. A detail can be found in Table 3.

4.6 Discussion

Our data suggest that the slow decomposition of the buried Brady soil in the depositional landform is attributed to two main factors. First, the long-time persistence of the buried Brady soil (Figure. 1.b) is due to the environmental conditions that have prevented microbial decomposition of this soil SOM, and second is the thermal transformation of the SOM into a highly condensed aromatic compound (Marin-Spiotta et al., 2014), which is not easily decomposable by all microbial communities (Schmidt et al., 2011). Our two-pool model decay constant of the slow pool (Figure 4.B) shows that Brady soils present in the depositional landform have the slowest decay constant rate while the erosional landform Brady soil decay constant is comparable with the modern soils.

The decline in the respiration rate over time that we see in both continuous wet and wet-dry experiments indicates a decline in the decomposition rate. This can be connected to the labile S-POM present in the soils (Figure. 3). Although there was no significant difference in the S-POM area between depositional modern vs erosional modern and depositional Brady vs erosional Brady soils, the highest CO_2 evolution occurred in erosional modern soils, which might indicate that there might be a priming effect in the erosional soils compared to the depositional soils (Kuzyakov et al., 2002). We know that higher EC decreases the soil microbial activity, hence the decomposition, and we see significantly higher EC in depositional Brady soil compared to the erosional Brady soils, which might have contributed to the high evolved CO_2, although there is no significant difference between these soils in clay, sand, silt, S-POM, and TOC% content. As total organic carbon (TOC%) (Figure 2. a) declines exponentially from modern to deep-buried Brady soil, it is likely that the microbial biomass also declined and shifted to either a less diverse or starvation-tolerated community (Fierer et al., 2003), but the exact mechanism that drives this pattern is unknown. As the amount of organic carbon declines from topsoil to the deeper soil profile, environmental variability also changes. Topsoil goes through a wide range of temperatures and moisture fluctuations, while deeper soil has a more constant environment (Rumpel et al., 2012). Xiang et al. (2008) indicated that the evolved CO_2 from soil not only depends on the amount of labile C availability but rather an inability of the microbes to access it physically, which is a likely condition for the deeply buried Brady soils in the depositional landform. Fierer et al. (2003) argued that the presence of low labile compounds in the deeper soil prevents decomposition, and the availability of the labile C can prime deep soil OM decomposition. This might be true for our deeply buried Brady soils, where the amount of labile compound is smaller, and the condensed aromatic structure (Marin-Spiotta et al., 2014) is preventing the microbial community from decomposition. But the shallowest-depth Brady soil in the erosional landform emitted more CO_2 compared to the deeper Brady soils might be due to the presence of newer carbon input that primed the previously stabilized ancient carbon.

We noted a significant difference in evolved CO_2 from the erosional modern soil compared to depositional Brady soil at the end of 225 days of the continuous wet experiment (Figure 7, Table 2). This higher rate of OM decomposition in erosional modern soil can be attributed to the differences in soil OM availability and soil physiochemical properties due to the different landforms and soil positions (Berhe et al., 2012). The difference in respiration can be supported by further research on the microbial community present in the depositional vs erosional landform. So, we see that soil burial can act as a significant C-sink where SOC can stay longer due to the unfavorable environment for microbial decomposition. On the first day of incubation, erosional Brady soil's initial respiration was around double that of the depositional Brady soil, which suggests that erosional Brady soil has an easily decomposable C compound and may have a smaller long-time mineralizable C pool. This can be supported by the study of Marin-Spiotta et al. (2014) on a similar site depositional landform, Brady soil. The study indicated that 40% of the Brady soil SOM is derived from fire, which has helped the SOM to transform thermally, thus not easily decomposable. Although, there was no significant difference among the Brady soils for simple, complex and microbially derived organic matter (Figure 3, Table 1.B) erosional Brady soil evolved more CO_2 than depositional. This finding ca be supported by a soil physical fractionation study by Szymanski (2021) on this similar soil where she reported that more than 50% of the SOC of these Brady soils are associated with mineral-associated fraction, hence less accessibility for microbial decomposition. Ventura et al. 2014 study found a higher decomposition rate for biochar when the plant roots are present in a field experiment. A

study by Sing et al. 2012 based on a modeling approach to understand biochar decomposition revealed that for one-pool average turnover time can be 88yearss. For a two-pool approach, it can be 3 years for a fast-cycling pool and 870 years for a slow-cycling pool. Since we did the experiment in a laboratory setting, we might have missed several environmental factors which can be present in a field. As freezing/thawing can disperse biochar, bioturbation and aggregate destruction by root can have a priming effect due to increased microbial activity (Pausch et al., 2012) in the field environment. This indicates that our deeper Brady soils can become vulnerable to available fire-derived SOC mineralization if they come to the modern environment and accommodate newer carbon. Thus, a detailed analysis of the combustion temperature of these PyC present in the depositional landform Brady soil and longer incubation experiment (years to decades) with higher temperatures and microbial biomass might show the effect of the decomposition rate will be on these fire-derived SOC (Abney et al., 2019; Sing et al., 2012; Kuzyakov et al., 2014).

Overall, there might be several factors that might have interacted to cause the higher decomposition of SOC in erosional vs depositional landform soils. A two-pool decay model was used to fit our data to see the slow cycling and fast cycling C-pool. Our slow pool decay rates were ~1000-fold higher than the fast pool decay rates, which may suggest that the calculated pools are representative of the non-labile carbon. A priming effect is noticed in the erosional modern, and erosional Brady soils as the F_m value is significantly higher (Table 1. B) in them compared to depositional Brady and depositional modern soil consecutively (Chapter 1), indicating the incorporation of newer carbon.

Fierer and Schimel (2003) study on surface soil showed that just after wetting, most of the C respired is dominated by microbial C and also noted a large release of non-microbial extractable organic carbon (EOC), which might be taken up by the remaining alive microbes for osmolyte production during the drought cycle. Mikha et al. (2005) did a multiple wet-dry cycle study on agricultural soil and noticed that it reduced respiration even below the continuous moist cycle and concluded that high microbial stress is affecting CO_2 emission. We see a similar result for our Brady soils collected from the ~5.5m, ~3.5m, and ~1.5m of the depositional and erosional landform, which can be tied to the limited labile organic carbon resource in these buried soils where the microbial stress mechanism is dominating. Miller et al. (2005) study on California soil indicated that rewetting could expose the substrate to enzymatic attack during a dry period. Xiang et al. (2008) indicated that dry soil processes liberated EOC, and this increased over the incubation period, and it was similar in the continuously wet experimental system. There are mainly 2 mechanisms by which CO_2 pulse occurs in the wet-dry experiment. Water addition disrupts the soil structure and makes the previously protected organic matter available, and as this product is getting used by microbes, the pulse starts to decrease every cycle. But for buried soil that has not experienced this type of disruption, the first addition of moisture will disrupt the aggregate, and bioavailable organic matter will be decomposed by microbes by producing a large pulse. But the first pulses were not significantly larger than the next pulses. Another mechanism can be the carbon movement to microbes limiting their use of the bioavailable carbon. When the water is always there, diffusion can be the mechanism for microbes to get the carbon, and in soil, that process is generally slow, especially for the deeper soil where the substrate is low and can prevent the microbial population from growing (Xiang et al., 2008). This indicates bioavailable C in the deeper soil is diffusion limited; when the soil is rewetted, the C will move through the soil and will become microbially available. As every

rewetting event will equilibrate the available C and a small portion of it will be used, we will see a slower decrease in the soil pulses through multiple cycles, which we saw in our Brady soil samples. So, with all this evidence, it can be concluded that transport is playing an important role compared to the physical disruption, especially in the buried Brady soils, but this remains to be further testing of the soils.

In our control experiment, the deeper Brady soils at depositional landform with 5% WHC evolved the highest CO_2, followed by the shallower Brady soils in both continuous wet and wet-dry experimental setups, although Szymanski (2021) study reported no particulate organic matter (POM) in the deeper Brady soils, and there was not enough increase in POM with the increasing exposure to the erosional landform Brady soil either. More interestingly, wet-dry experiment, Brady soils are only 10 times more active than the 5% control. This indicates that water stress is probably higher in deeper Brady soils compared to the shallower Brady soils. This higher CO_2 flux can be also attributed to high microbial stress in the presence of very little moisture after a long drying period. This also tells us that changes in precipitation patterns with prolonged drought will make these Brady soils more vulnerable to SOC decomposition.

The soils of this area are calcareous soils with visible carbonate filaments and small nodules, as explained by Szymanski (2021), and there is a possibility of chemical dissolution of carbonates which might show higher CO_2 fluxes (Tamir et al., 2011). We must remember that 30% of the earth's surface is covered by Ca-rich soils (Rowley et al., 2018), and if there is any small change in the moisture, new CO_2 fluxes will be added to the atmosphere through calcite dissolution (Schlesinger, 1985) too. This study on calcareous soil gives us an overview of how much total (organic + inorganic) carbon-CO_2 can be added to our environment from this area alone in case of any change in moisture.

Marin-Spiotta et al (2014) study suggested that the Brady soil in this area can store up to 675.2 Mg organic carbon (OC), and we do not know how much of this OC is under the erosional landform. For both the continuous wet and wet-dry experiment, erosional Brady soil CO_2 efflux was similar to the erosional modern CO_2 efflux and higher than the depositional landform modern soil efflux. Although these modern and Brady soil's >97% SOC is present in a slow-cycling pool, the rate constant of the slow-cycling pool is similar for erosional Brady and modern soils present in depositional and erosional landforms. The fast-cycling pool decay constant for the erosional Brady soil is also similar to the modern soils of the study area (Figure 5. c). Our study suggests that Brady soil in erosional landforms is more vulnerable to future disturbances. Erosion suggests an increase in wetness along with an increased temperature compared with depositional landforms, which can eventually increase the carbon mineralization processes. Our finding also supported that the erosional landform Brady soil is more vulnerable and can act as a source of climate change as the decomposition rate of the fast and slow-cycling pool is similar to modern soils.

4.7 Conclusion

We found that the decomposition of the SOC is controlled by the moisture and landform where the soil is situated, as indicated by the wide range of decomposition rates observed in our incubation study. Water has disproportionate effects on these modern and Brady soils at erosional and depositional landforms. Moreover, erosional landform soils are more vulnerable to water addition as the slope accelerates the transport of the dissolved

material. The Great Plains area is projected to experience a temperature increase of 3.5 to 9.5 degrees, along with a 1-inch of precipitation increase in a year (National Climate Assessment, 2018). Anthropogenic activities such as agriculture and overgrazing, along with wind and high precipitation, can accelerate the erosion of this area. This increase in precipitation can remove the topsoil from the erosional landform and eventually bring the buried Brady soil to modern environments. Drying rewetting has higher stress on the shallowest Brady soil in the erosional landform compared to the other different depth Brady soil, and with 60% WHC and 5%WHC, it was seen that frequency of drying will have a larger effect on the Brady soils. Prolonged drought, change in precipitation pattern, and increased temperature in this area will mostly affect the ancient Brady soil present in the erosional landform to decomposition. We also found that depth is playing an important role in slow cycling C-pool as the depth decay constant significantly decreased where the depositional landform deepest Brady soil has a much slower slow-C-pool decay constant compared to the Brady soils collected from depositional Brady at~0.5m, ~1.2m, ~1.5m, ~3.5m and ~5.5m. With the study, we understand that the soil microbial activity in the deep soil can change with soil conditions, and the persistence of the SOC is an ecosystem property rather than a molecular property, as soil depositional depth is playing a major role in SOC stabilization in these soils. IPCC 2018 report indicated that due to large CO_2 emissions, global temperature has increased by 1℃ after the industrial era indicating anthropogenic climate change. IPCC has also concluded that keeping the global temperature rise below 2℃ will help humans and the ecosystem. It will be difficult to achieve this target by only reducing greenhouse gas emissions. While we are struggling to reduce greenhouse gas emissions, it is important to make an effort to increase the soil C sink as the soil has the potential to help in climate mitigation.

4.8 Reference

Abney, R. B., Jin, L., and Berhe, A. A. (2019). Soil properties and combustion temperature: Controls on the decomposition rate of pyrogenic organic matter. CATENA,182,

Berhe, A. A., Harte, J., Harden, J. W. and Torn, M.S. (2007). The significance of the erosion-induced terrestrial carbon sink. Bioscience, 57, 337-346, https://doi.org/10.1641/B570408

Berhe, A. A., Harden, J. W., Torn, M. S., Kleber, M., Burton, S. D., and Harte, J. (2012). Persistence of soil organic matter in eroding versus depositional landform positions. J. Geophys. Res., 117, G02019, doi:10.1029/2011JG001790.

Chaopricha, N. T., and Marin-Spiotta, E. (2014). Soil Burial Contributes to Deep Soil Organic Carbon Storage. Soil Biology and Biogeochemistry, 56, 251-264, https://doi.org/10.1016/j.soilbio.2013.11.011.

Doetterl, S.,Six, J., Wesemael, B. V., and Oost, K. V. (2012). Carbon Cycling in Eroding Landscapes: Geomorphic Controls on Soil Organic C Pool Composition and C Stabilization. Global Change Biology, 18, 2218–2232, https://doi.org/10.1111/j.1365-2486.2012.02680.x

Ellerbrock, R. H. and Gerke, H. H. (2004). Characterizing organic matter of soil aggregate coatings and biopores by Fourier transform infrared spectroscopy. Eur. J. Soil Sci., 55, 219–228, https://doi.org/10.1046/j.1365-2389.2004.00593.x,

Fontaine, S., Barot, S., Barré, P., Bdioui, N., Mary, B., and Rumpel C. (2007), Stability of organic carbon in deep soil layers controlled by fresh carbon supply. Nature 450, 277–280. https://doi.org/10.1038/nature06275

Fierer, N., Schimel, J. P., and Holden, P. A. (2003) Influence of drying–rewetting frequency on soil bacterial community structure Microbial Ecology, 45 , 63-71

Gee, G.W. and Bauder, J.W. (1986.) Particle-size analysis, in Klute, A., ed., Methods of soil analysis: Part 1: Madison, Wisconsin, American Society of Agronomy, 383-411.

Harrison, R. B., Footen, P.W., and Strahn, B. D. (2011), Deep soil horizons- Contribution and importance to soil C pools and in assessing whole-ecosystem response to management and global change. Forest science, 57: 67-76, https://doi.org/10.1093/forestscience/57.1.67

Hall, S. J., Berhe, A. A., and Thompson, A. (2018) Order from disorder: do soil organic matter composition and turnover co-vary with iron phase crystallinity?. Biogeochemistry, 140, 93–110, https://doi.org/10.1007/s10533-018-0476-4, 2018

Jacobs, P. M., and Mason, J. A. (2004), Pedology of soils in thick Holocene loess, Nebraska, USA, Revista Mexicana de Ciencias Geológicas, 21(1),54-70

Jacobs, P.M. and Mason, J.A. 2007. Late Quaternary climate change, loess sedimentation, and soil profile development in the central Great Plains: A pedosedimentary model. Geological Society of America Bulletin 119:462. doi: 10.1130/B25868.1

Jickells, T. D., An, Z.S., Andersen, K. K., Baker, A.R., Bergametti, G., Brooks, N., Cao, J. J., Boyd, P.W., Duce, R. A., Hunter, K. A., Kawahata, H., Kubilay, N., laRoche, J., Liss, P. S., Mahowald, Prospero, J. M., Ridgwell, A. J., Tegen, L., and Torres, R. (2005). Global iron connections between desert dust, ocean biogeochemistry, and climate. Science, 308 (5718)

Jobbagy, E. G., and Jackson, R. B. (2000). The vertical distribution of soil organic carbon and its relation to climate and vegetation, Ecological Applications,10(2), 423–436, https://doi.org/10.1890/1051-0761(2000)010[0423:TVDOSO]2.0.CO;2

Johnson, W. C., Willey, K. L., Mason, J. A., and May, D. W. (2007), Stratigraphy and environmental reconstruction at the middle Wisconsinan Gilman Canyon formation type locality, Buzzard's Roost, southwestern /Nebraska, USA. Quaternary research,67, 474-486, https://doi.org/10.1016/j.yqres.2007.01.011

Kilmer, V.J., and Alexander, L.T. (1949). Methods of making mechanical analysis of soils. Soil Science, 68,15–24.

Kögel-Knaber, I. and Amelung, W. (2014). Dynamics, Chemistry, and Preservation of Organic Matter in Soils, in: Treatise on Geochemistry, edited by: Holland, H. D. and Turekian, K. K., Elsevier, Oxford, 157–215, ISBN 9780080959757

Kuzyakov, Y. (2002). Review: Factors affecting rhizosphere priming effects. Journal of Plant Nutrition and Soil Science, 165, 382– 396

Lal, R., Sobecki, T. M., Livari, T., and Kimble, J. M. (2003). Soil Degradation in the United States: Extent, Severity, and Trends. Lewis Publisher, Boca Raton, Florida

Kuzyakov, Y., Bogomolova, I., and Glaser, B. (2014). Biochar stability in soil: Decomposition during eight years and transformation as assessed by compound-specific 14C analysis. Soil Biology and Biochemistry,70,229-236, https://doi.org/10.1016/j.soilbio.2013.12.021

Mainka, M., Summerauer., L., Wasner, D., Garland, G., Griepentrog, M., Berhe, A. A., and Doetterl, S. (2022). Soil geochemistry as a driver of soil organic matter composition: insight from a soil chronosequences. Biogeosciences, 19,1675-1689.

Marin-Spiotta, E., Chaopricha, N. T., Plante, A. F., Diefendorf, A. F., Muller, C. W., Grandy, A. S., and Mason, J. A. (2014). Long-term Stabilization of Deep Soil Carbon by Fire and Burial During Early Holocene Climate Change. Nature Geoscience, May 25, 2014. DOI: 10.1038/NGEO2169

Mason, J.A., and Kuzila, M.S. (2000). Episodic Holocene loess deposition in central Nebraska. Quaternary International ,67,119–131.

Mason, J. A., Miao, X., Hanson, P. R., Jhonson, W.C., Jacob, P. M., and Goble, R. J. (2008). Loess record of the Pleistocene-Holocene transition on the northern and central Great Plains, USA. Quaternary science review, 37,947-950, https://doi.org/10.1016/j.quascirev.2008.07.004

Miller, A. E., Schimel, J. P., Meixner, T., Sickman, J. O., and Melack, J. M. (2005). Episodic rewetting enhances carbon and nitrogen release from chaparral soils. Soil Biology & Biochemistry,37,2195-2204

Mikha, M. M., Rice, C.W., and Milliken, G. A. (2005). Carbon and nitrogen mineralization as affected by drying and wetting cycles. Soil Biology & Biochemistry, 37,339-347

National Climate Assessment (2018) northern great plains (https://forestadaptation.org/sites/default/files/2019-06/Great-Plains-Climate-Impacts.pdf)

Neff, J. C., Ballantyne, A. P., Famer, G. L., Mahowald, N. M., Conroy, J. L., Landry, C. C., Overpeck, J. T., Painter, T. H., Lawrence, C. R., and Reynolds, R. L. (2008). Increasing eolian dust deposition in the western United States linked to human activity. Nature – Geosciences. doi:10.1038/ngeo133

Parikh, S. J., Goyne, K. W., Margenot, A. J., Mukome, F. N. D., and Calderón, F. J. (2014). Soil chemical insights provided through vibrational spectroscopy, 126, 1–148, https://doi.org/10.1016/B978-0- 12-800132-5.00001-8.

Pausch, J., and Kuzyakov, Y. (2012). Soil organic carbon decomposition from recently added and older sources estimated by δ13 C values of CO2 and organic matter Soil Biol. Biochem., 55, 40-47

Reynolds, R., Belnap, J., Reheis, M., Lamothe, P., and Luiszer, F. (2001). Aeolian dust in Colorado Plateau soils: nutrient inputs and recent change in source. Proc. Natl. Acad. Sci. USA 98, 7123–7127

Ruhe, R.V (1983), Depositional environment of late Wisconsin loess in the midcontinental United States. In: Porter, S.C. (Ed.), Late-Quaternary Environments of the United States, Vol. 1, The Pleistocene. University of Minnesota Press, Minneapolis, 130-137

Rumpel, C., and Kögel-Knabner, I. (2010). Deep soil organic matter—a key but poorly understood component of terrestrial C cycle. Plant and Soil, 338, 143-158.

Rumpel, C., Chabbi, A., and Marschner, B. (2012). Carbon Storage and Sequestration in Subsoil Horizons: Knowledge, Gaps and Potentials. Recarbonization of the biosphere, 445-464.

Ryals, R., Kaiser, M., Torn, M. S., Berhe, A. A., and Silver, W. L. (2014). Impacts of organic matter amendments on carbon and nitro gen dynamics in grassland soils. Soil Biol. Biochem., 68, 52–61, https://doi.org/10.1016/j.soilbio.2013.09.011.

Sankey, J. B., Germino, M. J., and Glenn, N. F. (2009). Aeolian sediment transport following wildfire in sagebrush steppe. Journal of arid environments,73, 912-919

Schmidt, M. W. I., Torn, M .S., Abiven, S., Dittmar, T., Guggenberger, G., Janssens, I. A., Kleber, M., Kogel-Knabner, I., Lehmann, D J., Manning, A. C., Nannipieri, P., Rasse, D. P., Weiner, S., and Trumbore, S. E. (2011). Persistence of soil organic matter as an ecosystem property, Nature, 478, 49-56, doi:10.1038/nature10386

Schlesinger, W. H. (1985). The formation of caliche in soils of the Mojave Desert, California. Geochimica et Cosmochimica Acta, 49, 57– 66.

Singh, N., Abiven, S., Torn, M. S., and Schmidt, M. W. I. (2012). Fire-derived organic carbon in soil turns over on a centennial scale. Biogeosciences, 9,2847-2857

Soong, J. L., Castanha, C., Hicks Pries, C. E., Ofiti, N., Porras, R. C., Riley, W. J., and Torn, M. S. (2021). Five years of whole-soil warming led to loss of subsoil carbon stocks and increased CO2 efflux. Science advances, 7(21), eabd1343.

Stacy, E. M., Hart, S. C., Hunsaker, C. T., Johnson, D. W., and Berhe, A. A. (2015). Soil carbon and nitrogen erosion in forested catchments: implications for erosion-induced terrestrial carbon sequestration. Biogeosciences, 12(16), 4861-4874.

Stuiver, M., Reimer, P. J., and Braziunas, T. F. (1998). High-precision radiocarbon age calibration for terrestrial and marine samples. Radiocarbon, 403,1127–1151

Szymanski, L. M. (2021). Spatial distribution and long-time persistence of ancient carbon in buried soils and its vulnerability to landscape disturbance (Publication No. 28720040) [Doctoral dissertation, University of Wisconsin, Madison]. ProQuest Dissertations & Theses Global

Tamir, G., Shenker, M., Heller, H., Bloom, P.R., and Bar-Tal, A. (2011). Can soil carbonate dissolution lead to overestimation of soil respiration? Soil Science Society of America Journal

Viscarra Rossel, R. A., Behrens, T., Ben-Dor, E., Brown, D. J., Demattê, J. A. M., Shepherd, K. D., Shi, Z., Stenberg, B., Stevens, A., Adamchuk, V., Aïchi, H., Barthès, B. G., Bartholomeus, H. M., Bayer, A. D., Bernoux, M., Böttcher, K., Brodský, L., Du, C. W., Chappell, A., Fouad, Y., Genot, V., Gomez, C., Grunwald, S., Gubler, A., Guerrero, C., Hedley, C. B., Knadel, M., Morrás, H. J. M., Nocita, M., Ramirez-Lopez, L., Roudier, P., Campos, E. M. R., Sanborn, P., Sellitto, V. M., Sudduth, K. A., Rawlins, B. G., Walter, C., Winowiecki, L. A., Hong, S. Y., and Ji, W. (2016). A global spectral library to characterize the world's soil, Earth-Sci. Rev., 155, 198–230, https://doi.org/10.1016/j.earscirev.2016.01.012

Vogel, J. S., Southon, J. R., Nelson, D. E., and Brown, T. A. (1984). Performance of catalytically condensed carbon for use in accelerator mass-spectrometry. Nucl Instrum Methods Phys Res, B5,289–293

Woodburn, T., Johnson, W. C., Mason, J. A, Bozarth, S. R., and Halfen, A. F. (2017). Vegetation dynamics during the pleistocene- Holocene transition in the central great plains, USA. The Holocene, 27(1), 155-163.

Xiang, S.H., Doyle, A., Holden, P. A, and Schimel, J. P. (2008). Drying and rewetting effects on C and N mineralization and microbial activity in surface and subsurface California grassland soils. Soil biology and biochemistry, 40(9), 2281-2289.

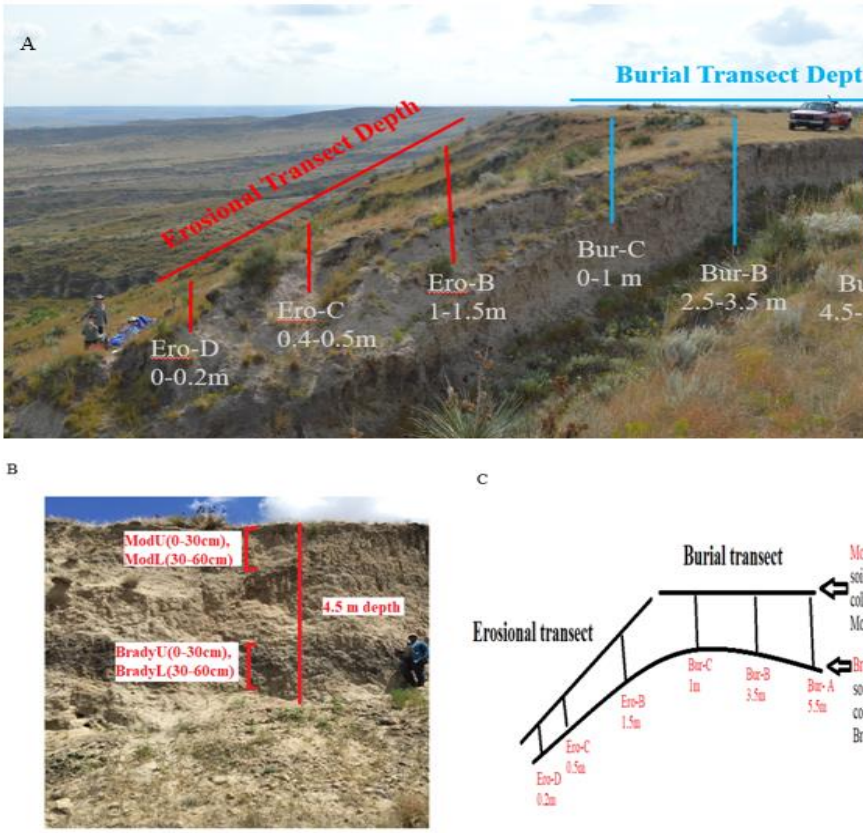

Figure 4-1 Schematic representation of sampling locations in the study system located in Nebraska. The depth of the Brady soil varies along topographic gradients, depending on whether one considers different layers of aeolian deposits the Brady soil was buried under originally (i.e., burial transect or depositional transect) vs. areas that are currently eroding (i.e., erosional). Pictures B and C is showing a detail of how the soil

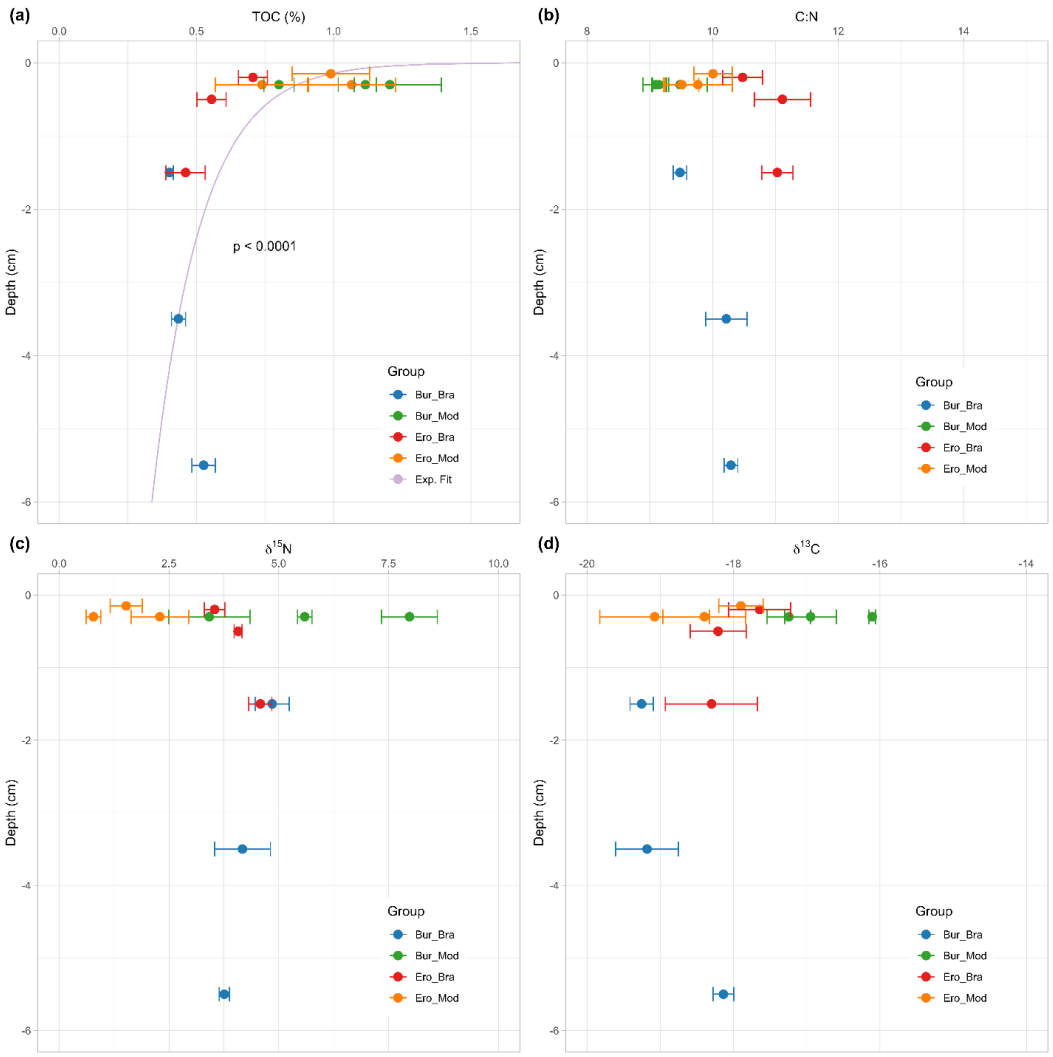

Figure 4-2 Figures indicating mean ± SE of the bulk soil's (a) total organic carbon (TOC%), (b) C: N ratio, (c) d15N, and (d) d13C at different soil layers of the depositional and erosional transect. TOC% has an exponential decay fitted curve with a $p<0.001$.

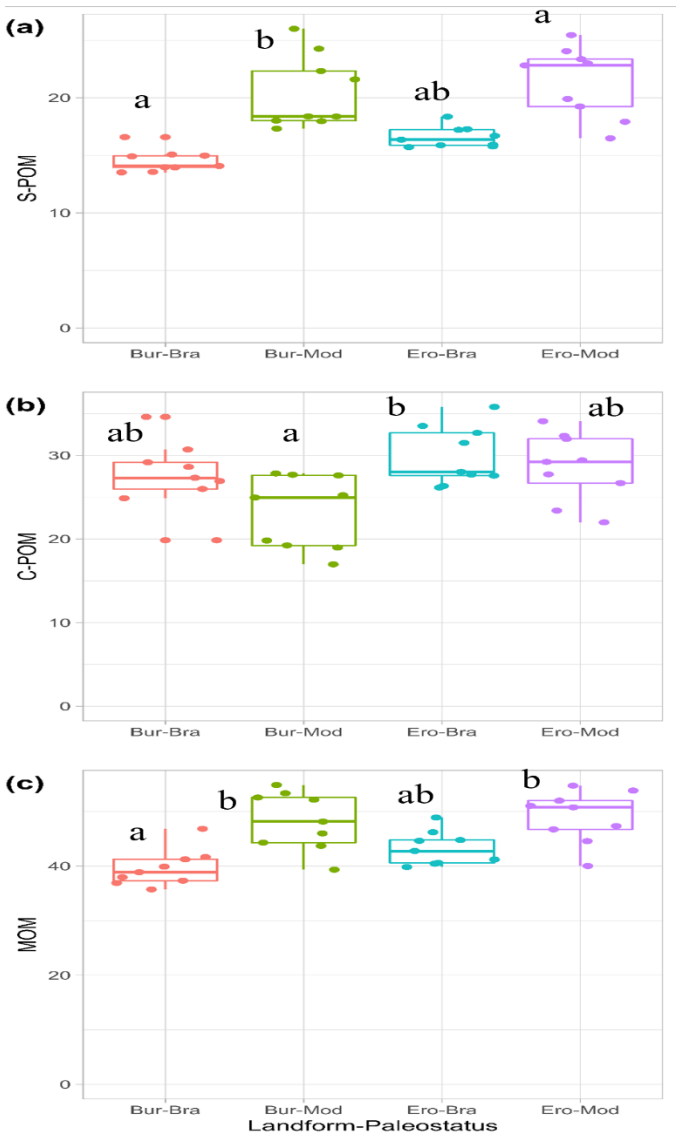

Figure 4-3 DRIFT area of simple organic compound present at 2898-2976 cm^{-1} (S-POM1), 2839-2870 cm^{-1} (S-POM2), 1500-1550 cm^{-1} as C-POM and 1660- 1580 cm^{-1} as microbially derived organic compound (MOM)

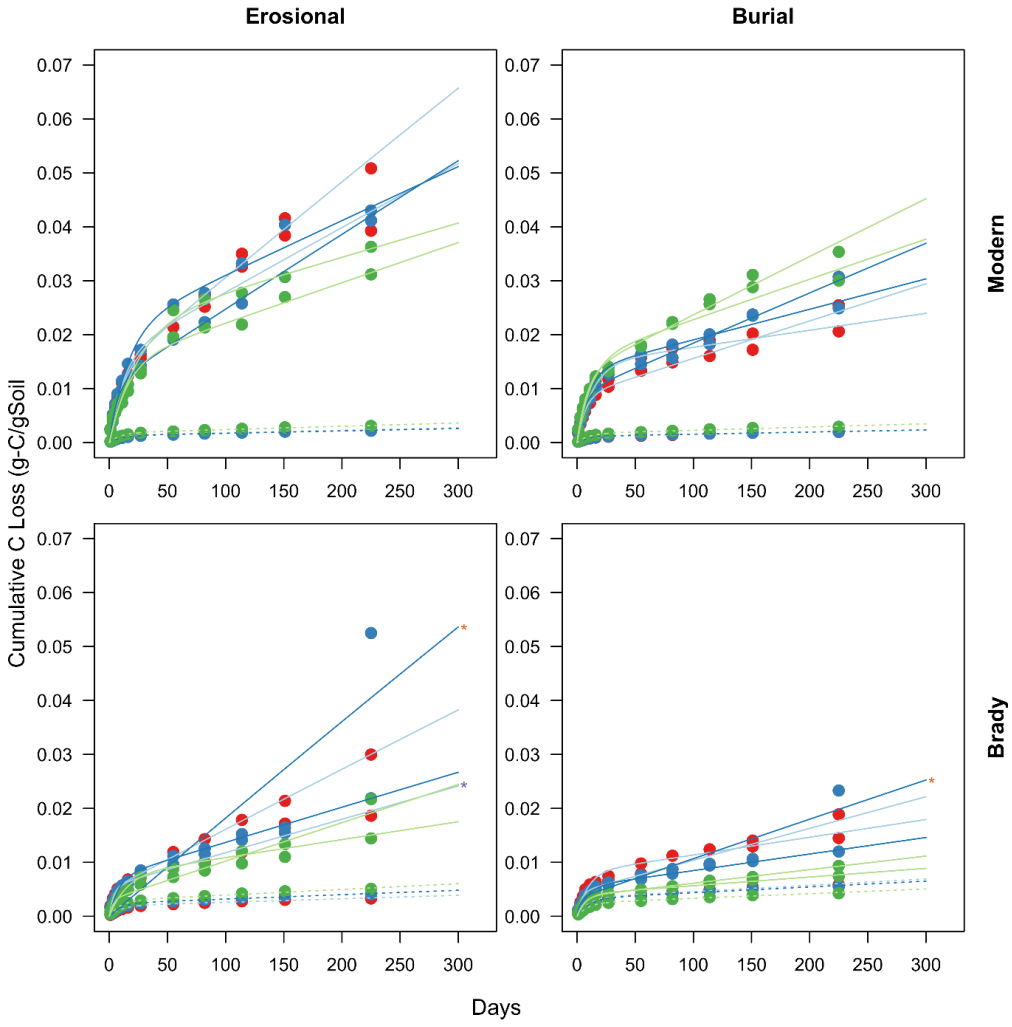

Figure 4-4 Cumulative respiration with a fitted model of the continuous wet experiment. Different colors indicate different depths from where Brady soils have been collected. Blue color represents the deepest, green represents the intermediate, and red color represents the shallowest depth of the Brady soils. A similar color was also provided for the modern soils that were collected from the topsoil at the particular depth of the Brady soils.

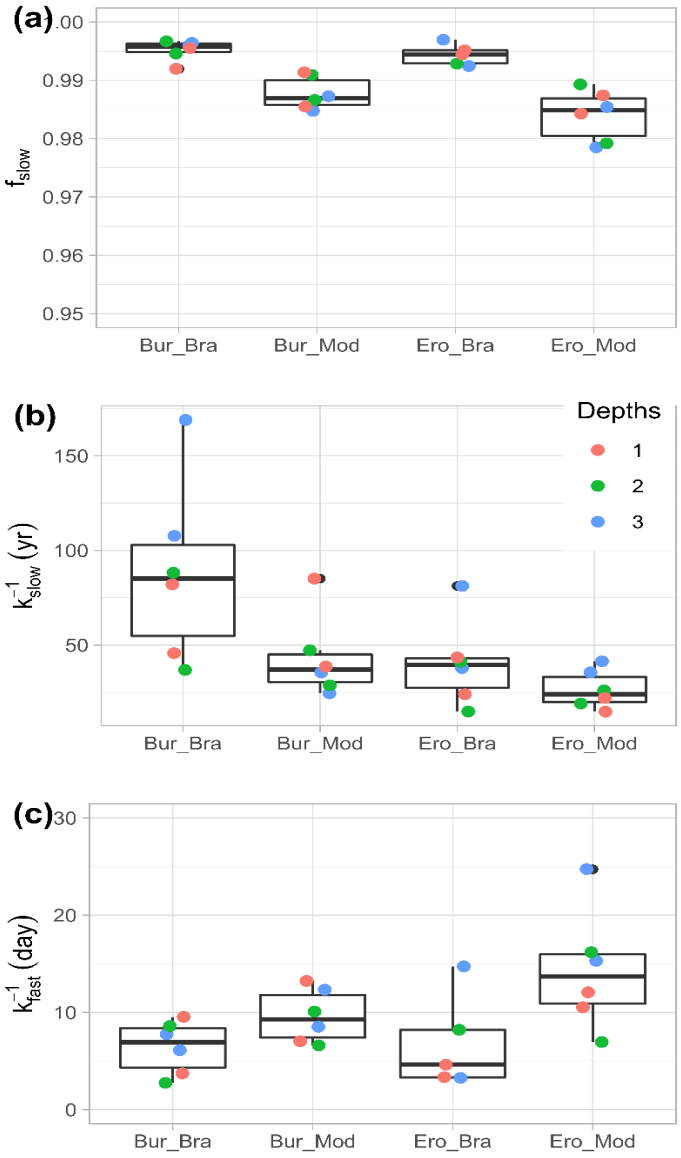

Figure 4-5 Figure a describes the fraction of the slow-cycling pool, figure b describes the decomposition rate of the slow-cycling pool, and figure c is describing the decomposition rate of the fast-cycling pool in depositional landform modern soil (Bur_Mod), depositional landform Brady soil (Bur_Bra), erosional landform modern soil (Ero_Mod) and erosional landform Brady soil (Ero-Bra). 1, 2, and 3 indicate different depth categories, where 3 is the deepest depth, 2 is the intermediate depth, and 1 is the shallowest depth of the Brady soil collected from depositional and erosional landform

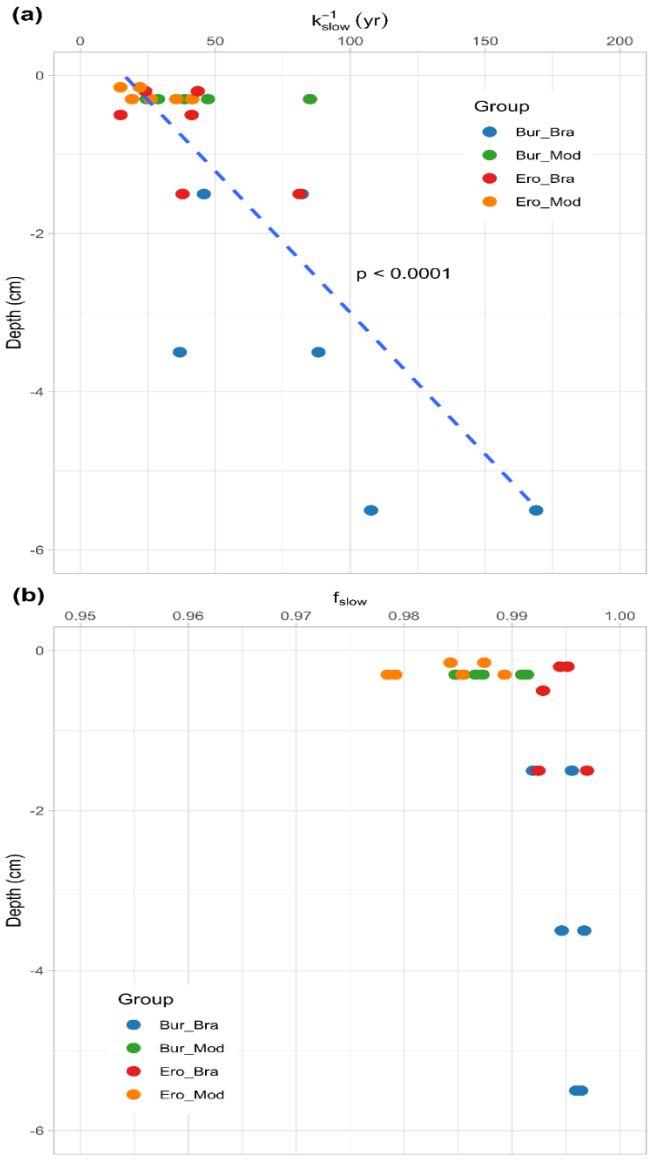

Figure 4-6 Figure a indicates the effect of the depth of decay constant of the slow cycling pool on modern and Brady soils at depositional and erosional landforms where the blue dotted line indicates exponential decay. Figure b indicates the slow-cycling pools present at different depths of the modern and Brady soils in depositional and erosional landforms.

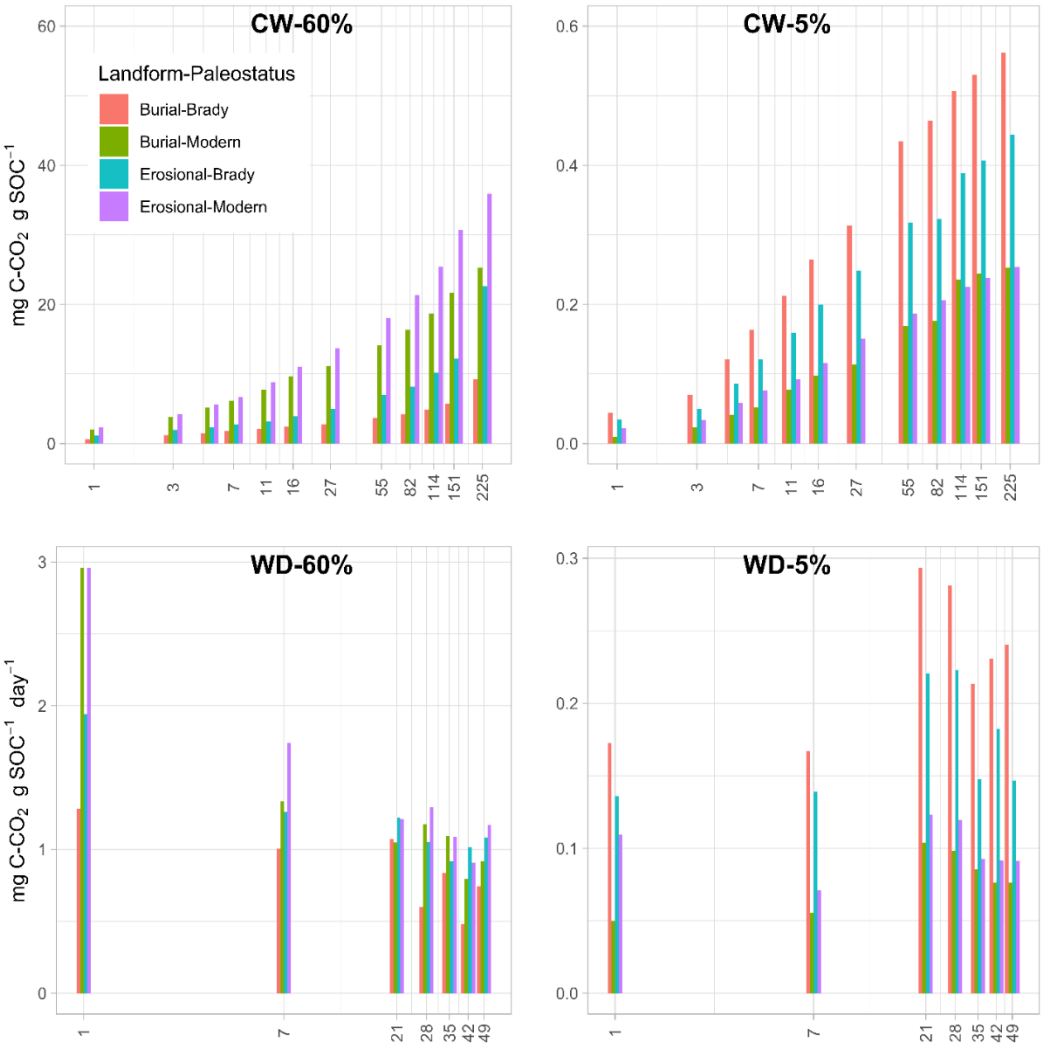

Figure 4-7Measured concentration of respired CO2 values plotted vs. days. CW 60% indicates continuous wet experiment with 60% water holding capacity, CW-5% indicates continuous wet control with 5% water holding capacity, WD-60% indicates wet-dry experiment with 60% water holding capacity, and WD-5% indicates wet-dry experiment control with 5% water holding capacity

Table 4-1. Selected properties of the study sites. Values with n.s indicate no significance has been noticed

A.

Landform (n= 9)	pH	EC	Clay	Silt	Sand
Burial Brady- Burial Modern	<0.001	<0.001	<0.001	0.08	<0.001
Burial Brady- Erosional Brady	>0.1	<0.001	>0.1	>0.1	>0.1
Burial Modern- Erosional Brady	<0.001	>0.1	0.03	n. s	1
Burial Brady- Erosional Modern	<0.001	<0.001	<0.001	<0.001	<0.001
Burial Modern- Erosional Modern	n. s	>0.1	n. s	>0.1	>0.1
Erosional Brady- Erosional Modern	0.0247	n. s	0.04	0.08	0.02

B.

Landform (n= 9)	TOC%	TC	TIC	TN	C: N
Burial Brady- Burial Modern	<0.001	<0.001	0.001	<0.001	>0.1
Burial Brady- Erosional Brady	>0.1	0.05	n. s	n. s	0.004
Burial Modern- Erosional Brady	0.018	>0.1	<0.004	<0.001	<0.001
Burial Brady- Erosional Modern	0.001	<0.001	0.64	<0.001	n. s
Burial Modern- Erosional Modern	n. s	n. s	<0.001	>0.1	>0.1
Erosional Brady- Erosional Modern	>0.1	0.04	n. s	0.05	<0.001

C.

Landform (n= 9)	Smectite	Vermiculite	Illite	Kaolinite
Burial Brady- Burial Modern	0.003	0.11	<0.001	n. s
Burial Brady- Erosional Brady	n. s	n. s	n. s	>0.1
Burial Modern- Erosional Brady	0.03	0.05	0.03	>0.1
Burial Brady- Erosional Modern	n. s	n. s	n. s	>0.1
Burial Modern- Erosional Modern	<0.001	>0.1	0.001	n. s
Erosional Brady- Erosional Modern	n. s	n. s	n. s	n. s

Table 4-2. Continuous wet experiment (60% WHC) and control (5% WHC) respired cumulative CO_2 from modern and Brady soils collected from burial and erosional landform at 6 different depth category.

Landform	Paleostatus	Soil Layers	Depth to Brady (m)	Water%	Rep	Day	Depth	ug-CO2/gC(cumulative)
Burial	Modern	Upper	5.5	60%	1	1	3	2265.99
Burial	Modern	Upper	5.5	60%	2	1	3	2312.12
Burial	Brady	Upper	5.5	60%	1	1	3	340.95
Burial	Brady	Upper	5.5	60%	2	1	3	362.82
Burial	Modern	Upper	3.5	60%	1	1	2	2146.64
Burial	Modern	Upper	3.5	60%	2	1	2	1775.77
Burial	Brady	Upper	3.5	60%	1	1	2	543.13
Burial	Brady	Upper	3.5	60%	2	1	2	753.36
Burial	Modern	Upper	1.5	60%	1	1	1	1760.12
Burial	Modern	Upper	1.5	60%	2	1	1	1593.81
Burial	Brady	Upper	1.5	60%	1	1	1	772.17
Burial	Brady	Upper	1.5	60%	2	1	1	768.10
Erosional	Modern	Upper	1.5	60%	1	1	3	2013.08
Erosional	Modern	Upper	1.5	60%	2	1	3	2289.21
Erosional	Brady	Upper	1.5	60%	1	1	3	522.54
Erosional	Brady	Upper	1.5	60%	2	1	3	496.66
Erosional	Modern	Upper	0.5	60%	1	1	2	2391.73
Erosional	Modern	Upper	0.5	60%	2	1	2	2390.21
Erosional	Brady	Upper	0.5	60%	1	1	2	1155.12
Erosional	Brady	Upper	0.5	60%	2	1	2	1305.41
Erosional	Modern	Upper	0.2	60%	1	1	1	2353.62
Erosional	Modern	Upper	0.2	60%	2	1	1	2351.63
Erosional	Brady	Upper	0.2	60%	1	1	1	1690.82
Erosional	Brady	Upper	0.2	60%	2	1	1	1515.39
Burial	Modern	Upper	5.5	60%	1	3	3	4185.88
Burial	Modern	Upper	5.5	60%	2	3	3	4350.09
Burial	Brady	Upper	5.5	60%	1	3	3	742.09
Burial	Brady	Upper	5.5	60%	2	3	3	771.15
Burial	Modern	Upper	3.5	60%	1	3	2	4211.57
Burial	Modern	Upper	3.5	60%	2	3	2	3309.93
Burial	Brady	Upper	3.5	60%	1	3	2	977.11
Burial	Brady	Upper	3.5	60%	2	3	2	1358.89
Burial	Modern	Upper	1.5	60%	1	3	1	3607.99
Burial	Modern	Upper	1.5	60%	2	3	1	3166.86
Burial	Brady	Upper	1.5	60%	1	3	1	1782.39

Landform	Paleostatus	Soil Layers	Depth to Brady (m)	Water%	Rep	Day	Depth	ug-CO2/gC(cumulative)
Burial	Brady	Upper	1.5	60%	2	3	1	1577.96
Erosional	Modern	Upper	1.5	60%	1	3	3	3663.78
Erosional	Modern	Upper	1.5	60%	2	3	3	4150.37
Erosional	Brady	Upper	1.5	60%	1	3	3	1142.11
Erosional	Brady	Upper	1.5	60%	2	3	3	1104.39
Erosional	Modern	Upper	0.5	60%	1	3	2	4888.33
Erosional	Modern	Upper	0.5	60%	2	3	2	3637.37
Erosional	Brady	Upper	0.5	60%	1	3	2	2021.08
Erosional	Brady	Upper	0.5	60%	2	3	2	2212.63
Erosional	Modern	Upper	0.2	60%	1	3	1	4536.37
Erosional	Modern	Upper	0.2	60%	2	3	1	4509.50
Erosional	Brady	Upper	0.2	60%	1	3	1	2771.98
Erosional	Brady	Upper	0.2	60%	2	3	1	2464.43
Burial	Modern	Upper	5.5	60%	1	5	3	5600.27
Burial	Modern	Upper	5.5	60%	2	5	3	5831.62
Burial	Brady	Upper	5.5	60%	1	5	3	955.50
Burial	Brady	Upper	5.5	60%	2	5	3	988.17
Burial	Modern	Upper	3.5	60%	1	5	2	5584.50
Burial	Modern	Upper	3.5	60%	2	5	2	4581.09
Burial	Brady	Upper	3.5	60%	1	5	2	1131.39
Burial	Brady	Upper	3.5	60%	2	5	2	1681.40
Burial	Modern	Upper	1.5	60%	1	5	1	5002.19
Burial	Modern	Upper	1.5	60%	2	5	1	4235.77
Burial	Brady	Upper	1.5	60%	1	5	1	2392.88
Burial	Brady	Upper	1.5	60%	2	5	1	1978.82
Erosional	Modern	Upper	1.5	60%	1	5	3	4847.16
Erosional	Modern	Upper	1.5	60%	2	5	3	4868.04
Erosional	Brady	Upper	1.5	60%	1	5	3	1402.59
Erosional	Brady	Upper	1.5	60%	2	5	3	1437.78
Erosional	Modern	Upper	0.5	60%	1	5	2	6700.43
Erosional	Modern	Upper	0.5	60%	2	5	2	5399.35
Erosional	Brady	Upper	0.5	60%	1	5	2	2041.32
Erosional	Brady	Upper	0.5	60%	2	5	2	2750.89
Erosional	Modern	Upper	0.2	60%	1	5	1	5597.53
Erosional	Modern	Upper	0.2	60%	2	5	1	6097.18
Erosional	Brady	Upper	0.2	60%	1	5	1	3387.96
Erosional	Brady	Upper	0.2	60%	2	5	1	3001.52
Burial	Modern	Upper	5.5	60%	1	7	3	6769.41

Landform	Paleostatus	Soil Layers	Depth to Brady (m)	Water%	Rep	Day	Depth	ug-CO2/gC(cumulative)
Burial	Modern	Upper	5.5	60%	2	7	3	6992.23
Burial	Brady	Upper	5.5	60%	1	7	3	1101.28
Burial	Brady	Upper	5.5	60%	2	7	3	1156.33
Burial	Modern	Upper	3.5	60%	1	7	2	6306.14
Burial	Modern	Upper	3.5	60%	2	7	2	5615.06
Burial	Brady	Upper	3.5	60%	1	7	2	1459.38
Burial	Brady	Upper	3.5	60%	2	7	2	1971.23
Burial	Modern	Upper	1.5	60%	1	7	1	6176.03
Burial	Modern	Upper	1.5	60%	2	7	1	5132.83
Burial	Brady	Upper	1.5	60%	1	7	1	2873.11
Burial	Brady	Upper	1.5	60%	2	7	1	2434.90
Erosional	Modern	Upper	1.5	60%	1	7	3	5406.86
Erosional	Modern	Upper	1.5	60%	2	7	3	5995.66
Erosional	Brady	Upper	1.5	60%	1	7	3	1566.26
Erosional	Brady	Upper	1.5	60%	2	7	3	1717.79
Erosional	Modern	Upper	0.5	60%	1	7	2	8233.33
Erosional	Modern	Upper	0.5	60%	2	7	2	6760.31
Erosional	Brady	Upper	0.5	60%	1	7	2	2475.38
Erosional	Brady	Upper	0.5	60%	2	7	2	3236.95
Erosional	Modern	Upper	0.2	60%	1	7	1	6345.43
Erosional	Modern	Upper	0.2	60%	2	7	1	7468.45
Erosional	Brady	Upper	0.2	60%	1	7	1	3874.71
Erosional	Brady	Upper	0.2	60%	2	7	1	3426.13
Burial	Modern	Upper	5.5	60%	1	11	3	8418.26
Burial	Modern	Upper	5.5	60%	2	11	3	8694.08
Burial	Brady	Upper	5.5	60%	1	11	3	1266.05
Burial	Brady	Upper	5.5	60%	2	11	3	1336.76
Burial	Modern	Upper	3.5	60%	1	11	2	8034.51
Burial	Modern	Upper	3.5	60%	2	11	2	7241.19
Burial	Brady	Upper	3.5	60%	1	11	2	1790.08
Burial	Brady	Upper	3.5	60%	2	11	2	2325.58
Burial	Modern	Upper	1.5	60%	1	11	1	7548.12
Burial	Modern	Upper	1.5	60%	2	11	1	6464.07
Burial	Brady	Upper	1.5	60%	1	11	1	3337.24
Burial	Brady	Upper	1.5	60%	2	11	1	2806.38
Erosional	Modern	Upper	1.5	60%	1	11	3	7047.57
Erosional	Modern	Upper	1.5	60%	2	11	3	7592.40
Erosional	Brady	Upper	1.5	60%	1	11	3	1880.05

Landform	Paleostatus	Soil Layers	Depth to Brady (m)	Water%	Rep	Day	Depth	ug-CO2/gC(cumulative)
Erosional	Brady	Upper	1.5	60%	2	11	3	1985.32
Erosional	Modern	Upper	0.5	60%	1	11	2	10535.88
Erosional	Modern	Upper	0.5	60%	2	11	2	9053.76
Erosional	Brady	Upper	0.5	60%	1	11	2	3054.37
Erosional	Brady	Upper	0.5	60%	2	11	2	3900.01
Erosional	Modern	Upper	0.2	60%	1	11	1	8613.56
Erosional	Modern	Upper	0.2	60%	2	11	1	10027.77
Erosional	Brady	Upper	0.2	60%	1	11	1	4432.48
Erosional	Brady	Upper	0.2	60%	2	11	1	4043.57
Burial	Modern	Upper	5.5	60%	1	16	3	10592.66
Burial	Modern	Upper	5.5	60%	2	16	3	10781.27
Burial	Brady	Upper	5.5	60%	1	16	3	1471.51
Burial	Brady	Upper	5.5	60%	2	16	3	1602.22
Burial	Modern	Upper	3.5	60%	1	16	2	10366.59
Burial	Modern	Upper	3.5	60%	2	16	2	9066.80
Burial	Brady	Upper	3.5	60%	1	16	2	2247.43
Burial	Brady	Upper	3.5	60%	2	16	2	2721.57
Burial	Modern	Upper	1.5	60%	1	16	1	9378.73
Burial	Modern	Upper	1.5	60%	2	16	1	7849.49
Burial	Brady	Upper	1.5	60%	1	16	1	3487.47
Burial	Brady	Upper	1.5	60%	2	16	1	3306.12
Erosional	Modern	Upper	1.5	60%	1	16	3	9173.80
Erosional	Modern	Upper	1.5	60%	2	16	3	9528.23
Erosional	Brady	Upper	1.5	60%	1	16	3	2320.03
Erosional	Brady	Upper	1.5	60%	2	16	3	2338.88
Erosional	Modern	Upper	0.5	60%	1	16	2	13488.85
Erosional	Modern	Upper	0.5	60%	2	16	2	11396.73
Erosional	Brady	Upper	0.5	60%	1	16	2	3894.61
Erosional	Brady	Upper	0.5	60%	2	16	2	4372.50
Erosional	Modern	Upper	0.2	60%	1	16	1	11547.14
Erosional	Modern	Upper	0.2	60%	2	16	1	11145.91
Erosional	Brady	Upper	0.2	60%	1	16	1	5684.77
Erosional	Brady	Upper	0.2	60%	2	16	1	5035.38
Burial	Modern	Upper	5.5	60%	1	27	3	11544.21
Burial	Modern	Upper	5.5	60%	2	27	3	12350.51
Burial	Brady	Upper	5.5	60%	1	27	3	1582.64
Burial	Brady	Upper	5.5	60%	2	27	3	1699.86
Burial	Modern	Upper	3.5	60%	1	27	2	11886.53

Landform	Paleostatus	Soil Layers	Depth to Brady (m)	Water%	Rep	Day	Depth	ug-CO2/gC(cumulative)
Burial	Modern	Upper	3.5	60%	2	27	2	11543.69
Burial	Brady	Upper	3.5	60%	1	27	2	2621.85
Burial	Brady	Upper	3.5	60%	2	27	2	3081.44
Burial	Modern	Upper	1.5	60%	1	27	1	10609.43
Burial	Modern	Upper	1.5	60%	2	27	1	9226.69
Burial	Brady	Upper	1.5	60%	1	27	1	4141.43
Burial	Brady	Upper	1.5	60%	2	27	1	3634.31
Erosional	Modern	Upper	1.5	60%	1	27	3	11806.10
Erosional	Modern	Upper	1.5	60%	2	27	3	12587.63
Erosional	Brady	Upper	1.5	60%	1	27	3	2907.78
Erosional	Brady	Upper	1.5	60%	2	27	3	4405.82
Erosional	Modern	Upper	0.5	60%	1	27	2	15912.09
Erosional	Modern	Upper	0.5	60%	2	27	2	12970.62
Erosional	Brady	Upper	0.5	60%	1	27	2	5236.01
Erosional	Brady	Upper	0.5	60%	2	27	2	6070.35
Erosional	Modern	Upper	0.2	60%	1	27	1	14043.60
Erosional	Modern	Upper	0.2	60%	2	27	1	14895.99
Erosional	Brady	Upper	0.2	60%	1	27	1	6135.66
Erosional	Brady	Upper	0.2	60%	2	27	1	5299.68
Burial	Modern	Upper	5.5	60%	1	55	3	16155.58
Burial	Modern	Upper	5.5	60%	2	55	3	15908.04
Burial	Brady	Upper	5.5	60%	1	55	3	2043.34
Burial	Brady	Upper	5.5	60%	2	55	3	2023.15
Burial	Modern	Upper	3.5	60%	1	55	2	12831.41
Burial	Modern	Upper	3.5	60%	2	55	2	13200.72
Burial	Brady	Upper	3.5	60%	1	55	2	3289.94
Burial	Brady	Upper	3.5	60%	2	55	2	4037.66
Burial	Modern	Upper	1.5	60%	1	55	1	14526.46
Burial	Modern	Upper	1.5	60%	2	55	1	12046.95
Burial	Brady	Upper	1.5	60%	1	55	1	6041.18
Burial	Brady	Upper	1.5	60%	2	55	1	4444.64
Erosional	Modern	Upper	1.5	60%	1	55	3	22470.15
Erosional	Modern	Upper	1.5	60%	2	55	3	18998.51
Erosional	Brady	Upper	1.5	60%	1	55	3	3927.35
Erosional	Brady	Upper	1.5	60%	2	55	3	5506.37
Erosional	Modern	Upper	0.5	60%	1	55	2	16774.21
Erosional	Modern	Upper	0.5	60%	2	55	2	14429.95
Erosional	Brady	Upper	0.5	60%	1	55	2	6816.26

Landform	Paleostatus	Soil Layers	Depth to Brady (m)	Water%	Rep	Day	Depth	ug-CO2/gC(cumulative)
Erosional	Brady	Upper	0.5	60%	2	55	2	8428.89
Erosional	Modern	Upper	0.2	60%	1	55	1	19896.03
Erosional	Modern	Upper	0.2	60%	2	55	1	15816.17
Erosional	Brady	Upper	0.2	60%	1	55	1	10282.19
Erosional	Brady	Upper	0.2	60%	2	55	1	6843.39
Burial	Modern	Upper	5.5	60%	1	82	3	19884.07
Burial	Modern	Upper	5.5	60%	2	82	3	20209.11
Burial	Brady	Upper	5.5	60%	1	82	3	2172.86
Burial	Brady	Upper	5.5	60%	2	82	3	2344.74
Burial	Modern	Upper	3.5	60%	1	82	2	14491.91
Burial	Modern	Upper	3.5	60%	2	82	2	14238.29
Burial	Brady	Upper	3.5	60%	1	82	2	3929.41
Burial	Brady	Upper	3.5	60%	2	82	2	4783.83
Burial	Modern	Upper	1.5	60%	1	82	1	16084.47
Burial	Modern	Upper	1.5	60%	2	82	1	13455.17
Burial	Brady	Upper	1.5	60%	1	82	1	7038.99
Burial	Brady	Upper	1.5	60%	2	82	1	4850.27
Erosional	Modern	Upper	1.5	60%	1	82	3	24284.96
Erosional	Modern	Upper	1.5	60%	2	82	3	20608.11
Erosional	Brady	Upper	1.5	60%	1	82	3	4765.50
Erosional	Brady	Upper	1.5	60%	2	82	3	6033.56
Erosional	Modern	Upper	0.5	60%	1	82	2	18741.44
Erosional	Modern	Upper	0.5	60%	2	82	2	17496.05
Erosional	Brady	Upper	0.5	60%	1	82	2	8488.74
Erosional	Brady	Upper	0.5	60%	2	82	2	9500.16
Erosional	Modern	Upper	0.2	60%	1	82	1	25588.19
Erosional	Modern	Upper	0.2	60%	2	82	1	21263.20
Erosional	Brady	Upper	0.2	60%	1	82	1	12436.52
Erosional	Brady	Upper	0.2	60%	2	82	1	7652.23
Burial	Modern	Upper	5.5	60%	1	114	3	23304.57
Burial	Modern	Upper	5.5	60%	2	114	3	24209.72
Burial	Brady	Upper	5.5	60%	1	114	3	2501.41
Burial	Brady	Upper	5.5	60%	2	114	3	3020.76
Burial	Modern	Upper	3.5	60%	1	114	2	16236.83
Burial	Modern	Upper	3.5	60%	2	114	2	16624.45
Burial	Brady	Upper	3.5	60%	1	114	2	5018.96
Burial	Brady	Upper	3.5	60%	2	114	2	5316.84
Burial	Modern	Upper	1.5	60%	1	114	1	17387.70

Landform	Paleostatus	Soil Layers	Depth to Brady (m)	Water%	Rep	Day	Depth	ug-CO2/gC(cumulative)
Burial	Modern	Upper	1.5	60%	2	114	1	14476.05
Burial	Brady	Upper	1.5	60%	1	114	1	7774.42
Burial	Brady	Upper	1.5	60%	2	114	1	5366.11
Erosional	Modern	Upper	1.5	60%	1	114	3	25169.34
Erosional	Modern	Upper	1.5	60%	2	114	3	20911.28
Erosional	Brady	Upper	1.5	60%	1	114	3	5676.86
Erosional	Brady	Upper	1.5	60%	2	114	3	7925.94
Erosional	Modern	Upper	0.5	60%	1	114	2	24082.15
Erosional	Modern	Upper	0.5	60%	2	114	2	20805.01
Erosional	Brady	Upper	0.5	60%	1	114	2	10780.05
Erosional	Brady	Upper	0.5	60%	2	114	2	11862.23
Erosional	Modern	Upper	0.2	60%	1	114	1	33093.70
Erosional	Modern	Upper	0.2	60%	2	114	1	28528.18
Erosional	Brady	Upper	0.2	60%	1	114	1	15752.17
Erosional	Brady	Upper	0.2	60%	2	114	1	9186.45
Burial	Modern	Upper	5.5	60%	1	151	3	26219.45
Burial	Modern	Upper	5.5	60%	2	151	3	28498.76
Burial	Brady	Upper	5.5	60%	1	151	3	2813.98
Burial	Brady	Upper	5.5	60%	2	151	3	3378.72
Burial	Modern	Upper	3.5	60%	1	151	2	19761.93
Burial	Modern	Upper	3.5	60%	2	151	2	21723.32
Burial	Brady	Upper	3.5	60%	1	151	2	5408.31
Burial	Brady	Upper	3.5	60%	2	151	2	5813.79
Burial	Modern	Upper	1.5	60%	1	151	1	18480.87
Burial	Modern	Upper	1.5	60%	2	151	1	15480.77
Burial	Brady	Upper	1.5	60%	1	151	1	8944.31
Burial	Brady	Upper	1.5	60%	2	151	1	8163.58
Erosional	Modern	Upper	1.5	60%	1	151	3	27919.70
Erosional	Modern	Upper	1.5	60%	2	151	3	25747.29
Erosional	Brady	Upper	1.5	60%	1	151	3	6493.99
Erosional	Brady	Upper	1.5	60%	2	151	3	8863.27
Erosional	Modern	Upper	0.5	60%	1	151	2	31043.77
Erosional	Modern	Upper	0.5	60%	2	151	2	25523.27
Erosional	Brady	Upper	0.5	60%	1	151	2	11763.40
Erosional	Brady	Upper	0.5	60%	2	151	2	12697.87
Erosional	Modern	Upper	0.2	60%	1	151	1	39491.11
Erosional	Modern	Upper	0.2	60%	2	151	1	34120.39
Erosional	Brady	Upper	0.2	60%	1	151	1	19022.14

Landform	Paleostatus	Soil Layers	Depth to Brady (m)	Water%	Rep	Day	Depth	ug-CO2/gC(cumulative)
Erosional	Brady	Upper	0.2	60%	2	151	1	14266.25
Burial	Modern	Upper	5.5	60%	1	225	3	27222.31
Burial	Modern	Upper	5.5	60%	2	225	3	32545.72
Burial	Brady	Upper	5.5	60%	1	225	3	3186.62
Burial	Brady	Upper	5.5	60%	2	225	3	5090.16
Burial	Modern	Upper	3.5	60%	1	225	2	20748.58
Burial	Modern	Upper	3.5	60%	2	225	2	28770.57
Burial	Brady	Upper	3.5	60%	1	225	2	6752.14
Burial	Brady	Upper	3.5	60%	2	225	2	18067.58
Burial	Modern	Upper	1.5	60%	1	225	1	18746.92
Burial	Modern	Upper	1.5	60%	2	225	1	23585.92
Burial	Brady	Upper	1.5	60%	1	225	1	8954.38
Burial	Brady	Upper	1.5	60%	2	225	1	13638.78
Erosional	Modern	Upper	1.5	60%	1	225	3	33245.77
Erosional	Modern	Upper	1.5	60%	2	225	3	29711.33
Erosional	Brady	Upper	1.5	60%	1	225	3	16811.48
Erosional	Brady	Upper	1.5	60%	2	225	3	9532.30
Erosional	Modern	Upper	0.5	60%	1	225	2	31661.08
Erosional	Modern	Upper	0.5	60%	2	225	2	37678.43
Erosional	Brady	Upper	0.5	60%	1	225	2	48475.87
Erosional	Brady	Upper	0.5	60%	2	225	2	17845.68
Erosional	Modern	Upper	0.2	60%	1	225	1	48566.31
Erosional	Modern	Upper	0.2	60%	2	225	1	34809.29
Erosional	Brady	Upper	0.2	60%	1	225	1	27353.19
Erosional	Brady	Upper	0.2	60%	2	225	1	15462.80
Burial	Modern	Upper	5.5	5%	0	1	3	15.04
Burial	Brady	Upper	5.5	5%	0	1	3	32.80
Burial	Modern	Upper	3.5	5%	0	1	2	7.23
Burial	Brady	Upper	3.5	5%	0	1	2	45.39
Burial	Modern	Upper	1.5	5%	0	1	1	4.83
Burial	Brady	Upper	1.5	5%	0	1	1	53.54
Erosional	Modern	Upper	1.5	5%	0	1	3	33.50
Erosional	Brady	Upper	1.5	5%	0	1	3	56.67
Erosional	Modern	Upper	0.5	5%	0	1	2	16.79
Erosional	Brady	Upper	0.5	5%	0	1	2	27.58
Erosional	Modern	Upper	0.2	5%	0	1	1	15.92
Erosional	Brady	Upper	0.2	5%	0	1	1	19.13
Burial	Modern	Upper	5.5	5%	0	3	3	24.63

Landform	Paleostatus	Soil Layers	Depth to Brady (m)	Water%	Rep	Day	Depth	ug-CO2/gC(cumulative)
Burial	Brady	Upper	5.5	5%	0	3	3	47.35
Burial	Modern	Upper	3.5	5%	0	3	2	28.26
Burial	Brady	Upper	3.5	5%	0	3	2	63.13
Burial	Modern	Upper	1.5	5%	0	3	1	16.20
Burial	Brady	Upper	1.5	5%	0	3	1	99.16
Erosional	Modern	Upper	1.5	5%	0	3	3	45.24
Erosional	Brady	Upper	1.5	5%	0	3	3	74.87
Erosional	Modern	Upper	0.5	5%	0	3	2	31.91
Erosional	Brady	Upper	0.5	5%	0	3	2	44.97
Erosional	Modern	Upper	0.2	5%	0	3	1	25.16
Erosional	Brady	Upper	0.2	5%	0	3	1	29.83
Burial	Modern	Upper	5.5	5%	0	5	3	55.40
Burial	Brady	Upper	5.5	5%	0	5	3	96.88
Burial	Modern	Upper	3.5	5%	0	5	2	40.60
Burial	Brady	Upper	3.5	5%	0	5	2	112.20
Burial	Modern	Upper	1.5	5%	0	5	1	28.31
Burial	Brady	Upper	1.5	5%	0	5	1	155.33
Erosional	Modern	Upper	1.5	5%	0	5	3	68.95
Erosional	Brady	Upper	1.5	5%	0	5	3	121.67
Erosional	Modern	Upper	0.5	5%	0	5	2	54.80
Erosional	Brady	Upper	0.5	5%	0	5	2	67.04
Erosional	Modern	Upper	0.2	5%	0	5	1	52.55
Erosional	Brady	Upper	0.2	5%	0	5	1	68.62
Burial	Modern	Upper	5.5	5%	0	7	3	72.85
Burial	Brady	Upper	5.5	5%	0	7	3	122.86
Burial	Modern	Upper	3.5	5%	0	7	2	48.20
Burial	Brady	Upper	3.5	5%	0	7	2	156.63
Burial	Modern	Upper	1.5	5%	0	7	1	35.47
Burial	Brady	Upper	1.5	5%	0	7	1	210.19
Erosional	Modern	Upper	1.5	5%	0	7	3	92.13
Erosional	Brady	Upper	1.5	5%	0	7	3	165.99
Erosional	Modern	Upper	0.5	5%	0	7	2	66.26
Erosional	Brady	Upper	0.5	5%	0	7	2	112.13
Erosional	Modern	Upper	0.2	5%	0	7	1	71.17
Erosional	Brady	Upper	0.2	5%	0	7	1	83.51
Burial	Modern	Upper	5.5	5%	0	11	3	115.27
Burial	Brady	Upper	5.5	5%	0	11	3	144.54
Burial	Modern	Upper	3.5	5%	0	11	2	57.62

Landform	Paleostatus	Soil Layers	Depth to Brady (m)	Water%	Rep	Day	Depth	ug-CO2/gC(cumulative)
Burial	Brady	Upper	3.5	5%	0	11	2	232.83
Burial	Modern	Upper	1.5	5%	0	11	1	59.05
Burial	Brady	Upper	1.5	5%	0	11	1	260.45
Erosional	Modern	Upper	1.5	5%	0	11	3	116.40
Erosional	Brady	Upper	1.5	5%	0	11	3	203.09
Erosional	Modern	Upper	0.5	5%	0	11	2	81.47
Erosional	Brady	Upper	0.5	5%	0	11	2	156.03
Erosional	Modern	Upper	0.2	5%	0	11	1	80.06
Erosional	Brady	Upper	0.2	5%	0	11	1	118.86
Burial	Modern	Upper	5.5	5%	0	16	3	135.24
Burial	Brady	Upper	5.5	5%	0	16	3	166.15
Burial	Modern	Upper	3.5	5%	0	16	2	83.03
Burial	Brady	Upper	3.5	5%	0	16	2	296.63
Burial	Modern	Upper	1.5	5%	0	16	1	74.11
Burial	Brady	Upper	1.5	5%	0	16	1	330.88
Erosional	Modern	Upper	1.5	5%	0	16	3	137.41
Erosional	Brady	Upper	1.5	5%	0	16	3	232.05
Erosional	Modern	Upper	0.5	5%	0	16	2	93.71
Erosional	Brady	Upper	0.5	5%	0	16	2	186.58
Erosional	Modern	Upper	0.2	5%	0	16	1	115.73
Erosional	Brady	Upper	0.2	5%	0	16	1	181.04
Burial	Modern	Upper	5.5	5%	0	27	3	158.12
Burial	Brady	Upper	5.5	5%	0	27	3	208.67
Burial	Modern	Upper	3.5	5%	0	27	2	95.26
Burial	Brady	Upper	3.5	5%	0	27	2	376.05
Burial	Modern	Upper	1.5	5%	0	27	1	88.52
Burial	Brady	Upper	1.5	5%	0	27	1	355.46
Erosional	Modern	Upper	1.5	5%	0	27	3	184.56
Erosional	Brady	Upper	1.5	5%	0	27	3	294.81
Erosional	Modern	Upper	0.5	5%	0	27	2	127.99
Erosional	Brady	Upper	0.5	5%	0	27	2	234.52
Erosional	Modern	Upper	0.2	5%	0	27	1	138.96
Erosional	Brady	Upper	0.2	5%	0	27	1	217.05
Burial	Modern	Upper	5.5	5%	0	55	3	225.59
Burial	Brady	Upper	5.5	5%	0	55	3	236.43
Burial	Modern	Upper	3.5	5%	0	55	2	171.12
Burial	Brady	Upper	3.5	5%	0	55	2	576.61
Burial	Modern	Upper	1.5	5%	0	55	1	110.91

Landform	Paleostatus	Soil Layers	Depth to Brady (m)	Water%	Rep	Day	Depth	ug-CO2/gC(cumulative)
Burial	Brady	Upper	1.5	5%	0	55	1	489.81
Erosional	Modern	Upper	1.5	5%	0	55	3	207.38
Erosional	Brady	Upper	1.5	5%	0	55	3	371.71
Erosional	Modern	Upper	0.5	5%	0	55	2	182.28
Erosional	Brady	Upper	0.5	5%	0	55	2	288.50
Erosional	Modern	Upper	0.2	5%	0	55	1	169.62
Erosional	Brady	Upper	0.2	5%	0	55	1	293.19
Burial	Modern	Upper	5.5	5%	0	82	3	231.55
Burial	Brady	Upper	5.5	5%	0	82	3	248.83
Burial	Modern	Upper	3.5	5%	0	82	2	173.08
Burial	Brady	Upper	3.5	5%	0	82	2	602.20
Burial	Modern	Upper	1.5	5%	0	82	1	124.91
Burial	Brady	Upper	1.5	5%	0	82	1	541.53
Erosional	Modern	Upper	1.5	5%	0	82	3	215.63
Erosional	Brady	Upper	1.5	5%	0	82	3	375.69
Erosional	Modern	Upper	0.5	5%	0	82	2	222.03
Erosional	Brady	Upper	0.5	5%	0	82	2	294.42
Erosional	Modern	Upper	0.2	5%	0	82	1	180.65
Erosional	Brady	Upper	0.2	5%	0	82	1	297.92
Burial	Modern	Upper	5.5	5%	0	114	3	312.17
Burial	Brady	Upper	5.5	5%	0	114	3	287.58
Burial	Modern	Upper	3.5	5%	0	114	2	181.71
Burial	Brady	Upper	3.5	5%	0	114	2	630.93
Burial	Modern	Upper	1.5	5%	0	114	1	213.81
Burial	Brady	Upper	1.5	5%	0	114	1	601.61
Erosional	Modern	Upper	1.5	5%	0	114	3	230.89
Erosional	Brady	Upper	1.5	5%	0	114	3	474.72
Erosional	Modern	Upper	0.5	5%	0	114	2	237.01
Erosional	Brady	Upper	0.5	5%	0	114	2	337.34
Erosional	Modern	Upper	0.2	5%	0	114	1	208.45
Erosional	Brady	Upper	0.2	5%	0	114	1	354.11
Burial	Modern	Upper	5.5	5%	0	151	3	320.90
Burial	Brady	Upper	5.5	5%	0	151	3	315.36
Burial	Modern	Upper	3.5	5%	0	151	2	184.70
Burial	Brady	Upper	3.5	5%	0	151	2	656.75
Burial	Modern	Upper	1.5	5%	0	151	1	226.78
Burial	Brady	Upper	1.5	5%	0	151	1	618.90
Erosional	Modern	Upper	1.5	5%	0	151	3	253.52

Landform	Paleostatus	Soil Layers	Depth to Brady (m)	Water%	Rep	Day	Depth	ug-CO2/gC(cumulative)
Erosional	Brady	Upper	1.5	5%	0	151	3	505.80
Erosional	Modern	Upper	0.5	5%	0	151	2	246.08
Erosional	Brady	Upper	0.5	5%	0	151	2	351.77
Erosional	Modern	Upper	0.2	5%	0	151	1	213.56
Erosional	Brady	Upper	0.2	5%	0	151	1	362.31
Burial	Modern	Upper	5.5	5%	0	225	3	328.57
Burial	Brady	Upper	5.5	5%	0	225	3	341.96
Burial	Modern	Upper	3.5	5%	0	225	2	190.32
Burial	Brady	Upper	3.5	5%	0	225	2	699.81
Burial	Modern	Upper	1.5	5%	0	225	1	240.19
Burial	Brady	Upper	1.5	5%	0	225	1	642.70
Erosional	Modern	Upper	1.5	5%	0	225	3	277.91
Erosional	Brady	Upper	1.5	5%	0	225	3	577.35
Erosional	Modern	Upper	0.5	5%	0	225	2	260.55
Erosional	Brady	Upper	0.5	5%	0	225	2	382.07
Erosional	Modern	Upper	0.2	5%	0	225	1	222.57
Erosional	Brady	Upper	0.2	5%	0	225	1	372.81

Table 4-3. Wet-drying experiment (60% WHC) and control (5% WHC) respired CO_2 from modern and Brady soils collected from burial and erosional landform at 6 different depth categories.

Landform	Paleostatus	Soil Layers	Depth to Brady (m)	Water%	Replication	Day	Depth	ugCO2/gC (per Day)
Burial	Modern	Upper	5.5	60%	1	1	3	3574.455
Burial	Modern	Upper	5.5	60%	2	1	3	3827.949
Burial	Brady	Upper	5.5	60%	1	1	3	1131.659
Burial	Brady	Upper	5.5	60%	2	1	3	1073.063
Burial	Modern	Upper	3.5	60%	1	1	2	2821.981
Burial	Modern	Upper	3.5	60%	2	1	2	3309.154
Burial	Brady	Upper	3.5	60%	1	1	2	1353.308
Burial	Brady	Upper	3.5	60%	2	1	2	1555.894
Burial	Modern	Upper	1.5	60%	1	1	1	2174.895
Burial	Modern	Upper	1.5	60%	2	1	1	2061.929
Burial	Brady	Upper	1.5	60%	1	1	1	1140.753
Burial	Brady	Upper	1.5	60%	2	1	1	1442.384
Erosional	Modern	Upper	1.5	60%	1	1	3	3555.185
Erosional	Modern	Upper	1.5	60%	2	1	3	2741.646
Erosional	Brady	Upper	1.5	60%	1	1	3	1244.457
Erosional	Brady	Upper	1.5	60%	2	1	3	1119.221
Erosional	Modern	Upper	0.5	60%	1	1	2	3297.817
Erosional	Modern	Upper	0.5	60%	2	1	2	3529.43
Erosional	Brady	Upper	0.5	60%	1	1	2	1306.45
Erosional	Brady	Upper	0.5	60%	2	1	2	1320.591
Erosional	Modern	Upper	0.2	60%	1	1	1	2372.104
Erosional	Modern	Upper	0.2	60%	2	1	1	2271.408
Erosional	Brady	Upper	0.2	60%	1	1	1	3194.95
Erosional	Brady	Upper	0.2	60%	2	1	1	3471.173
Burial	Modern	Upper	5.5	60%	1	7	3	1053.529
Burial	Modern	Upper	5.5	60%	2	7	3	1173.822
Burial	Brady	Upper	5.5	60%	1	7	3	1163.938
Burial	Brady	Upper	5.5	60%	2	7	3	756.8482
Burial	Modern	Upper	3.5	60%	1	7	2	1536.59
Burial	Modern	Upper	3.5	60%	2	7	2	1737.08
Burial	Brady	Upper	3.5	60%	1	7	2	1397.679
Burial	Brady	Upper	3.5	60%	2	7	2	1319.492
Burial	Modern	Upper	1.5	60%	1	7	1	1464.341

Landform	Paleostatus	Soil Layers	Depth to Brady (m)	Water%	Replication	Day	Depth	ugCO2/gC (per Day)
Burial	Modern	Upper	1.5	60%	2	7	1	1050.381
Burial	Brady	Upper	1.5	60%	1	7	1	848.2157
Burial	Brady	Upper	1.5	60%	2	7	1	544.0116
Erosional	Modern	Upper	1.5	60%	1	7	3	1809.61
Erosional	Modern	Upper	1.5	60%	2	7	3	1656.429
Erosional	Brady	Upper	1.5	60%	1	7	3	867.327
Erosional	Brady	Upper	1.5	60%	2	7	3	1139.899
Erosional	Modern	Upper	0.5	60%	1	7	2	1685.059
Erosional	Modern	Upper	0.5	60%	2	7	2	1789.988
Erosional	Brady	Upper	0.5	60%	1	7	2	1322.177
Erosional	Brady	Upper	0.5	60%	2	7	2	990.3232
Erosional	Modern	Upper	0.2	60%	1	7	1	1634.289
Erosional	Modern	Upper	0.2	60%	2	7	1	1864.999
Erosional	Brady	Upper	0.2	60%	1	7	1	1476.622
Erosional	Brady	Upper	0.2	60%	2	7	1	1770.948
Burial	Modern	Upper	5.5	60%	1	21	3	1106.383
Burial	Modern	Upper	5.5	60%	2	21	3	1305.787
Burial	Brady	Upper	5.5	60%	1	21	3	1156.34
Burial	Brady	Upper	5.5	60%	2	21	3	1007.607
Burial	Modern	Upper	3.5	60%	1	21	2	695.0272
Burial	Modern	Upper	3.5	60%	2	21	2	1254.486
Burial	Brady	Upper	3.5	60%	1	21	2	1425.98
Burial	Brady	Upper	3.5	60%	2	21	2	1228.556
Burial	Modern	Upper	1.5	60%	1	21	1	1092.343
Burial	Modern	Upper	1.5	60%	2	21	1	847.0728
Burial	Brady	Upper	1.5	60%	1	21	1	961.1488
Burial	Brady	Upper	1.5	60%	2	21	1	657.5733
Erosional	Modern	Upper	1.5	60%	1	21	3	1477.425
Erosional	Modern	Upper	1.5	60%	2	21	3	1266.266
Erosional	Brady	Upper	1.5	60%	1	21	3	1104.154
Erosional	Brady	Upper	1.5	60%	2	21	3	873.2996
Erosional	Modern	Upper	0.5	60%	1	21	2	1527.3
Erosional	Modern	Upper	0.5	60%	2	21	2	1060.278
Erosional	Brady	Upper	0.5	60%	1	21	2	1370.649
Erosional	Brady	Upper	0.5	60%	2	21	2	1345.661
Erosional	Modern	Upper	0.2	60%	1	21	1	970.3736
Erosional	Modern	Upper	0.2	60%	2	21	1	975.3993
Erosional	Brady	Upper	0.2	60%	1	21	1	1387.656

Landform	Paleostatus	Soil Layers	Depth to Brady (m)	Water%	Replication	Day	Depth	ugCO2/gC (per Day)
Erosional	Brady	Upper	0.2	60%	2	21	1	1244.439
Burial	Modern	Upper	5.5	60%	1	28	3	1223.451
Burial	Modern	Upper	5.5	60%	2	28	3	1311.868
Burial	Brady	Upper	5.5	60%	1	28	3	579.2929
Burial	Brady	Upper	5.5	60%	2	28	3	631.9666
Burial	Modern	Upper	3.5	60%	1	28	2	1203.231
Burial	Modern	Upper	3.5	60%	2	28	2	1124.539
Burial	Brady	Upper	3.5	60%	1	28	2	950.3627
Burial	Brady	Upper	3.5	60%	2	28	2	815.7742
Burial	Modern	Upper	1.5	60%	1	28	1	1029.325
Burial	Modern	Upper	1.5	60%	2	28	1	1168.91
Burial	Brady	Upper	1.5	60%	1	28	1	233.139
Burial	Brady	Upper	1.5	60%	2	28	1	391.545
Erosional	Modern	Upper	1.5	60%	1	28	3	1490.72
Erosional	Modern	Upper	1.5	60%	2	28	3	1495.171
Erosional	Brady	Upper	1.5	60%	1	28	3	1054.085
Erosional	Brady	Upper	1.5	60%	2	28	3	695.4041
Erosional	Modern	Upper	0.5	60%	1	28	2	1300.814
Erosional	Modern	Upper	0.5	60%	2	28	2	1463.954
Erosional	Brady	Upper	0.5	60%	1	28	2	1420.668
Erosional	Brady	Upper	0.5	60%	2	28	2	1228.822
Erosional	Modern	Upper	0.2	60%	1	28	1	1227.23
Erosional	Modern	Upper	0.2	60%	2	28	1	786.6592
Erosional	Brady	Upper	0.2	60%	1	28	1	715.842
Erosional	Brady	Upper	0.2	60%	2	28	1	1216.397
Burial	Modern	Upper	5.5	60%	1	35	3	1279.166
Burial	Modern	Upper	5.5	60%	2	35	3	1196.802
Burial	Brady	Upper	5.5	60%	1	35	3	1067.889
Burial	Brady	Upper	5.5	60%	2	35	3	975.8202
Burial	Modern	Upper	3.5	60%	1	35	2	993.907
Burial	Modern	Upper	3.5	60%	2	35	2	1443.765
Burial	Brady	Upper	3.5	60%	1	35	2	1180.71
Burial	Brady	Upper	3.5	60%	2	35	2	664.988
Burial	Modern	Upper	1.5	60%	1	35	1	910.9239
Burial	Modern	Upper	1.5	60%	2	35	1	729.8793
Burial	Brady	Upper	1.5	60%	1	35	1	556.7395
Burial	Brady	Upper	1.5	60%	2	35	1	573.0568
Erosional	Modern	Upper	1.5	60%	1	35	3	1388.342

Landform	Paleostatus	Soil Layers	Depth to Brady (m)	Water%	Replication	Day	Depth	ugCO2/gC (per Day)
Erosional	Modern	Upper	1.5	60%	2	35	3	980.3039
Erosional	Brady	Upper	1.5	60%	1	35	3	496.2832
Erosional	Brady	Upper	1.5	60%	2	35	3	524.6612
Erosional	Modern	Upper	0.5	60%	1	35	2	1200.093
Erosional	Modern	Upper	0.5	60%	2	35	2	1165.962
Erosional	Brady	Upper	0.5	60%	1	35	2	1315.937
Erosional	Brady	Upper	0.5	60%	2	35	2	700.1521
Erosional	Modern	Upper	0.2	60%	1	35	1	694.2941
Erosional	Modern	Upper	0.2	60%	2	35	1	1098.185
Erosional	Brady	Upper	0.2	60%	1	35	1	1427.087
Erosional	Brady	Upper	0.2	60%	2	35	1	1047.553
Burial	Modern	Upper	5.5	60%	1	42	3	865.4368
Burial	Modern	Upper	5.5	60%	2	42	3	996.0393
Burial	Brady	Upper	5.5	60%	1	42	3	517.4835
Burial	Brady	Upper	5.5	60%	2	42	3	558.4316
Burial	Modern	Upper	3.5	60%	1	42	2	1023.018
Burial	Modern	Upper	3.5	60%	2	42	2	709.6119
Burial	Brady	Upper	3.5	60%	1	42	2	577.9844
Burial	Brady	Upper	3.5	60%	2	42	2	936.328
Burial	Modern	Upper	1.5	60%	1	42	1	453.977
Burial	Modern	Upper	1.5	60%	2	42	1	734.8177
Burial	Brady	Upper	1.5	60%	1	42	1	44.2793
Burial	Brady	Upper	1.5	60%	2	42	1	256.2662
Erosional	Modern	Upper	1.5	60%	1	42	3	1146.557
Erosional	Modern	Upper	1.5	60%	2	42	3	598.1293
Erosional	Brady	Upper	1.5	60%	1	42	3	992.2005
Erosional	Brady	Upper	1.5	60%	2	42	3	1399.628
Erosional	Modern	Upper	0.5	60%	1	42	2	729.6351
Erosional	Modern	Upper	0.5	60%	2	42	2	1154.268
Erosional	Brady	Upper	0.5	60%	1	42	2	1050.87
Erosional	Brady	Upper	0.5	60%	2	42	2	935.4375
Erosional	Modern	Upper	0.2	60%	1	42	1	1025.35
Erosional	Modern	Upper	0.2	60%	2	42	1	799.713
Erosional	Brady	Upper	0.2	60%	1	42	1	817.0655
Erosional	Brady	Upper	0.2	60%	2	42	1	893.701
Burial	Modern	Upper	5.5	60%	1	49	3	1097.394
Burial	Modern	Upper	5.5	60%	2	49	3	1031.739
Burial	Brady	Upper	5.5	60%	1	49	3	953.8884

Landform	Paleostatus	Soil Layers	Depth to Brady (m)	Water%	Replication	Day	Depth	ugCO2/gC (per Day)
Burial	Brady	Upper	5.5	60%	2	49	3	1110.208
Burial	Modern	Upper	3.5	60%	1	49	2	1077.268
Burial	Modern	Upper	3.5	60%	2	49	2	1303.184
Burial	Brady	Upper	3.5	60%	1	49	2	1098.654
Burial	Brady	Upper	3.5	60%	2	49	2	505.7281
Burial	Modern	Upper	1.5	60%	1	49	1	622.1719
Burial	Modern	Upper	1.5	60%	2	49	1	374.535
Burial	Brady	Upper	1.5	60%	1	49	1	415.4754
Burial	Brady	Upper	1.5	60%	2	49	1	372.8782
Erosional	Modern	Upper	1.5	60%	1	49	3	1271.08
Erosional	Modern	Upper	1.5	60%	2	49	3	1280.797
Erosional	Brady	Upper	1.5	60%	1	49	3	1158.855
Erosional	Brady	Upper	1.5	60%	2	49	3	1112.638
Erosional	Modern	Upper	0.5	60%	1	49	2	1280.822
Erosional	Modern	Upper	0.5	60%	2	49	2	1197.11
Erosional	Brady	Upper	0.5	60%	1	49	2	1291.633
Erosional	Brady	Upper	0.5	60%	2	49	2	558.8833
Erosional	Modern	Upper	0.2	60%	1	49	1	1033.471
Erosional	Modern	Upper	0.2	60%	2	49	1	957.5217
Erosional	Brady	Upper	0.2	60%	1	49	1	1201.713
Erosional	Brady	Upper	0.2	60%	2	49	1	1184.1
Burial	Modern	Upper	5.5	5%	1	1	0	81.37199
Burial	Brady	Upper	5.5	5%	1	1	0	129.0195
Burial	Modern	Upper	3.5	5%	1	1	0	24.11923
Burial	Brady	Upper	3.5	5%	1	1	0	108.4926
Burial	Modern	Upper	1.5	5%	1	1	0	44.08719
Burial	Brady	Upper	1.5	5%	1	1	0	279.5932
Erosional	Modern	Upper	1.5	5%	1	1	0	136.9782
Erosional	Brady	Upper	1.5	5%	1	1	0	279.8257
Erosional	Modern	Upper	0.5	5%	1	1	0	97.65442
Erosional	Brady	Upper	0.5	5%	1	1	0	98.93884
Erosional	Modern	Upper	0.2	5%	1	1	0	94.17696
Erosional	Brady	Upper	0.2	5%	1	1	0	28.93858
Burial	Modern	Upper	5.5	5%	1	7	0	69.82241
Burial	Brady	Upper	5.5	5%	1	7	0	103.9235
Burial	Modern	Upper	3.5	5%	1	7	0	53.44611
Burial	Brady	Upper	3.5	5%	1	7	0	177.6976
Burial	Modern	Upper	1.5	5%	1	7	0	42.91534

Landform	Paleostatus	Soil Layers	Depth to Brady (m)	Water%	Replication	Day	Depth	ugCO2/gC (per Day)
Burial	Brady	Upper	1.5	5%	1	7	0	219.4396
Erosional	Modern	Upper	1.5	5%	1	7	0	92.73663
Erosional	Brady	Upper	1.5	5%	1	7	0	177.2782
Erosional	Modern	Upper	0.5	5%	1	7	0	45.80117
Erosional	Brady	Upper	0.5	5%	1	7	0	180.3752
Erosional	Modern	Upper	0.2	5%	1	7	0	74.50819
Erosional	Brady	Upper	0.2	5%	1	7	0	59.59475
Burial	Modern	Upper	5.5	5%	1	21	0	158.1469
Burial	Brady	Upper	5.5	5%	1	21	0	205.8561
Burial	Modern	Upper	3.5	5%	1	21	0	78.91915
Burial	Brady	Upper	3.5	5%	1	21	0	334.0008
Burial	Modern	Upper	1.5	5%	1	21	0	73.94648
Burial	Brady	Upper	1.5	5%	1	21	0	340.782
Erosional	Modern	Upper	1.5	5%	1	21	0	199.1242
Erosional	Brady	Upper	1.5	5%	1	21	0	322.0202
Erosional	Modern	Upper	0.5	5%	1	21	0	118.386
Erosional	Brady	Upper	0.5	5%	1	21	0	180.3906
Erosional	Modern	Upper	0.2	5%	1	21	0	51.31167
Erosional	Brady	Upper	0.2	5%	1	21	0	159.7988
Burial	Modern	Upper	5.5	5%	1	28	0	151.3277
Burial	Brady	Upper	5.5	5%	1	28	0	195.5792
Burial	Modern	Upper	3.5	5%	1	28	0	74.1908
Burial	Brady	Upper	3.5	5%	1	28	0	321.2941
Burial	Modern	Upper	1.5	5%	1	28	0	69.41598
Burial	Brady	Upper	1.5	5%	1	28	0	327.1313
Erosional	Modern	Upper	1.5	5%	1	28	0	191.7381
Erosional	Brady	Upper	1.5	5%	1	28	0	310.1373
Erosional	Modern	Upper	0.5	5%	1	28	0	113.2874
Erosional	Brady	Upper	0.5	5%	1	28	0	170.6715
Erosional	Modern	Upper	0.2	5%	1	28	0	53.21694
Erosional	Brady	Upper	0.2	5%	1	28	0	187.8014
Burial	Modern	Upper	5.5	5%	1	35	0	120.0528
Burial	Brady	Upper	5.5	5%	1	35	0	164.4986
Burial	Modern	Upper	3.5	5%	1	35	0	85.67712
Burial	Brady	Upper	3.5	5%	1	35	0	156.856
Burial	Modern	Upper	1.5	5%	1	35	0	50.89711
Burial	Brady	Upper	1.5	5%	1	35	0	318.9727
Erosional	Modern	Upper	1.5	5%	1	35	0	122.2267

Landform	Paleostatus	Soil Layers	Depth to Brady (m)	Water%	Replication	Day	Depth	ugCO2/gC (per Day)
Erosional	Brady	Upper	1.5	5%	1	35	0	143.2479
Erosional	Modern	Upper	0.5	5%	1	35	0	108.7851
Erosional	Brady	Upper	0.5	5%	1	35	0	147.361
Erosional	Modern	Upper	0.2	5%	1	35	0	47.09499
Erosional	Brady	Upper	0.2	5%	1	35	0	152.1243
Burial	Modern	Upper	5.5	5%	1	42	0	123.0724
Burial	Brady	Upper	5.5	5%	1	42	0	153.0274
Burial	Modern	Upper	3.5	5%	1	42	0	54.62736
Burial	Brady	Upper	3.5	5%	1	42	0	268.6079
Burial	Modern	Upper	1.5	5%	1	42	0	50.67269
Burial	Brady	Upper	1.5	5%	1	42	0	270.5479
Erosional	Modern	Upper	1.5	5%	1	42	0	161.1081
Erosional	Brady	Upper	1.5	5%	1	42	0	260.858
Erosional	Modern	Upper	0.5	5%	1	42	0	92.16153
Erosional	Brady	Upper	0.5	5%	1	42	0	130.4421
Erosional	Modern	Upper	0.2	5%	1	42	0	21.66889
Erosional	Brady	Upper	0.2	5%	1	42	0	155.913
Burial	Modern	Upper	5.5	5%	1	49	0	153.2972
Burial	Brady	Upper	5.5	5%	1	49	0	151.0813
Burial	Modern	Upper	3.5	5%	1	49	0	44.818
Burial	Brady	Upper	3.5	5%	1	49	0	197.8194
Burial	Modern	Upper	1.5	5%	1	49	0	30.8672
Burial	Brady	Upper	1.5	5%	1	49	0	372.0786
Erosional	Modern	Upper	1.5	5%	1	49	0	152.0315
Erosional	Brady	Upper	1.5	5%	1	49	0	215.0842
Erosional	Modern	Upper	0.5	5%	1	49	0	60.84605
Erosional	Brady	Upper	0.5	5%	1	49	0	151.897
Erosional	Modern	Upper	0.2	5%	1	49	0	61.03821
Erosional	Brady	Upper	0.2	5%	1	49	0	73.03173

Chapter 5.
Conclusion

Through this research we have investigated the local topographic variability of buried soils at different depth in burial and erosional landforms and the modern soil layers present on these buried soils. This research will be contributing to the growing number of studies on deeper soils and how does the soil organic matter (SOM), stabilization of the SOM and vulnerability of the deeper soils will react due to the increased precipitation which can lead to erosion and hence removal of the top modern soil layer and connecting the buried soil to the modern environment. Our results also highlight that burial can be an important mechanism for soil carbon storage and reconnecting the buried soil will make the previously stored soil carbon vulnerable to microbial decomposition.

The buried soil studied are found to be different in pH, EC, total organic carbon (TOC), total inorganic carbon (TIC), total nitrogen (TN) and C:N ratio at different landform (burial vs erosional) and paleostatus (modern vs Brady). Soil organic carbon was found to be increasing as the buried soil near to the modern surface in erosional landform. We also found that the source of the TOCs present in modern and buried soils at different landform are different. While the major source of TOC in the burial landform modern soils were C4 plant, the other soils have a good mixture of C4 and C3 plant derived carbon. Buried soils were more alkaline and has higher soluble salt (EC) content compared to the modern soils. Analysis of functional group level chemical composition indicated that the erosional landform buried soils has relatively high amount of easily decomposable aliphatic compound (C-H) and can become vulnerable if come in contact to the modern environment where the factors for microbial decompositions are present. Radiocarbon analysis indicated, although the deeper buried soils are older with depth in the burial landform, there is a shift in the values of fraction modern in the erosional landform where it is shallower and prone to expose to the modern environment. From our turnover time model, we noticed that burial landform deeper soils have higher turnover time indicating acting as a storage of soil organic carbon (SOC) while the erosional landform buried soils has shorter turnover time indicating they might be acting as a carbon source and also incorporating newer carbon due to shallow depth.

As we noticed the difference in soil chemical components, we focused on the stabilization mechanism of the SOC in these soils. Due to the previous observation of alkalinity and higher EC in the buried soils, we thought calcium (Ca) mediated SOC stabilization will be the dominant mechanism for SOC stabilization in these soils. Our observations indicated that the relative importance of chemical and physical storage of SOC are not consistent in different landform. Analysis of base cation exchange capacity indicated the amount of monovalent and divalent cation concentrations are different in modern and buried soils at different landforms. Buried soils has higher exchangeable potassium (K) and sodium (Na) compared to the modern soils while erosional modern soils were lower in exchangeable magnesium (Mg). The dominant cation present in these

soils were Ca and it was higher in the erosional landform modern and buried soils compared to the burial landform modern soils and there was no exchangeable Na in both burial and erosional landform modern soils. Overall soil physical structure was identified from the EC and sodium adsorption ratio (SAR), and we found all our soils are flocculated in structure indicating flocculation can be the major mechanism of aggregate formation of our studied soils. During flocculation, a chemical coagulates with water makes bonds between particles and create larger aggregates. Flocculating cations are divided into two categories, good flocculants which include Ca and Mg, and bad flocculants include Na. Presence of Na can disperse the soils and break down the soil aggregates eventually. As we know that this study area soils have agricultural practices where the topography permits, irrigation with high Na concentration water can make the soil aggregates destabilize easily. We noticed higher TOC content was positively correlated to the exchangeable Ca in the erosional landform modern soil, buried soil and burial landform modern soils which indicated that formation of aggregates or organo-mineral complexation through Ca bridging can be the major mechanism of SOC stabilization in these soils. For the burial landform buried soils, there can be an extra mechanism of SOC stabilization through compaction from the top along with aggregate formation and organo-mineral complexation. Due to compaction the pore space is smaller than the microbial bodies which can prevent the microbial activity from SOC decomposition.

With the understanding of how the SOC is different and the mechanism of stabilization can be different we investigated the vulnerability of these ancient carbon present in different landform with their modern soil counterparts in an in-situ laboratory incubation study with the addition of two different moisture intensity. We studied continuous wet and periodic wet dry incubation experiments at 60% water holding capacity (WHC) for the experiments and 5% WHC for the control. We designed the experiment to see if there is any change in seasonal precipitation, how the soil carbons will be impacted. Our continuous wet experiment with 60% WHC evolved highest CO_2 compared to the wet-dry experiment. In both experiments (continuous wet and wet-dry), erosional landform modern soils produced the largest amount of CO_2 at the end of the experiments. We didn't find any significant differences in evolved CO_2 from the buried soils and modern soils in our wet-dry experiment study. Our incubation study indicated erosional landform modern and buried soils are more vulnerable to decomposition in addition of moisture compared to the burial modern and buried soils. We also found that 5% WHC has highest effects on buried soils compared to the modern soils. We did a two-pool first order decay model with the continuous wet cumulative data to understand which pool is more responsive to the change in moisture. Our data indicated slow cycling pool is dominant in these soils as >97% SOC are stored in the slow-cycling pool. Burial landform buried soil has the highest amount of slow cycling pool and erosional landform modern soil has the least amount of slow-cycling pool. Decay constant of the slow cycling pools were thousand-fold high compared to the slow cycling pools. Fast-cycling pool of the buried soils are slightly faster than the modern soils, perhaps indicating that there is fast cycling SOC available that is protected at depth will decompose faster when brought to modern environment conditions. Our research indicated that persistence of soil organic carbon is an ecosystem property and not a molecular property. This research highlights the fact that buried soils can serve as a model system to understand -accumulation, long time stabilization and potential vulnerabilities to disturbances of carbon in deeper soil horizons.

This research provided evidence that soil burial can act as a significant C-sink where SOC can stay longer due to the unfavorable environment for microbial decomposition. To further our understanding of the ability of the buried soil to act as a carbon sink, we will need to quantify the total amount of carbon present in these soils at this depth ranging from 0.2m to 5.5m, while reminding that the TOC present today in these soils also include addition of newer organic matter which are staying at this deep because of the unfavorable environment. To better understand the vulnerability of these ancient carbon we will need to study a longer period of incubation with higher temperatures as previous study has indicated presence of PyC in these soils. A longer incubation study with change in microbial community and composition of SOM can tell us the fate of these buried carbon in presence of future disturbances.

There is now an urgent need to improve our understanding and prediction capability of buried C vulnerability to changes in climate and landscape disturbance; and identify the mechanisms that regulate storage and turnover in these C pools and evaluate their response to changing environmental conditions in-situ.

Acknowledgements
We would like to acknowledge the funding from NSF EAR-1623814 and Lawrence Livermore National Laboratory (LLNL) student training program. We also thank the landowners, for access to the field sites.